ETH
Eidgenössische Technische Hochschule Zürich
Swiss Federal Institute of Technology Zurich

Seminar for Applied Mathematics SAM

Exponential Convergence for hp-Version and Spectral Finite Element Methods for Elliptic Problems in Polyhedra

D. Schötzau and Ch. Schwab

Research Report No. 2014-38
December 2014

Seminar für Angewandte Mathematik
Eidgenössische Technische Hochschule
CH-8092 Zürich
Switzerland

Funding ERC: AdG grant STAHDPDE 247277
Funding: Natural Sciences and Engineering Research Council of Canada (NSERC)

EXPONENTIAL CONVERGENCE FOR *hp*-VERSION AND SPECTRAL FINITE ELEMENT METHODS FOR ELLIPTIC PROBLEMS IN POLYHEDRA

DOMINIK SCHÖTZAU AND CHRISTOPH SCHWAB

Abstract. We establish exponential convergence of conforming *hp*-version and spectral finite element methods for second-order, elliptic boundary-value problems with constant coefficients and homogeneous Dirichlet boundary conditions in bounded, axiparallel polyhedra. The source terms are assumed to be piecewise analytic. The conforming *hp*-approximations are based on σ-geometric meshes of mapped, possibly anisotropic hexahedra and on the uniform and isotropic polynomial degree $p \geq 1$. The principal new results are the construction of conforming, patchwise *hp*-interpolation operators in edge, corner and corner-edge patches which are the three basic building blocks of geometric meshes. In particular, we prove, for each patch type, exponential convergence rates for the H^1-norm of the corresponding *hp*-version (quasi)interpolation errors for functions which belong to a suitable, countably normed space on the patches. The present work extends the discontinuous Galerkin approaches in [14, 15] to conforming *hp*-Galerkin finite element methods.

Contents

2010 *Mathematics Subject Classification.* 65N30.

Key words and phrases. *hp*-FEM, spectral FEM, second-order elliptic problems in polyhedra, exponential convergence.

This work was supported in part by the Natural Sciences and Engineering Research Council of Canada (NSERC), the European Research Council AdG grant STAHDPDE 247277.

1. Introduction

The *hp*-version of the finite element method (FEM) is a realization of so-called variable-degree, variable knot spline approximations in the context of Galerkin approximations for elliptic partial differential equations; cp. [6, 13] and the references therein. While in [6, 13] exponential convergence rates in L^∞-norm were proved for particular, singular functions in one space dimension, in [9] exponential convergence of *hp*-FEM in H^1-norm was shown, for a model second-order, elliptic boundary-value problem, again with a model singular solution in one space dimension. Subsequently, these concepts were substantially generalized to *hp*-version FEMs for second-order, elliptic boundary-value problems in two space dimensions: on the one hand, rather than for particular singular solutions, in [10] exponential convergence of *hp*-FEM on geometrically refined triangulations was now proved for solutions belonging to *countably normed, weighted Sobolev spaces*. On the other hand, in [1] an *elliptic regularity shift theorem* was shown in these spaces.

In recent years, the corresponding elliptic regularity shifts in countably normed, weighted Sobolev spaces in polyhedral domains have been established in [11, 12, 4], at least for certain classes of second-order, elliptic boundary-value problems in three dimensions. Based on these analytic regularity results, in [15], exponential convergence in broken H^1-norms has been proved for an *hp*-version discontinuous Galerkin (DG) method for second-order, elliptic problems in axiparallel polyhedra. Corresponding exponential convergence results on regular, anisotropic geometric meshes of tetrahedral elements have been announced in [2].

The purpose of the present paper is to establish exponential convergence of conforming *hp*-version approximations on families of geometrically refined meshes of axiparallel hexahedra, in the setting of [14, 15]. Our proof consists in the construction of H^1-conforming piecewise polynomial approximations of *uniform polynomial degree* $p \geq 1$, by modifying our *discontinuous hp-version base interpolants* from [15] with the aid of suitable *polynomial trace lifting operators* in the presence of *irregular* geometric mesh refinements towards corners and edges. This construction is accompanied with the proof that the trace liftings thus constructed do not disrupt the exponential convergence of the base interpolants.

Therefore, the main results of the paper are, for each geometric mesh patch of corner, edge and corner-edge type, the construction and analysis of *hp*-version patch projectors onto spaces of continuous, piecewise polynomials which converge exponentially for solutions belonging belong to a certain analytic class of functions in each patch type. By Céa's lemma, this result in conjunction with the analytic regularity in [4] implies exponential convergence of *hp*-FEM on polyhedra for the model diffusion equation considered in the paper. We emphasize, however, that the *hp-patch approximation results* proved here apply more generally to any solutions

whose pull-backs into the reference patches belong to one of the weighted analytic classes.

As we consider uniform elemental polynomial degrees, the present hp-version consistency error analysis covers, in particular, also *spectral element methods*; there, additional quadrature errors due to elemental under-integration arise, which are not dicussed in the present paper. We also mention that conforming hp-FE spaces have been implemented in [8], and also in [7].

The outline of this paper is as follows. In Section 2 we present an elliptic model problem in an axiparallel polyhedral domain, and recapitulate the analytic regularity theory of [4] for solutions with piecewise analytic source terms. Section 3 addresses the construction of the hp-version subspaces, and it presents and discusses our main result on exponential convergence of conforming hp-FEM. Section 4 reviews the construction and exponential error bounds of the base hp-version projector from [15] which are obtained by tensorization of univariate hp-projectors. In Section 5, we construct and analyze polynomial trace liftings which preserve exponential convergence estimates for all types of irregular interfaces.

The notation employed throughout this paper is consistent with [14, 15]. In particular, we shall frequently use the notations "$\lesssim$" or "$\simeq$" to mean an inequality or an equivalence containing generic positive multiplicative constants which are independent of the local mesh size, the polynomial degree $p \geq 1$, the regularity parameters, and the geometric refinement level ℓ, but which may depend on the geometric refinement ratio σ.

2. Elliptic Model Dirichlet Problem and Analytic Regularity

In this section, we introduce an elliptic model problem in an axiparallel polyhedron in three dimensions, and specify the (analytic) regularity of its solutions in terms of countably normed weighted Sobolev spaces. We follow [4], based on the notations already introduced in [14, 15].

2.1. **Model Problem.** Let $\Omega \subset \mathbb{R}^3$ be an open, bounded and axiparallel polyhedron with Lipschitz boundary $\Gamma = \partial\Omega$ that consists of a finite union of plane faces; cp. [14, 15]. We consider the elliptic model Dirichlet problem

$$-\nabla \cdot (\boldsymbol{A}\nabla u) = f \qquad \text{in } \Omega, \tag{2.1}$$

$$\gamma_0(u) = 0 \qquad \text{on } \Gamma, \tag{2.2}$$

where γ_0 denotes the trace operator on Γ. We assume that the diffusion tensor $\boldsymbol{A}$ is constant and symmetric positive definite. With the standard Sobolev space $H^1_0(\Omega) = \{v \in H^1(\Omega) : \gamma_0(v) = 0\}$, the variational form of problem (2.1)–(2.2) is to find $u \in H^1_0(\Omega)$ such that

$$a(u,v) := \int_\Omega \boldsymbol{A}\nabla u \cdot \nabla v \, \mathrm{d}\boldsymbol{x} = \int_\Omega fv \, \mathrm{d}\boldsymbol{x} \qquad \forall v \in H^1_0(\Omega)\,. \tag{2.3}$$

Under the above assumptions, the bilinear form a is coercive, and for every right hand side f in $H^{-1}(\Omega)$, the dual space of $H^1_0(\Omega)$, problem (2.3) admits a unique weak solution $u \in H^1_0(\Omega)$.

2.2. **Subdomains and Weights.** To specify the analytic regularity of solutions of (2.3), we follow [4], based on the notations already introduced in [14, 15]. We

denote by $\mathcal{C}$ the set of corners $\boldsymbol{c}$, and by $\mathcal{E}$ the set of open edges $\boldsymbol{e}$ of Ω. The *singular set of* Ω is given by

$$\mathcal{S} := \left(\bigcup_{\boldsymbol{c}\in\mathcal{C}} \boldsymbol{c}\right) \cup \left(\bigcup_{\boldsymbol{e}\in\mathcal{E}} \boldsymbol{e}\right) \subset \Gamma. \tag{2.4}$$

For $\boldsymbol{c} \in \mathcal{C}$, $\boldsymbol{e} \in \mathcal{E}$, and $\boldsymbol{x} \in \Omega$, we define the following distance functions:

$$r_{\boldsymbol{c}}(\boldsymbol{x}) := \operatorname{dist}(\boldsymbol{x}, \boldsymbol{c}), \qquad r_{\boldsymbol{e}}(\boldsymbol{x}) := \operatorname{dist}(\boldsymbol{x}, \boldsymbol{e}), \qquad \rho_{\boldsymbol{ce}}(\boldsymbol{x}) := r_{\boldsymbol{e}}(\boldsymbol{x})/r_{\boldsymbol{c}}(\boldsymbol{x}). \tag{2.5}$$

As in [14, Section 2.1], the vertices of Ω are assumed to be separated. For each corner $\boldsymbol{c} \in \mathcal{C}$, we denote by $\mathcal{E}_{\boldsymbol{c}} := \{\, \boldsymbol{e} \in \mathcal{E} \,:\, \boldsymbol{c} \cap \overline{\boldsymbol{e}} \neq \emptyset \,\}$ the set of all edges which meet at $\boldsymbol{c}$. Similarly, for $\boldsymbol{e} \in \mathcal{E}$, the set of corners of $\boldsymbol{e}$ is $\mathcal{C}_{\boldsymbol{e}} := \{\, \boldsymbol{c} \in \mathcal{C} \,:\, \boldsymbol{c} \cap \overline{\boldsymbol{e}} \neq \emptyset \,\}$. Then, for $\varepsilon > 0$, $\boldsymbol{c} \in \mathcal{C}$, $\boldsymbol{e} \in \mathcal{E}$ respectively $\boldsymbol{e} \in \mathcal{E}_{\boldsymbol{c}}$, we define the neighborhoods

$$\begin{aligned}
\omega_{\boldsymbol{c}} &= \{\, \boldsymbol{x} \in \Omega \,:\, r_{\boldsymbol{c}}(\boldsymbol{x}) < \varepsilon \;\wedge\; \rho_{\boldsymbol{ce}}(\boldsymbol{x}) > \varepsilon \quad \forall\, \boldsymbol{e} \in \mathcal{E}_{\boldsymbol{c}} \,\},\\
\omega_{\boldsymbol{e}} &= \{\, \boldsymbol{x} \in \Omega \,:\, r_{\boldsymbol{e}}(\boldsymbol{x}) < \varepsilon \;\wedge\; r_{\boldsymbol{c}}(\boldsymbol{x}) > \varepsilon \quad \forall\, \boldsymbol{c} \in \mathcal{C}_{\boldsymbol{e}} \,\},\\
\omega_{\boldsymbol{ce}} &= \{\, \boldsymbol{x} \in \Omega \,:\, r_{\boldsymbol{c}}(\boldsymbol{x}) < \varepsilon \;\wedge\; \rho_{\boldsymbol{ce}}(\boldsymbol{x}) < \varepsilon \,\}.
\end{aligned} \tag{2.6}$$

By choosing $\varepsilon > 0$ sufficiently small as in [14], the domain Ω can be partitioned into four *disjoint* subdomains, $\overline{\Omega} = \overline{\Omega_{\mathcal{C}} \,\dot\cup\, \Omega_{\mathcal{E}} \,\dot\cup\, \Omega_{\mathcal{CE}} \,\dot\cup\, \Omega_0}$, referred to as *corner*, *edge*, *corner-edge* and *interior* neighborhoods of Ω, respectively, where

$$\Omega_{\mathcal{C}} = \bigcup_{\boldsymbol{c}\in\mathcal{C}} \omega_{\boldsymbol{c}}, \qquad \Omega_{\mathcal{E}} = \bigcup_{\boldsymbol{e}\in\mathcal{E}} \omega_{\boldsymbol{e}}, \qquad \Omega_{\mathcal{CE}} = \bigcup_{\boldsymbol{c}\in\mathcal{C}} \bigcup_{\boldsymbol{e}\in\mathcal{E}_{\boldsymbol{c}}} \omega_{\boldsymbol{ce}},$$

and $\Omega_0 := \Omega \setminus \overline{\Omega_{\mathcal{C}} \cup \Omega_{\mathcal{E}} \cup \Omega_{\mathcal{CE}}}$.

2.3. **Weighted Sobolev Spaces.** To each $\boldsymbol{c} \in \mathcal{C}$ and $\boldsymbol{e} \in \mathcal{E}$, we associate a corner and an edge exponent $\beta_{\boldsymbol{c}}, \beta_{\boldsymbol{e}} \in \mathbb{R}$, respectively. We collect these quantities in the multi-exponent

$$\boldsymbol{\beta} = \{\, \beta_{\boldsymbol{c}} \,:\, \boldsymbol{c} \in \mathcal{C} \,\} \cup \{\, \beta_{\boldsymbol{e}} \,:\, \boldsymbol{e} \in \mathcal{E} \,\} \in \mathbb{R}^{|\mathcal{C}|+|\mathcal{E}|}. \tag{2.7}$$

Inequalities of the form $\boldsymbol{\beta} < 1$ and expressions like $\boldsymbol{\beta} \pm s$, for $s \in \mathbb{R}$, are to be understood componentwise, i.e., $\boldsymbol{\beta} + s = \{\, \beta_{\boldsymbol{c}} + s \,:\, \boldsymbol{c} \in \mathcal{C} \,\} \cup \{\, \beta_{\boldsymbol{e}} + s \,:\, \boldsymbol{e} \in \mathcal{E} \,\}$.

To review the analytic regularity results of [4] for solutions to (2.1)–(2.2), we choose local coordinate systems in $\omega_{\boldsymbol{e}}$ and $\omega_{\boldsymbol{ce}}$, for $\boldsymbol{c} \in \mathcal{C}$, $\boldsymbol{e} \in \mathcal{E}$ resp. $\boldsymbol{e} \in \mathcal{E}_{\boldsymbol{c}}$, such that the edge $\boldsymbol{e}$ corresponds to the direction $(0, 0, 1)$. Then, we indicate quantities transversal to $\boldsymbol{e}$ by $(\cdot)^{\perp}$, and quantities parallel to $\boldsymbol{e}$ by $(\cdot)^{\parallel}$. In particular, if $\boldsymbol{\alpha} = (\alpha_1, \alpha_2, \alpha_3) \in \mathbb{N}_0^3$ is a multi-index of order $|\boldsymbol{\alpha}| = \alpha_1 + \alpha_2 + \alpha_3$, then we write $\boldsymbol{\alpha} = (\boldsymbol{\alpha}^{\perp}, \alpha^{\parallel})$ with $\boldsymbol{\alpha}^{\perp} = (\alpha_1, \alpha_2)$ and $\alpha^{\parallel} = \alpha_3$, and denote the partial derivative operator $\mathsf{D}^{\boldsymbol{\alpha}}$ by $\mathsf{D}^{\boldsymbol{\alpha}} = \mathsf{D}_{\perp}^{\boldsymbol{\alpha}^{\perp}} \mathsf{D}_{\parallel}^{\alpha^{\parallel}}$, where $\mathsf{D}_{\perp}^{\boldsymbol{\alpha}^{\perp}}$ and $\mathsf{D}_{\parallel}^{\alpha^{\parallel}}$ signify the derivative operators in perpendicular and parallel directions, respectively.

For $k \in \mathbb{N}_0$, we define the weighted semi-norm $|\cdot|_{M^k_{\boldsymbol{\beta}}(\Omega)}$ by

$$\begin{aligned}
|u|^2_{M^k_{\boldsymbol{\beta}}(\Omega)} := \sum_{|\boldsymbol{\alpha}|=k} \Bigg\{ &\|\mathsf{D}^{\boldsymbol{\alpha}} u\|^2_{L^2(\Omega_0)} + \sum_{\boldsymbol{c}\in\mathcal{C}} \big\| r_{\boldsymbol{c}}^{\beta_{\boldsymbol{c}}+|\boldsymbol{\alpha}|} \mathsf{D}^{\boldsymbol{\alpha}} u \big\|^2_{L^2(\omega_{\boldsymbol{c}})} \\
&+ \sum_{\boldsymbol{e}\in\mathcal{E}} \big\| r_{\boldsymbol{e}}^{\beta_{\boldsymbol{e}}+|\boldsymbol{\alpha}^{\perp}|} \mathsf{D}^{\boldsymbol{\alpha}} u \big\|^2_{L^2(\omega_{\boldsymbol{e}})} + \sum_{\boldsymbol{c}\in\mathcal{C}} \sum_{\boldsymbol{e}\in\mathcal{E}_{\boldsymbol{c}}} \big\| r_{\boldsymbol{c}}^{\beta_{\boldsymbol{c}}+|\boldsymbol{\alpha}|} \rho_{\boldsymbol{ce}}^{\beta_{\boldsymbol{e}}+|\boldsymbol{\alpha}^{\perp}|} \mathsf{D}^{\boldsymbol{\alpha}} u \big\|^2_{L^2(\omega_{\boldsymbol{ce}})} \Bigg\}.
\end{aligned} \tag{2.8}$$

The norm $\|\cdot\|_{M^m_{\beta}(\Omega)}$ is defined by $\|u\|^2_{M^m_{\boldsymbol{\beta}}(\Omega)} = \sum_{k=0}^m |u|^2_{M^k_{\boldsymbol{\beta}}(\Omega)}$, and the weighted Sobolev space $M^m_{\boldsymbol{\beta}}(\Omega)$ is obtained as the closure of $C_0^\infty(\Omega)$ with respect to the

norm $\|\cdot\|_{M^m_{\boldsymbol{\beta}}(\Omega)}$. For $D \subseteq \Omega$, we denote by $|\cdot|_{M^m_{\boldsymbol{\beta}}(D)}$ and $\|\cdot\|_{M^m_{\boldsymbol{\beta}}(D)}$ the above seminorm and norm, respectively, with all domains of integration replaced by their intersections with $D \subseteq \Omega$.

2.4. **Analytic Regularity of Variational Solutions.** We adopt the following classes of analytic functions from [4].

Definition 2.1. For subdomains $D \subseteq \Omega$ the space $A_{\boldsymbol{\beta}}(D)$ consists of all functions u such that $u \in M^k_{\boldsymbol{\beta}}(D)$ for all $k \geq 0$, and such that there exists a constant $C_u > 0$ (independent of D) with the property that

$$|u|_{M^k_{\boldsymbol{\beta}}(D)} \leq C_u^{k+1}\Gamma(k+1) \qquad \forall\, k \in \mathbb{N}_0\,, \tag{2.9}$$

where Γ is the standard Gamma function satisfying $\Gamma(k+1) = k!$ for any $k \in \mathbb{N}_0$.

In [4, Corollary 7.1]), the following analytic regularity result for variational solutions of (2.1)–(2.2) in the case of constant coefficients considered here has been shown.

Proposition 2.2. *There are bounds $b_{\mathcal{C}}, b_{\mathcal{E}} > 0$ (depending on Ω and on the diffusion matrix $\boldsymbol{A}$) such that, for weight vectors $\boldsymbol{b}$ satisfying*

$$0 \leq b_{\boldsymbol{c}} < b_{\mathcal{C}}, \quad 0 \leq b_{\boldsymbol{e}} < b_{\mathcal{E}}, \qquad \boldsymbol{c} \in \mathcal{C},\ \boldsymbol{e} \in \mathcal{E}, \tag{2.10}$$

the weak solution $u \in H^1_0(\Omega)$ in (2.3) of the Dirichlet problem (2.1)-(2.2) satisfies:

$$f \in A_{1-\boldsymbol{b}}(\Omega) \implies u \in A_{-1-\boldsymbol{b}}(\Omega)\,. \tag{2.11}$$

Remark 2.3. In the following and as in [15], we shall exclude the limit cases $b_{\boldsymbol{c}} = 0$ and $b_{\boldsymbol{e}} = 0$, and assume without loss of generality that in (2.10) there holds

$$0 < b_{\mathcal{C}},\ b_{\mathcal{E}} < 1. \tag{2.12}$$

We further note that Proposition 2.2 is a reformulation of [6, Corollary 7.1], which results from a straightforward substitution of the weights there; cp. [15]. We have chosen this alternative formulation since our weights in (2.10) are now non-negative and, thereby, the ensuing error analysis is slightly facilitated.

3. hp-Version Discretization and Exponential Convergence

In this section, we adjust the construction of hp-version finite element spaces in [14, 15] from the discontinuous to the continuous Galerkin framework. Then we introduce conforming hp-version finite element approximations on geometric mesh families. Finally, we state our main exponential convergence result (Theorem 3.6) and outline the structure of its proof.

3.1. **Geometric Meshes.** We start by reviewing the construction of geometric mesh (families) from [14, 15].

3.1.1. *Patch Mesh $\mathcal{M}^0$.* We start from a coarse regular and *quasiuniform patch mesh* $\mathcal{M}^0 = \{Q_{\mathfrak{p}}\}_{\mathfrak{p}=1}^{\mathfrak{P}}$, which partitions Ω into $\mathfrak{P}$ convex axiparallel hexahedra also referred to as *patches*. Throughout, we shall assume that the initial mesh $\mathcal{M}^0$ is sufficiently fine so that an element $K \in \mathcal{M}^0$ has non-trivial intersection with at most one corner $\boldsymbol{c} \in \mathcal{C}$, and either none, one or several edges $\boldsymbol{e} \in \mathcal{E}_{\boldsymbol{c}}$ meeting in $\boldsymbol{c}$. Each of these patch subdomains $Q_{\mathfrak{p}} \in \mathcal{M}^0$ is the image under an affine mapping $G_{\mathfrak{p}}$ of the *reference patch domain* $\widetilde{Q} = (-1,1)^3$, i.e., $Q_{\mathfrak{p}} = G_{\mathfrak{p}}(\widetilde{Q})$. We assume that the patch maps are geometrically exact.

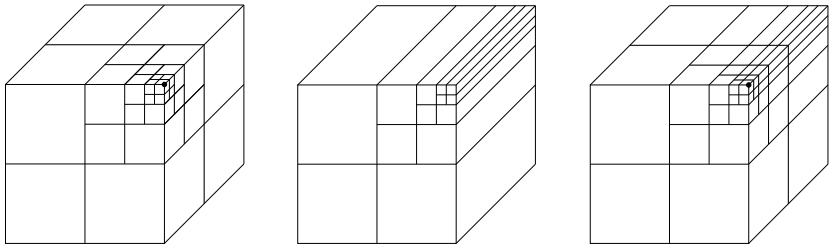

FIGURE 1. Three basic geometric mesh patches in the reference patch $\widetilde{Q}$ as considered in [14] with subdivision ratio $\sigma = 0.5$: corner patch $\widetilde{\mathcal{M}}_\sigma^{\ell,\boldsymbol{c}}$ with isotropic geometric refinement towards the corner $\boldsymbol{c}$ (left), edge patch $\widetilde{\mathcal{M}}_\sigma^{\ell,\boldsymbol{e}}$ with anisotropic geometric refinement towards the edge $\boldsymbol{e}$ (center), and corner-edge patch $\widetilde{\mathcal{M}}_\sigma^{\ell,\boldsymbol{ce}}$ with geometric refinement towards the corner-edge pair $\boldsymbol{ce}$ (right). The singular supports $\boldsymbol{c}, \boldsymbol{e}, \boldsymbol{ce}$ are shown in bold face.

3.1.2. *Geometric Reference Mesh Patches.* With each patch $Q_{\mathfrak{p}} \in \mathcal{M}^0$, we associate a *geometric reference mesh patch* $\widetilde{\mathcal{M}}_{\mathfrak{p}}$ *on* $\widetilde{Q}$. We allow for *four types of geometric refinements*, as constructed in [14, Section 3.3] in terms of four different *hp*-extensions (Ex1)–(Ex4). That is, we take

$$\widetilde{\mathcal{M}}_{\mathfrak{p}} \in \widetilde{\mathcal{RP}} := \{\widetilde{\mathcal{M}}_\sigma^{\ell,\boldsymbol{c}}, \widetilde{\mathcal{M}}_\sigma^{\ell,\boldsymbol{e}}, \widetilde{\mathcal{M}}_\sigma^{\ell,\boldsymbol{ce}}, \widetilde{\mathcal{M}}_\sigma^{\ell,\mathrm{int}}\} = \{\widetilde{\mathcal{M}}_\sigma^{\ell,\mathrm{t}}\}_{\mathrm{t}\in\{\boldsymbol{c},\boldsymbol{e},\boldsymbol{ce},\mathrm{int}\}}. \tag{3.1}$$

More specifically, whenever $Q_{\mathfrak{p}}$ abuts at the singular set $\mathcal{S}$, we assign to $\widetilde{\mathcal{M}}_{\mathfrak{p}}$ (a suitably rotated and oriented version) of the geometrically refined reference mesh patches shown in Figure 1 and denoted by $\widetilde{\mathcal{M}}_\sigma^{\ell,\boldsymbol{c}}$ (corner patch), $\widetilde{\mathcal{M}}_\sigma^{\ell,\boldsymbol{e}}$ (edge patch), and $\widetilde{\mathcal{M}}_\sigma^{\ell,\boldsymbol{ce}}$ (corner-edge patch), respectively. We implicitly allow for simultaneous geometric refinements towards several edges in the corner-edge patch $\widetilde{\mathcal{M}}^{\ell,\boldsymbol{ce}}$, which corresponds to an overlap of at most three rotated versions of the basic corner-edge patch; see also Figures 10 and 11 ahead. The geometric refinements in these reference patches are characterized by (i) a fixed parameter $\sigma \in (0,1)$ defining the subdivision ratio of the geometric refinements and (ii) the index ℓ defining the number of refinements. For interior patches $Q_{\mathfrak{p}} \in \mathcal{M}^0$, which have empty intersection with $\mathcal{S}$, we assign to $\widetilde{\mathcal{M}}_{\mathfrak{p}}$ a geometric reference mesh patch $\widetilde{\mathcal{M}}_\sigma^{\ell,\mathrm{int}}$ on $\widetilde{Q}$, which comprises only *finitely many regular refinements* and does not introduce irregular faces within $\widetilde{Q}$. In the refinement process, the reference mesh $\widetilde{\mathcal{M}}_\sigma^{\ell,\mathrm{int}}$ is kept unchanged and is independent of the refinement level ℓ.

To ensure continuity across mesh patches, we shall always work under the following *inter-patch compatibility* hypothesis.

Assumption 3.1. We assume that:

(i) Any two distinct geometric mesh patches $Q_{\mathfrak{p}}, Q_{\mathfrak{p}'} \in \mathcal{M}^0$, $\mathfrak{p} \neq \mathfrak{p}'$, with nonempty intersection $\Gamma_{\mathfrak{p}\,\mathfrak{p}'} := \overline{Q}_{\mathfrak{p}} \cap \overline{Q}_{\mathfrak{p}'} \neq \emptyset$, are geometrically conforming, i.e., the parametrizations induced by patch maps on patch interfaces $\Gamma_{\mathfrak{p}\,\mathfrak{p}'}$ coincide "from either side":

$$G_{\mathfrak{p}} \circ \left(G_{\mathfrak{p}'}^{-1}\,|_{\Gamma_{\mathfrak{p}\,\mathfrak{p}'}}\right) = G_{\mathfrak{p}'} \circ \left(G_{\mathfrak{p}}^{-1}\,|_{\Gamma_{\mathfrak{p}\,\mathfrak{p}'}}\right) .$$

(ii) The types of reference geometric meshes $\widetilde{\mathcal{M}}_{\mathfrak{p}}$ on $\widetilde{Q}$ considered above, see also Figure 1, in any two distinct geometric mesh patches $Q_{\mathfrak{p}}, Q_{\mathfrak{p}'} \in \mathcal{M}^0$ coincide on the nonempty intersection $\Gamma_{\mathfrak{p}\,\mathfrak{p}'}$ of $Q_{\mathfrak{p}}, Q_{\mathfrak{p}'}$.

We note that Assumption 3.1 (ii) mandates that the parameters σ and ℓ are equal in all geometric reference mesh patches. It further may mandate the introduction of finitely many regular refinements in interior reference patches $\widetilde{\mathcal{M}}_{\mathfrak{p}}$, in contrast to the discontinuous setting in [14, 15] where the interior reference mesh patch is left unrefined and consists of the single element $\widetilde{Q}$.

3.1.3. *Geometric Mesh Families.* If we denote by $\widetilde{\mathcal{M}}_{\mathfrak{p}} = \{\widetilde{K}\}$ the axiparallel reference mesh on $\widetilde{Q}$ associated with the patch $Q_{\mathfrak{p}}$, then the corresponding patch partition $\mathcal{M}_{\mathfrak{p}}$ on $Q_{\mathfrak{p}}$ will be given by $\mathcal{M}_{\mathfrak{p}} := \{\, K : K = (G_{\mathfrak{p}} \circ H_{\mathfrak{p},\widetilde{K}})(\widetilde{K}),\ \widetilde{K} \in \widetilde{\mathcal{M}}_{\mathfrak{p}} \,\}$, where $H_{\mathfrak{p},\widetilde{K}}(\widetilde{K})$ is a possibly anisotropic dilation-translation of the reference cube $\widehat{K} = (-1,1)^3$ onto $\widetilde{K}$. For $\sigma \in (0,1)$ and $\ell \in \mathbb{N}$, a σ-geometric mesh on Ω is now given by the disjoint union

$$\mathcal{M} = \mathcal{M}_\sigma^{(\ell)} := \bigcup_{\mathfrak{p}=1}^{\mathfrak{P}} \mathcal{M}_{\mathfrak{p}}\,. \tag{3.2}$$

By construction, each axiparallel element K in a geometric mesh $\mathcal{M}$ is the image of the reference cube $\widehat{K}$ under an element mapping $K = \Phi_K(\widehat{K})$, where Φ_K is the composition of the corresponding patch map $G_{\mathfrak{p}}$ with an anisotropic dilation-translation from $\widehat{K}$ to K.

To achieve a proper geometric refinement towards corners and edges of Ω, it is important to note that the geometric refinements $\mathcal{M}_{\mathfrak{p}}$ in the patches $Q_{\mathfrak{p}}$ have to be suitably selected and oriented in order to achieve a proper geometric refinement towards corners and edges of Ω without violating Assumption 3.2.

For a fixed subdivision ratio $\sigma \in (0,1)$, we call the sequence $\mathfrak{M}_\sigma = \{\mathcal{M}_\sigma^{(\ell)}\}_{\ell \geq 1}$ of geometric meshes a *σ-geometric mesh family*; see [14, Definition 3.4]. As before, we shall refer to the index ℓ as *refinement level*.

3.1.4. *Edges and Faces.* Next, we introduce some notation related to edges and faces of a geometric mesh $\mathcal{M} = \mathcal{M}_\sigma^{(\ell)}$. We denote the sets of all interior and boundary edges e of $\mathcal{M}$ by $\mathcal{E}_I(\mathcal{M})$ and $\mathcal{E}_B(\mathcal{M})$, respectively, and set $\mathcal{E}(\mathcal{M}) := \mathcal{E}_I(\mathcal{M}) \cup \mathcal{E}_B(\mathcal{M})$. We denote by $e_{K,K'} = \mathrm{int}(\partial K \cap \partial K')$ an edge shared by K and K'. Similarly, we write $\mathcal{F}_I(\mathcal{M})$ and $\mathcal{F}_B(\mathcal{M})$ for the sets of interior and boundary faces f of $\mathcal{M}$, respectively, and define $\mathcal{F}(\mathcal{M}) := \mathcal{F}_I(\mathcal{M}) \cup \mathcal{F}_B(\mathcal{M})$. Again, we write $f_{K,K'} = \mathrm{int}(\partial K \cap \partial K')$ for the interior face shared by K and K'. For a piecewise smooth function v, we denote the jump of v over the face $f_{K,K'}$ by

$$[\![v]\!]_{f_{K,K'}} := v|_K - v|_{K'}. \tag{3.3}$$

Moreover, for an element K, we denote by $\mathcal{E}_K$ the set of its elemental edges, and by $\mathcal{F}_K$ the set of its elemental faces. We call an edge e *regular* if e is an entire elemental face of all elements K sharing it (i.e., if $\overline{e} \cap \overline{K} \neq \emptyset$, then $e \in \mathcal{E}_K$). Otherwise e is called *irregular*. Analogously, a face $f = f_{K,K'}$ is called regular if f is an elemental face of both K and K' (i.e., $f \in \mathcal{F}_K$ and $f \in F_{K'}$); otherwise it is irregular. We shall always assume that boundary edges or faces belong to exactly one boundary plane of Γ.

For the continuity of finite element functions across elements, we impose the following assumption.

Assumption 3.2. Under Assumption 3.1, for any two, distinct elements $K, K' \in \mathcal{M}$ which share either a common edge $e_{K,K'}$ or an interior face $f_{K,K'}$ the traces of the elemental polynomial spaces on $e_{K,K'}$ or $f_{K,K'}$ in local coordinates (induced by the corresponding patch maps) coincide.

3.1.5. *Mesh Layers.* Following [14, Section 3], we partition a geometric mesh $\mathcal{M}_\sigma^{(\ell)}$ into interior elements $\mathfrak{O}_\sigma^\ell$ away from $\mathcal{S}$ and into the terminal layer elements $\mathfrak{T}_\sigma^\ell$ at $\mathcal{S}$:

$$\mathcal{M}_\sigma^{(\ell)} := \mathfrak{O}_\sigma^\ell \,\dot\cup\, \mathfrak{T}_\sigma^\ell, \tag{3.4}$$

with $\mathfrak{O}_\sigma^\ell := \{K \in \mathcal{M}_\sigma^{(\ell)} : \overline{K} \cap \mathcal{S} = \emptyset\}$ and $\mathfrak{T}_\sigma^\ell := \{K \in \mathcal{M}_\sigma^{(\ell)} : \overline{K} \cap \mathcal{S} \neq \emptyset\}$. Following [14, Section 3.3.1], the interior mesh $\mathfrak{O}_\sigma^\ell$ can be further disjointly partitioned into ℓ *mesh layers* of the form

$$\mathfrak{O}_\sigma^\ell = \mathfrak{L}_\sigma^0 \,\dot\cup\, \cdots \,\dot\cup\, \mathfrak{L}_\sigma^{\ell-1}, \tag{3.5}$$

where mesh layer $0 \le \ell' \le \ell - 1$ consists of a group $\mathfrak{L}_\sigma^{\ell'}$ of elements with identical scaling properties as in [15, Section 3].

3.1.6. *Anisotropic Scaling.* For $K \in \mathcal{M}_\sigma^{(\ell)}$, we set $h_K := \operatorname{diam}(K)$. As in [14, 15], for possibly anisotropic edge-patch and corner-edge patch elements K, we denote by $h_K^\perp$ and $h_K^\parallel$ the elemental diameters of K transversal respectively parallel to the singular edge $\boldsymbol{e} \in \mathcal{E}$ situated nearest to K, defined as the corresponding quantities over the axiparallel element $\widetilde{K} = G_{\mathfrak{p}}^{-1}(K)$, where $G_{\mathfrak{p}}$ denotes the affine patch map associated with K. If $K \in \mathfrak{O}_\sigma^\ell$, these quantities are related to the relative distances to the sets $\mathcal{C}$ and $\mathcal{E}$; cp. [15, Proposition 3.2]. Corner-patch and interior-patch elements are isotropic, with $h_K^\parallel \simeq h_K^\perp \simeq h_K$. We further denote by $h_{K,F}^\perp$ the height of $K \in \mathcal{M}_\sigma^{(\ell)}$ in direction perpendicular to $F \in \mathcal{F}_K$, also defined as the corresponding height in the axiparallel element $\widetilde{K} = G_{\mathfrak{p}}^{-1}(K)$.

As in [15, Section 5.1.4], we may assume without loss of generality that $K \in \mathcal{M}_\sigma^{(\ell)}$ can be written in the form

$$K = K^\perp \times K^\parallel = (0, h_K^\parallel)^2 \times (0, h_K^\parallel). \tag{3.6}$$

The subsequent scalings will be crucially used in our analysis.

Lemma 3.3. *Let K be an axiparallel element of the form* (3.6) *and $\Phi_K : \widehat{K} \to K$ the element transformation. For $v : K \to \mathbb{R}$ and $\widehat{v} = v \circ \Phi_K$, we have the scalings:*

(i) $\|v\|^2_{L^2(K)} \simeq (h_K^\perp)^2 h_K^\parallel \|\widehat{v}\|^2_{L^2(\widehat{K})}$.

(ii) *If $h_K^\perp \lesssim h_K^\parallel$, then $\|\nabla u\|^2_{L^2(K)} \lesssim h_K^\parallel \|\widehat{\nabla}\widehat{u}\|^2_{L^2(\widehat{K})}$.*

(iii) *If $f \in \mathcal{F}_K$ is an elemental edge of K with $h_{K,f}^\perp \simeq h_K^\perp$ and $\widehat{f}$ the corresponding reference edge of $\widehat{K}$, then $\|\widehat{v}\|^2_{L^2(\widehat{f})} \simeq \left(h_K^\perp h_K^\parallel\right)^{-1} \|v\|^2_{L^2(f)}$.*

Proof. The following more general scaling property was established in [15, Equation (5.11)]:

$$\|\widehat{\mathsf{D}}_\perp^{\boldsymbol{\alpha}^\perp} \widehat{\mathsf{D}}_\parallel^{\alpha^\parallel} \widehat{v}\|^2_{L^2(\widehat{K})} = \Big(\frac{h_K^\perp}{2}\Big)^{2|\boldsymbol{\alpha}^\perp|-2} \Big(\frac{h_K^\parallel}{2}\Big)^{2\alpha^\parallel - 1} \|\mathsf{D}_\perp^{\boldsymbol{\alpha}^\perp} \mathsf{D}_\parallel^{\alpha^\parallel} v\|^2_{L^2(K)}. \tag{3.7}$$

The L^2-norm scaling in item (i) is an immediate consequence of (3.7). Similarly, we see that

$$\|\mathsf{D}_\perp u\|^2_{L^2(K)} \simeq h_K^{\|}\|\widehat{\mathsf{D}}_\perp \widehat{u}\|^2_{L^2(\widehat{K})}, \quad \|\mathsf{D}_\| u\|^2_{L^2(K)} \simeq (h_K^\perp)^2 (h_K^\|)^{-1}\|\widehat{\mathsf{D}}_\| \widehat{u}\|^2_{L^2(\widehat{K})}.$$

Hence, if $h_K^\perp \lesssim h_K^\|$, item (ii) follows. To show item (iii), we note that $h^\perp_{K,f} \simeq h^\perp_K$ implies that f can be written in the form $f = (0, h_K^\perp) \times (0, h_K^\|)$. Hence, item (iii) follows from a similar L^2-norm scaling argument. □

3.1.7. *Anisotropic Jump Estimate.* Finally, we establish the following anisotropic jump estimate. To state it, we introduce the weighted $H^1(K)$-norm:

$$N_K[v]^2 := \left(h^\perp_{\min,K}\right)^{-2}\|v\|^2_{L^2(K)} + \|\nabla v\|^2_{L^2(K)}, \qquad K \in \mathcal{M}^{(\ell)}_\sigma. \tag{3.8}$$

with $h^\perp_{\min,K} := \min_{F\in\mathcal{F}_K}\{h^\perp_{K,F}\}$. We then consider an interior face $f_{K,K'}$ parallel to a singular edge $\boldsymbol{e}$ and shared by two axiparallel and possibly non-matching hexahedra K, K' of the form $K = K^\perp \times (0, h^\|)$ and $K' = (K')^\perp \times (0, h^\|)$, cp. (3.6). The elements $K^\perp$, $(K')^\perp$ are shape-regular rectangles with $\operatorname{diam}(K^\perp) \simeq \operatorname{diam}((K')^\perp) \simeq h^\perp$, with $h^\perp \lesssim h^\|$.

Lemma 3.4. *In the setting above and for a piecewise smooth function v, we have*

$$(h^\perp)^{-1}\|[\![v]\!]_{f_{K,K'}}\|^2_{L^2(f_{K,K'})} \lesssim N_K[v]^2 + N_{K'}[v]^2. \tag{3.9}$$

Proof. We have $h^\perp_{K,f_{K,K'}} \simeq h^\perp_{K',f_{K,K'}} \simeq h^\perp_{\min,K} \simeq h^\perp_{\min,K'} \simeq h^\perp$. Hence, applying the anisotropic trace inequality from [14, Lemma 4.2] (formulated for axiparallel cuboids and for $t = 2$) yields

$$\begin{aligned}\|[\![v]\!]_{f_{K,K'}}\|^2_{L^2(f_{K,K'})} &\lesssim \|v|_K\|^2_{L^2(f_{K,K'})} + \|v|_{K'}\|^2_{L^2(f_{K,K'})}\\ &\lesssim (h^\perp)^{-1}\left(\|v\|^2_{L^2(K)} + \|v\|^2_{L^2(K')}\right) + h^\perp\left(\|\nabla v\|^2_{L^2(K)} + \|\nabla v\|^2_{L^2(K')}\right).\end{aligned}$$

The bound (3.9) follows. □

3.2. ***hp*-Version Discretizations.** The conforming finite element spaces to be considered here are based on *uniform and isotropic* polynomial degree $p \geq 1$ (throughout $K \in \mathcal{M}$). Unlike in the discontinous Galerkin framework considered in [14, 15], we *do not* consider here hp-spaces with variable and $\mathfrak{s}$-linearly increasing and anisotropic polynomial degree distributions.

More precisely, for a geometric mesh $\mathcal{M}$ satisfying Assumptions 3.1, 3.2 and for the polynomial degree $p \geq 1$, we introduce the hp-version finite element spaces

$$\begin{aligned}V_p(\mathcal{M}) &:= \left\{v \in H^1(\Omega) \,:\, v|_K \in \mathbb{Q}_p(K),\, K \in \mathcal{M}\right\},\\ V_p^0(\mathcal{M}) &:= V_p(\mathcal{M}) \cap H^1_0(\Omega).\end{aligned} \tag{3.10}$$

Here, the local polynomial approximation space $\mathbb{Q}_p(K)$ is defined as follows: first, on the reference element $\widehat{K}$, we introduce the tensor-product polynomial space

$$\mathbb{Q}_p(\widehat{K}) := \operatorname{span}\left\{\,\hat{\boldsymbol{x}}^{\boldsymbol{\alpha}} \,:\, \alpha_i \leq p,\ 1 \leq i \leq 3\,\right\}. \tag{3.11}$$

Then, for an hexahedral element $K \in \mathcal{M}$ with elemental mapping $\Phi_K : \widehat{K} \to K$, we set $\mathbb{Q}_p(K) := \left\{u \in L^2(K) : (u|_K \circ \Phi_K) \in \mathbb{Q}_p(\widehat{K})\right\}$. As compared to discontinuous spaces considered [14, 15], the spaces in (3.10) now feature interelement continuity and essential boundary conditions in the presence of geometric mesh refinements.

If $\mathfrak{M}_\sigma = \{\mathcal{M}_\sigma^{(\ell)}\}_{\ell=1}^\infty$ is now a σ-geometric mesh family, we introduce the following sequence of *hp*-version spaces:

$$V_\sigma^\ell := V_{p_\ell}^0(\mathcal{M}_\sigma^{(\ell)}), \qquad \ell \geq 1, \tag{3.12}$$

with the polynomial degree

$$p_\ell := \max\{3, \lfloor \mu \ell \rfloor\}, \qquad \ell \geq 1, \tag{3.13}$$

for a *proportionality parameter* $\mu > 0$. Note here that, as in [15], we shall always work under the (purely technical) assumption that $p_\ell \geq 3$; cp. Lemma 4.1 below.

Remark 3.5. Due to the possible occurence of irregular faces and edges which arise in geometric refinements of hexahedral meshes, it is a-priori not clear that the spaces (3.10), (3.12) are well-defined. That these definitions, indeed, define proper linear subspaces will also follow from our construction of polynomial trace liftings in Section 5 ahead.

With the definitions (3.12), (3.13) of the *hp*-FE spaces in place, the *hp*-version Galerkin discretization of the variational formulation (2.3) reads as usual:

$$u_\sigma^\ell \in V_\sigma^\ell: \quad a(u_\sigma^\ell, v) = \int_\Omega f v dx \quad \forall v \in V_\sigma^\ell \, . \tag{3.14}$$

For every $\ell \geq 1$, the discrete variational problem (3.14) admits a unique solution $u_\sigma^\ell \in V_\sigma^\ell$ which is quasioptimal: there exists a constant $C > 0$ (depending only on the domain Ω and on the diffusion tensor $\boldsymbol{A}$), such that for all parameters σ, ℓ there holds

$$\|u - u_\sigma^\ell\|_{H^1(\Omega)} \leq C \inf_{v \in V_\sigma^\ell} \|u - v\|_{H^1(\Omega)} \, . \tag{3.15}$$

3.3. **Exponential Convergence.** The quasioptimality (3.15) reduces the proof of our main result, exponential convergence rates for the conforming finite element approximations u_σ^ℓ in (3.14), to bounding the best approximation error of $u \in A_{-1-\boldsymbol{b}}(\Omega)$ in V_σ^ℓ, cp. Proposition 2.2.

Theorem 3.6. *Let $\mathfrak{M}_\sigma = \{\mathcal{M}_\sigma^{(\ell)}\}_{\ell \geq 1}$ be a family of σ-geometric meshes on Ω, and consider the hp-version discretizations based on the sequence V_σ^ℓ of subspaces defined in* (3.12) *with the polynomial degrees p_ℓ specified in* (3.13)*. Then, there exist projectors $\Pi^\ell : M^3_{-1-\boldsymbol{b}}(\Omega) \to V_\sigma^\ell$ such that for every $v \in A_{-1-\boldsymbol{b}}(\Omega) \subset M^3_{-1-\boldsymbol{b}}(\Omega)$, with weights as in* (2.12)*, there exist constants $b, C > 0$ such that, for every $\ell \geq 1$*

$$\left\|v - \Pi^\ell v\right\|_{H^1(\Omega)} \leq C \exp\left(-b\ell\right) \, . \tag{3.16}$$

The constants depend on the subdivision ratio σ, the macro-mesh $\mathcal{M}^0$ with its associated patch maps, $\min \boldsymbol{b} > 0$ (see Remark 2.3), and on the proportionality constant $\mu > 0$ in (3.13)*. They also depend on the function $v \in A_{-1-\boldsymbol{b}}(\Omega)$ through C_v in the analytic regularity estimate* (2.9)*.*

In particular, if the source term $f \in A_{1-\boldsymbol{b}}(\Omega)$ in (2.1) *with weights as in* (2.12) *(and hence $u \in A_{-1-\boldsymbol{b}}(\Omega)$ by Proposition 2.2), then, as $\ell \to \infty$, the hp-version approximations u_σ^ℓ in* (3.14) *converge exponentially:*

$$\left\|u - u_\sigma^\ell\right\|_{H^1(\Omega)} \leq C \exp\left(-b \sqrt[5]{N}\right) \, , \tag{3.17}$$

where the constants $b, C > 0$ are independent of $N = \dim(V_\sigma^\ell)$, the number of degrees of freedom of the hp-FE discretization.

3.4. **Outline of Proof.** We first note that the error bound (3.17) is an immediate consequence of the quasi-optimality property (3.15) and the exponential consistency bound (3.16). Therefore, the proof of Theorem 3.6 will follow from the construction and exponential convergence estimates for the *hp*-version (quasi)interpolants Π^ℓ. These estimates are of independent interest, and the rest of the paper is devoted to their proof, which is structured as follows.

3.4.1. *Reference Patch Projectors.* The *hp*-version projector Π^ℓ in (3.16) will be assembled from corresponding patch projectors $\Pi^\ell_{\mathfrak{p}}$ for $1 \le \mathfrak{p} \le \mathfrak{P}$. To do so, consider the mesh patch $\mathcal{M}_{\mathfrak{p}} = G_{\mathfrak{p}}(\widetilde{\mathcal{M}}_{\mathfrak{p}})$ on $Q_{\mathfrak{p}}$ (where $G_{\mathfrak{p}}$ is understood to be applied elementwise). Then, with the geometric reference mesh patch $\widetilde{\mathcal{M}}_{\mathfrak{p}}$, we associate a *reference patch projector* $\widetilde{\Pi}^\ell_{\mathfrak{p}}$ *on* $\widetilde{\mathcal{M}}_{\mathfrak{p}}$, which, in accordance with the four types of geometric refinements chosen for $\widetilde{\mathcal{M}}_{\mathfrak{p}} \in \widetilde{\mathcal{R}P}$ in (3.1), is taken as one of four types of reference projections

$$\widetilde{\Pi}^{\ell,\mathfrak{t}} \quad \text{on} \quad \widetilde{\mathcal{M}}^{\ell,\mathfrak{t}}_\sigma, \qquad \mathfrak{t} \in \{\boldsymbol{c}, \boldsymbol{e}, \boldsymbol{ce}, \mathrm{int}\}. \tag{3.18}$$

On the physical patch $\mathcal{M}_{\mathfrak{p}}$, the *patch projector* $\Pi^\ell_{\mathfrak{p}}$ is then defined via

$$(\Pi^\ell_{\mathfrak{p}} u)|_{Q_{\mathfrak{p}}} \circ G_{\mathfrak{p}} = \widetilde{\Pi}^\ell_{\mathfrak{p}} (u|_{Q_{\mathfrak{p}}} \circ G_{\mathfrak{p}}). \tag{3.19}$$

The *inter-patch continuity* of the projector Π^ℓ defined patchwise as $\Pi^\ell|_{Q_{\mathfrak{p}}} = \Pi^\ell_{\mathfrak{p}}$ will follow from Assumptions 3.1, 3.2.

3.4.2. *Patchwise Error Bounds.* Then the proof of (3.16) proceeds by bounding

$$\eta_{\mathfrak{p}} := u|_{Q_{\mathfrak{p}}} - \Pi^\ell_{\mathfrak{p}} u|_{Q_{\mathfrak{p}}}, \qquad \mathfrak{p} = 1, \dots, \mathfrak{P}, \tag{3.20}$$

respectively the pull-backs $\widetilde{\eta}_{\mathfrak{p}}$ to the reference patch $\widetilde{Q}$ given by

$$\widetilde{\eta}_{\mathfrak{p}} := \widetilde{u}_{\mathfrak{p}} - \widetilde{\Pi}^\ell_{\mathfrak{p}} \widetilde{u}_{\mathfrak{p}}, \qquad \mathfrak{p} = 1, \dots, \mathfrak{P}, \tag{3.21}$$

where $\widetilde{u}_{\mathfrak{p}} = u|_{Q_{\mathfrak{p}}} \circ G_{\mathfrak{p}}$ is the pull-back of $u|_{Q_{\mathfrak{p}}}$ to the reference patch $\widetilde{Q}$.

To bound (3.20), (3.21), for any set $\mathcal{D}$ of axiparallel elements K, we define

$$\Upsilon_{\mathcal{D}}[v] := \sum_{K \in \mathcal{D}} N_K[v]^2, \quad \text{with } N_K[v] \text{ in (3.8).} \tag{3.22}$$

Lemma 3.7. *For $1 \le \mathfrak{p} \le \mathfrak{P}$, there holds $\Upsilon_{\mathcal{M}_{\mathfrak{p}}}[\eta_{\mathfrak{p}}] \simeq \Upsilon_{\widetilde{\mathcal{M}}_{\mathfrak{p}}}[\widetilde{\eta}_{\mathfrak{p}}]$.*

Proof. This follows from the construction of the patch mesh $\mathcal{M}^0$; cp. also the boundedness properties of the patch maps in [14, Section 3.1]. □

Employing these definitions above in conjunction with Lemma 3.7, we see that the approximation error in (3.16) can be bounded by

$$\|u - \Pi^\ell u\|^2_{H^1(\Omega)} \le \sum_{\mathfrak{p}=1}^{\mathfrak{P}} \Upsilon_{\mathcal{M}_{\mathfrak{p}}}[\eta_{\mathfrak{p}}] \lesssim \sum_{\mathfrak{p}=1}^{\mathfrak{P}} \Upsilon_{\widetilde{\mathcal{M}}_{\mathfrak{p}}}[\widetilde{\eta}_{\mathfrak{p}}]. \tag{3.23}$$

Next, we notice that, up to rotation and orientation, there are four types of reference mesh patches in $\widetilde{\mathcal{RP}}$ in (3.1). Hence, to bound the right-hand side of (3.23), it is enough to provide error estimates for *the four reference cases* and we have

$$\|u - \Pi^\ell u\|^2_{H^1(\Omega)} \le \sum_{\mathfrak{t} \in \{\boldsymbol{c}, \boldsymbol{e}, \boldsymbol{ce}, \mathrm{int}\}} \Upsilon_{\widetilde{\mathcal{M}}^{\ell,\mathfrak{t}}_\sigma}[\widetilde{\eta}_{\mathfrak{t}}], \tag{3.24}$$

with $\widetilde{\eta}_{\mathfrak{t}} := \widetilde{u} - \widetilde{\Pi}^{\ell,\mathfrak{t}}\widetilde{u}$ for the pull-back $\widetilde{u}$ of u to $\widetilde{Q}$. We observe that, due to the patch maps being affine with (up to rotations and reflections) diagonal Jacobian, the analytic regularity (2.11) of solutions $u \in H^1_0(\Omega)$ to (2.1)–(2.2) is preserved under pull-back into the reference patch coordinates on $\widetilde{Q}$. That is, we may assume that $\widetilde{u} \in A_{-1-\boldsymbol{b}_{\mathfrak{t}}}(\widetilde{Q})$, with *reference weight vectors* $\boldsymbol{b}_{\mathfrak{t}}$ depending on the type $\mathfrak{t} \in \{\boldsymbol{c}, \boldsymbol{e}, \boldsymbol{ce}, \mathrm{int}\}$ as will be detailed in Section 4.4 below.

3.4.3. *hp-Base Projectors.* To define the reference patch projectors with exponential error bounds (3.16) on the geometric reference mesh patches $\widetilde{\mathcal{M}}^{\ell,\mathfrak{t}}$, we will proceed in two stages: first, we introduce *base hp-projectors*

$$\widetilde{\pi}_b^{\ell,\mathfrak{t}} \quad \text{on} \quad \widetilde{\mathcal{M}}_\sigma^{\ell,\mathfrak{t}}, \qquad \mathfrak{t} \in \{\boldsymbol{c}, \boldsymbol{e}, \boldsymbol{ce}, \mathrm{int}\}, \tag{3.25}$$

with exponential approximation bounds under the analytic regularity (2.9). As base projectors, we choose the non-conforming and tensorized projectors constructed in [15] and well-defined for $\widetilde{u} \in M^3_{-1-\boldsymbol{b}_{\mathfrak{t}}}(\widetilde{Q})$. The exponential convergence estimates in broken Sobolev norms established in [15, Section 5] apply directly on each mesh patch. We have

$$\mathfrak{t} \in \{\boldsymbol{c}, \boldsymbol{e}, \boldsymbol{ce}, \mathrm{int}\},\ \widetilde{u} \in A_{-1-\boldsymbol{b}_{\mathfrak{t}}}(\widetilde{Q}): \quad \Upsilon_{\widetilde{\mathcal{M}}_\sigma^{\ell,\mathfrak{t}}}[\widetilde{u} - \widetilde{\pi}_b^{\ell,\mathfrak{t}}\widetilde{u}] \le C\exp(-2b\ell), \tag{3.26}$$

with constants $b, C > 0$ independent of ℓ.

3.4.4. *Trace Liftings.* The base approximations $\widetilde{\pi}_b^{\ell,\mathfrak{t}}$ are nodally exact, continuous over matching faces and regular vertices and satisfy the homogeneous essential boundary conditions exactly (on corresponding patch boundary faces). The base approximations $\widetilde{\pi}_b^{\ell,\mathfrak{t}}$ are in general discontinuous across irregular inter-element faces, edges and vertices. To ensure *inner-patch continuity* (necessary for H^1-conformity) in geometrically refined patches, the second step of our proof therefore consists in constructing *jump lifting operators* $\widetilde{\mathcal{L}}_{\mathfrak{t}}$, $\mathfrak{t} \in \{\boldsymbol{c}, \boldsymbol{e}, \boldsymbol{ce}\}$, which remove the polynomial jumps in the base *hp*-projectors while preserving their exponential convergence estimates and the essential boundary conditions. These polynomial jump-liftings will be introduced and their stability will be analyzed in Section 5. The resulting *reference patch hp-projectors*

$$\widetilde{\Pi}^{\ell,\mathfrak{t}} := \widetilde{\pi}_b^{\ell,\mathfrak{t}} + \widetilde{\mathcal{L}}_{\mathfrak{t}}, \qquad \mathfrak{t} \in \{\boldsymbol{c}, \boldsymbol{e}, \boldsymbol{ce}\}, \tag{3.27}$$

then yield *continuous*, piecewise polynomial approximations, without disrupting the exponential convergence bounds in (3.26). In fact, we establish the following stability estimate.

Proposition 3.8. *For* $\mathfrak{t} \in \{\boldsymbol{c}, \boldsymbol{e}, \boldsymbol{ce}, \mathrm{int}\}$ *and* $\widetilde{u} \in M^3_{-1-\boldsymbol{b}_{\mathfrak{t}}}(\widetilde{Q})$, *we let* $\widetilde{\eta}_{\mathfrak{t}} = \widetilde{u} - \widetilde{\Pi}^{\ell,\mathfrak{t}}\widetilde{u}$ *and* $\widetilde{\eta}_{b,\mathfrak{t}} = \widetilde{u} - \widetilde{\pi}_b^{\ell,\mathfrak{t}}\widetilde{u}$. *Then we have*

$$\Upsilon_{\widetilde{\mathcal{M}}_\sigma^{\ell,\mathfrak{t}}}[\widetilde{\eta}_{\mathfrak{t}}] \lesssim p^{18}\Upsilon_{\widetilde{\mathcal{M}}_\sigma^{\ell,\mathfrak{t}}}[\widetilde{\eta}_{b,\mathfrak{t}}], \tag{3.28}$$

for any $\mathfrak{t} \in \{\boldsymbol{c}, \boldsymbol{e}, \boldsymbol{ce}, \mathrm{int}\}$.

The bound (3.28) will be established separately for each reference patch.

Conclusion of the Proof. The constructions of the reference patch hp-projectors lead to a family $\{\Pi^\ell\}_{\ell\geq 1}$ of globally conforming, piecewise polynomial and bounded hp-version (quasi)interpolants $\Pi^\ell : M^3_{-1-\boldsymbol{b}}(\Omega) \to V^\ell_\sigma$. They satisfy the homogeneous essential boundary conditions, and, by (3.24) and Proposition 3.8, converge at the same rates as the base projectors $\widetilde{\pi}^{\ell,\mathfrak{t}}_b$ on each of the reference mesh patches $\widetilde{\mathcal{M}}^{\ell,\mathfrak{t}}_\sigma$, up to an algebraic loss in the polynomial degree p:

$$\|u-\Pi^\ell u\|^2_{H^1(\Omega)} \lesssim p^{18} \sum_{\mathfrak{t}\in\{\boldsymbol{c},\boldsymbol{e},\boldsymbol{ce},\mathrm{int}\}} \Upsilon_{\widetilde{\mathcal{M}}^{\ell,\mathfrak{t}}_\sigma}[\widetilde{\eta}_{b,\mathfrak{t}}]\,. \tag{3.29}$$

If now $u \in A_{-1-\boldsymbol{b}}(\Omega)$ as in the statement of Theorem 3.6 and since the patch maps $G_{\mathfrak{p}}$ are *orthogonal* affine, the definition (2.8) of the $M^m_{-1-\boldsymbol{b}}(\Omega)$-seminorms and the analytic estimates (2.9) imply that the pull-back $\widetilde{u}$ of $u|_{Q_{\mathfrak{p}}}$ to $\widetilde{Q}$ belongs to one of the analytic reference classes $A_{1-\boldsymbol{b}_{\mathfrak{t}}}(\widetilde{Q})$, $\mathfrak{t}\in\{\boldsymbol{c},\boldsymbol{e},\boldsymbol{ce},\mathrm{int}\}$. The proof of (3.16) then follows from (3.29) and the exponential convergence rates of the base interpolants in (3.26). The algebraic loss in p in (3.29) is absorbed by suitably adjusting the constants b, C in the exponential convergence bounds.

Remark 3.9. The exponential error bounds for the hp-base interpolants in this section are based on the *patchwise analytic regularity* assumptions in (3.26) of the solution $\widetilde{u}$ *in local, patch coordinates*, which are satisfied in the axi-parallel case considered here. Our construction of exponentially consistent, H^1-conforming hp-interpolants can be readily extended to curvilinear patches. The exponential convergence bounds in Theorem 3.6 hold, provided that the pull-backs $\widetilde{u}$ of the solution u on the patches belongs to one of these regularity classes and the patch-maps satisfy the inter-patch compatibility Assumption 3.1.

Remark 3.10. The relatively large, algebraic loss in p in (3.28), (3.29) is an upper bound. It is a consequence of our trace liftings being taken as (bi)linear functions, rather than as polynomials of degree p (which is compatible with the constant polynomial degree p). By using polynomial trace-liftings with "minimal energy", as constructed in [18] or [17, Lemma 9.1], these exponents can be reduced.

It remains to review the definitions of the base projectors in (3.25) and the bounds (3.26) from [15, Section 5]. This will be done in Section 4. Finally, in Section 5, we present the construction and analysis of the polynomial jump liftings in (3.27) and prove Proposition 3.8.

4. Base Projectors and Exponential Convergence

In this section, we specify the non-conforming and tensorized hp-version base projectors in (3.25) and review their exponential convergence properties (3.26).

4.1. Tensorization of Univariate hp-Projectors.

We begin by introducing the univariate hp-approximation operators from [5]. To that end, let $\widehat{I}=(-1,1)$ denote the unit interval. For $p\geq 0$ we denote by $\widehat{\pi}_{p,0} : L^2(\widehat{I}) \to \mathbb{P}_p(\widehat{I})$ the $L^2(\widehat{I})$-projection. Univariate and C^1-conforming, univariate spectral projectors $\widehat{\pi}_{p,2}$ have been constructed in [5, Section 8].

Lemma 4.1. *For $p\geq 3$, there is a unique projector $\widehat{\pi}_{p,2} : H^2(\widehat{I}) \to \mathbb{P}_p(\widehat{I})$ that satisfies $(\widehat{\pi}_{p,2}v)^{(2)} = \widehat{\pi}_{p-2,0}(v^{(2)})$ and $(\widehat{\pi}_{p,k}v)^{(j)}(\pm 1) = v^{(j)}(\pm 1)$ for $j=0,1$.*

The projector $\widehat{\pi}_{p,2}$ is stable in $H^2(\widehat{I})$, cp. [5, Proposition 8.4]. Moreover, *hp*-version approximation properties of $\widehat{\pi}_{p,2}$ were established in [5, Theorem 8.3].

Next, we tensorize the one-dimensional projectors $\widehat{\pi}_{p,2}$. We follow [15, Section 5.1.2], and let $\widehat{I}^d = \widehat{I} \times \cdots \times \widehat{I}$ for $d \geq 2$. Coordinates in $\widehat{I}^d$ are written as $\widehat{\boldsymbol{x}} = (\widehat{x}_1, \ldots, \widehat{x}_d)$. On $\widehat{I}^d$ we introduce the tensor-product Sobolev space $H^2_{\mathrm{mix}}(\widehat{I}^d) := \bigotimes_{i=1}^d H^2(\widehat{I})$. Similarly, we set $\mathbb{Q}_p(\widehat{I}^d) := \bigotimes_{i=1}^d \mathbb{P}_p(\widehat{I})$, where $\mathbb{P}_p(\widehat{I})$ denotes the univariate polynomials on $\widehat{I}$ of degree less or equal than p. On $\widehat{I}^d$ and for $p \geq 3$, we now define the tensorized interpolation operator

$$\widehat{\pi}^d_{p,2} = \bigotimes_{i=1}^d \widehat{\pi}^{(i)}_{p,2}, \tag{4.1}$$

where $\widehat{\pi}^{(i)}_{p,2}$ denotes the univariate projector defined in Lemma 4.1, acting in the variable $\widehat{x}_i$. The projector is well-defined and stable on $H^2_{\mathrm{mix}}(\widehat{I}^d)$; see [15, Proposition 5.3]. For corresponding *hp*-approximation results, we refer to [15, Proposition 5.4].

In the discussion of interelement continuity of $\pi^d_{k,2}$, a crucial role is taken by the following property. It implies that traces of the tensorized interpolant and tensor projection commute. It is an immediate consequence of the defining properties of the univariate projector in Lemma 4.1.

Proposition 4.2. *For $d \geq 2$ and $1 \leq j \leq d$, there holds*

$$\Big(\widehat{\pi}^d_{p,2} v\Big)|_{\widehat{x}_j = \pm 1} = \Big(\bigotimes_{1 \leq i \neq j \leq d} \widehat{\pi}^{(i)}_{p,2} \Big)(v(\cdot, \widehat{x}_j = \pm 1)). \tag{4.2}$$

Remark 4.3. Observe that (4.2) is recursive: one may take repeated traces with respect to a sequence $\{\widehat{x}_{j(k)}\}_{k \geq 1}$ of coordinates, with $j(k) \neq j(k')$ for $k' \neq k$. In particular, by taking the traces twice, we see that $\big(\widehat{\pi}^3_{p,2} v\big)\,|_{\widehat{x}_i = \pm 1, \widehat{x}_j = \pm 1}$ corresponds to the univariate projections $\widehat{\pi}_{p,2}$ onto polynomials on the edges $\{\widehat{x}_i = \pm 1\} \cap \{\widehat{x}_j = \pm 1\}$, with $i \neq j$. Iterating this argument d times, we obtain nodal exactness of $\widehat{\pi}^d_{p,2} v$ in the vertices of $\widehat{I}^d$ follows: for $v \in H^2_{\mathrm{mix}}(\widehat{I}^d) \subset C^0(\overline{\widehat{I}^d})$, we have

$$v(Q) = (\widehat{\pi}^d_{p,k} v)(Q) \quad \text{for all vertices } Q \text{ of } \widehat{I}^d. \tag{4.3}$$

4.2. **Continuity Properties.** For an axiparallel hexahedron K and for a function $v : K \to \mathbb{R}$ with $\widehat{v} = v \circ \Phi_K \in H^2_{\mathrm{mix}}(\widehat{K})$, we now define the elemental interpolant $(\pi^3_{p,2} v)|_K \in \mathbb{Q}_p(K)$ in a standard way by setting

$$\big[\pi^3_{p,2} v\big]\,|_K \circ \Phi_K := \widehat{\pi}^3_{p,2}\,[v \circ \Phi_K]\,, \tag{4.4}$$

with $\widehat{\pi}^3_{p,2}$ the reference interpolant (4.1) and $\Phi_K : \widehat{K} \to K$ the elemental mapping. Analogously, we denote by $\pi^{(i)}_{p,2}|_K$ the univariate projector $\widehat{\pi}_{p,2}$ applied in direction x_i on element K.

Lemma 4.4. *The following properties hold.*

(i) *Let K, K' be two axiparallel hexahedra, $F_{K,K'} = \mathrm{int}(\partial K \cap \partial K')$ a regularly matching face, cp. Section 3.1, and assume that $v \in C^1(\overline{K} \cup \overline{K'})$. Then*

$$\big(\pi^3_{p,2}|_K v|_K\big)\,|_{\overline{F}} = \big(\pi^3_{p,2}|_{K'} v|_{K'}\big)\,|_{\overline{F}}, \tag{4.5}$$

implying that the projector $\pi^3_{p,2}$ yields a piecewise polynomial approximation which is continuous across a regular face F.

(ii) *Let K be an axiparallel hexahedron, and assume that $v \in C^1(\overline{K})$. If $v|_F \equiv 0$,*

$$\forall F \in \mathcal{F}_K : \quad \left(\pi^3_{p,2}|_K v|_K\right)|_{\overline{F}} \equiv 0, \tag{4.6}$$

implying that the projector $\pi^3_{p,2}$ preserves homogeneous Dirichlet boundary conditions on the face F. Additionally, if $\overline{E} \subset \overline{F}$ is an elemental edge of K (i.e., $E \in \mathcal{E}_K$), then

$$\left(\left(\pi^3_{p,2}|_K v|_K\right)|_{\overline{F}}\right)|_{\overline{E}} \equiv 0, \tag{4.7}$$

Proof. These are immediate consequences of (4.3) and Remark 4.3. □

4.3. **Definition of the Base Projectors.** Analogously to (3.4), we split the geometrically refined reference mesh patches into interior elements and terminal layer elements, with respect to the singular set on $\widetilde{Q}$ induced via the patch maps by the corresponding singular corners and edges on Ω:

$$\widetilde{\mathcal{M}}^{\ell,\mathfrak{t}}_\sigma := \widetilde{\mathfrak{O}}^{\ell,\mathfrak{t}}_\sigma \,\dot\cup\, \widetilde{\mathfrak{T}}^{\ell,\mathfrak{t}}_\sigma, \qquad \mathfrak{t} \in \{\boldsymbol{c}, \boldsymbol{e}, \boldsymbol{ce}\}. \tag{4.8}$$

For a sufficiently smooth function $\widetilde{u} : \widetilde{Q} \to \mathbb{R}$ and the polynomial degree p_ℓ in (3.13), we then define the non-conforming reference base interpolant $\widetilde{\pi}^{\ell,\mathfrak{t}}_b \widetilde{u} \in V_{p_\ell}(\widetilde{\mathcal{M}}^{\ell,\mathfrak{t}}_\sigma)$ elementwise as

$$\pi^{\ell,\mathfrak{t}}_b|_{\widetilde{K}} \widetilde{u}|_{\widetilde{K}} := \begin{cases} \pi^3_{p,2}|_{\widetilde{K}} \widetilde{u}|_{\widetilde{K}} & \mathfrak{t} = \text{int and } \widetilde{K} \in \widetilde{\mathcal{M}}^{\ell,\text{int}}_\sigma, \\ \pi^3_{p,2}|_{\widetilde{K}} \widetilde{u}|_{\widetilde{K}} & \mathfrak{t} \in \{\boldsymbol{c}, \boldsymbol{e}, \boldsymbol{ce}\} \text{ and } \widetilde{K} \in \widetilde{\mathfrak{O}}^{\ell,\mathfrak{t}}_\sigma, \\ 0 & \mathfrak{t} \in \{\boldsymbol{c}, \boldsymbol{e}, \boldsymbol{ce}\} \text{ and } \widetilde{K} \in \widetilde{\mathfrak{T}}^{\ell,\mathfrak{t}}_\sigma. \end{cases} \tag{4.9}$$

This interpolant is equal to the tensorized interpolant $\pi^3_{p,2}|_{\widetilde{K}}$ in (4.4) on all axiparallel elements away from singularities and equal to zero on all terminal layer elements (in the respective reference patches). The base interpolants are well-defined for functions in $M^3_{-1-\boldsymbol{b}_\mathfrak{t}}(\widetilde{Q})$, for the reference patch weights $\boldsymbol{b}_\mathfrak{t}$.

Remark 4.5. In view of Lemma 4.4, the base interpolants $\widetilde{\pi}^{\ell,\mathfrak{t}}_b \widetilde{u}$ in (4.9) are conforming over regularly matching faces within the reference mesh patch $\widetilde{\mathcal{M}}^{\ell,\mathfrak{t}}_\sigma$ and satisfy homogeneous boundary conditions on reference patch faces corresponding to boundary faces of a geometric mesh $\mathcal{M}$ on Ω. However, $\widetilde{\pi}^{\ell,\mathfrak{t}}_b \widetilde{u}$ is generally discontinuous over irregular faces within a reference mesh patch, as well as at the boundary of the terminal layers. These discontinuities will be suitably lifted in Section 5 ahead.

4.4. **Exponential Convergence on Reference Mesh Patches.** Next, we review the exponential convergence results from [15] for the reference base projectors in (4.9) on the reference mesh patches. Throughout, we assume $u \in A_{-1-\boldsymbol{b}}(\Omega)$ as in Theorem 3.6.

4.4.1. *Interior Patch $\widetilde{\mathcal{M}}^{\ell,\text{int}}_\sigma$.* Interior patches $\mathcal{M}_\mathfrak{p} = G_\mathfrak{p}(\widetilde{\mathcal{M}}^{\ell,\text{int}}_\sigma)$ consist of a fixed regular collection of axiparallel, hexahedral elements which do not abut at the singular set $\mathcal{S}$. That is, the distance functions $r_{\boldsymbol{e}}$, $r_{\boldsymbol{c}}$ and $\rho_{\boldsymbol{ce}}$ in (2.5) are bounded away from zero by an absolute distance. The analytic regularity (2.9) and the analyticity of the (affine) patch maps implies that

$$\|\widetilde{u}\|^2_{H^m(\widetilde{Q})} \le C^{2(m+1)} \Gamma(m+1)^2, \qquad m \in \mathbb{N}_0, \tag{4.10}$$

where $\widetilde{u}$ denotes the pull-back of u to the reference patch $\widetilde{Q}$, and $C > 1$ is a constant possibly different from C_u in (2.9). By proceeding as in [15, Proposition 5.10], we obtain the following exponential bound.

Proposition 4.6. *Let $\widetilde{u}$ satisfy the regularity assumption* (4.10)*. Consider the base projector $\widetilde{\pi}_b^{\ell,\mathrm{int}}\widetilde{u} \in V_{p_\ell}(\widetilde{\mathcal{M}}_\sigma^{\ell,\mathrm{int}})$ in* (4.9) *with polynomial degrees $p_\ell \simeq \ell$ as in* (3.13)*. Then, as $\ell \to \infty$, we have the error bound*

$$\Upsilon_{\widetilde{\mathcal{M}}_\sigma^{\ell,\mathrm{int}}}[\widetilde{u} - \widetilde{\pi}_b^{\ell,\mathrm{int}}\widetilde{u}] \le C\exp(-2b\ell)\ ,$$

with constants $b, C > 0$ independent of ℓ.

Corner Patch $\widetilde{\mathcal{M}}_\sigma^{\ell,\boldsymbol{c}}$. In the reference corner mesh $\widetilde{\mathcal{M}}_\sigma^{\ell,\boldsymbol{c}}$ on $\widetilde{Q}$, we assume that the pull-back $\widetilde{u}$ of the function u under $G_{\mathfrak{p}}$ satisfies

$$\sum_{|\boldsymbol{\alpha}|=m} \|r_{\boldsymbol{c}}^{-1-b_{\boldsymbol{c}}+|\boldsymbol{\alpha}|}\widetilde{\mathsf{D}}^{\boldsymbol{\alpha}}\widetilde{u}\|_{L^2(\widetilde{Q})}^2 \le C^{2(m+1)}\Gamma(m+1)^2, \qquad m \in \mathbb{N}_0, \tag{4.11}$$

where $r_{\boldsymbol{c}}$ is the distance to a corner of $\widetilde{Q}$, cp. Figure 1 (left), and $b_{\boldsymbol{c}} \in (0,1)$ a corner weight as in (2.12).

Proposition 4.7. *Let $\widetilde{u}$ satisfy the regularity assumption* (4.11)*. Consider the base projector $\widetilde{\pi}_b^{\ell,\boldsymbol{c}}\widetilde{u} \in V_{p_\ell}(\widetilde{\mathcal{M}}_\sigma^{\ell,\boldsymbol{c}})$ in* (4.9) *with polynomial degrees $p_\ell \simeq \ell$ as in* (3.13)*. Then, as $\ell \to \infty$, we have the error bound*

$$\Upsilon_{\widetilde{\mathcal{M}}_\sigma^{\ell,c}}[\widetilde{u} - \widetilde{\pi}_b^{\ell,\boldsymbol{c}}\widetilde{u}] \le C\exp(-2b\ell),\ .$$

with constants $b, C > 0$ independent of ℓ.

Proof. From (4.8), $\widetilde{\mathcal{M}}_\sigma^{\ell,\boldsymbol{c}} = \widetilde{\mathfrak{O}}_\sigma^{\ell,\boldsymbol{c}} \dot\cup \widetilde{\mathfrak{T}}_\sigma^{\ell,\boldsymbol{c}}$. On $\widetilde{\mathfrak{O}}_\sigma^{\ell,\boldsymbol{c}}$, exponential convergence follows from [15, Proposition 5.13]. On the mesh $\widetilde{\mathfrak{T}}_\sigma^{\ell,\boldsymbol{c}}$, the exponential bound results from [15, Proposition 5.21]. □

Edge Patch $\widetilde{\mathcal{M}}_\sigma^{\ell,\boldsymbol{e}}$. For the reference edge patch $\widetilde{\mathcal{M}}_\sigma^{\ell,\boldsymbol{e}}$ on $\widetilde{Q}$, we analogously shall assume that

$$\sum_{|\boldsymbol{\alpha}|=m} \|r_{\boldsymbol{e}}^{-1-b_{\boldsymbol{e}}+|\boldsymbol{\alpha}^\perp|}\widetilde{\mathsf{D}}^{\boldsymbol{\alpha}}\widetilde{u}\|_{L^2(\widetilde{Q})}^2 \le C^{2(m+1)}\Gamma(m+1)^2, \qquad m \in \mathbb{N}_0, \tag{4.12}$$

where $r_{\boldsymbol{e}}$ is the distance to an edge of $\widetilde{Q}$, as indicated in boldface in Figure 1 (middle), and $b_{\boldsymbol{e}} \in (0,1)$ an edge weight as in (2.12).

Proposition 4.8. *Let $\widetilde{u}$ satisfy the regularity assumption* (4.12)*. Consider the base projector $\widetilde{\pi}_b^{\ell,\boldsymbol{e}}\widetilde{u} \in V_{p_\ell}(\widetilde{\mathcal{M}}_\sigma^{\ell,\boldsymbol{e}})$ in* (4.9) *with polynomial degrees $p_\ell \simeq \ell$ as in* (3.13)*. Then, as $\ell \to \infty$, we have the error bound*

$$\Upsilon_{\widetilde{\mathcal{M}}_\sigma^{\ell,\boldsymbol{e}}}[\widetilde{u} - \widetilde{\pi}_b^{\ell,\boldsymbol{e}}\widetilde{u}] \le C\exp(-2b\ell)\ .$$

with constants $b, C > 0$ independent of ℓ.

Proof. This is a consequence of [15, Proposition 5.15] and [15, Proposition 5.22]. □

4.4.2. *Corner-edge Patch* $\widetilde{\mathcal{M}}_\sigma^{\ell,\boldsymbol{ce}}$. Finally, we consider the reference corner-edge mesh patch $\widetilde{\mathcal{M}}_\sigma^{\ell,\boldsymbol{ce}}$ on $\widetilde{Q}$. By superposition as in [15], we may restrict ourselves to the case of single corner $\boldsymbol{c}$ with a single edge $\boldsymbol{e} \in \mathcal{E}_{\boldsymbol{c}}$. We assume the corner-edge patch regularity

$$\sum_{|\boldsymbol{\alpha}|=m} \|r_{\boldsymbol{c}}^{-1-b_{\boldsymbol{c}}+|\boldsymbol{\alpha}|}\rho_{\boldsymbol{ce}}^{-1-b_{\boldsymbol{e}}+|\boldsymbol{\alpha}^\perp|}\widetilde{\mathsf{D}}^{\boldsymbol{\alpha}}\widetilde{u}\|_{L^2(\widetilde{Q})}^2 \leq C^{2(m+1)}\Gamma(m+1)^2, \quad m \in \mathbb{N}_0, \tag{4.13}$$

where $r_{\boldsymbol{c}}$ and $\rho_{\boldsymbol{ce}}$ are the distances to the corner-edge pair on $\widetilde{Q}$ formed by $\boldsymbol{c}$ and $\boldsymbol{e}$, as indicated in Figure 1 (right). The weights $b_{\boldsymbol{c}}, b_{\boldsymbol{e}} \in (0,1)$ are as in (2.12).

Proposition 4.9. *Let $\widetilde{u}$ satisfy the regularity assumption* (4.13)*. Consider the base projector $\widetilde{\pi}_b^{\ell,\boldsymbol{ce}}\widetilde{u} \in V_{p_\ell}(\widetilde{\mathcal{M}}_\sigma^{\ell,\boldsymbol{ce}})$ in* (4.9) *with polynomial degrees $p_\ell \simeq \ell$ as in* (3.13)*. Then, as $\ell \to \infty$, we have the error bound*

$$\Upsilon_{\widetilde{\mathcal{M}}_\sigma^{\ell,\boldsymbol{ce}}}[\widetilde{u} - \widetilde{\pi}_b^{\ell,\boldsymbol{ce}}\widetilde{u}] \leq C\exp(-2b\ell)\,,$$

with constants $b, C > 0$ independent of ℓ.

Proof. This follows from [15, Proposition 5.17] and [15, Proposition 5.23]. □

5. Polynomial Trace Liftings

In this section, we construct the H^1-conforming reference patch projectors $\widetilde{\Pi}^{\ell,\mathfrak{t}} = \widetilde{\pi}_b^{\ell,\mathfrak{t}} + \widetilde{\mathcal{L}}_{\mathfrak{t}}$ in (3.18), (3.27), by modifying the base projectors $\widetilde{\pi}_b^{\ell,\mathfrak{t}}$ with the introduction of suitable polynomial trace liftings $\widetilde{\mathcal{L}}_{\mathfrak{t}}$ over irregular edges and/or irregular faces. We then prove Proposition 3.8 by establishing the bound (3.28) separately for each reference mesh patch. To that end, we simply write $\pi_b := \widetilde{\pi}_b^{\ell,\mathfrak{t}}$ for the base *hp*-projector in (4.9) on the respective reference mesh patch $\widetilde{\mathcal{M}}_\sigma^{\ell,\mathfrak{t}}$, $\mathfrak{t} \in \{\boldsymbol{c}, \boldsymbol{e}, \boldsymbol{ce}, \mathrm{int}\}$, and $\Pi := \widetilde{\Pi}^{\ell,\mathfrak{t}}$ for the resulting patch projector. When clear from the context, we will omit "tildas" to denote quantities on reference patches, and, for a generic patch function $u \in M^3_{-1-\boldsymbol{b}_{\mathfrak{t}}}(\widetilde{Q})$, we use the notation

$$\eta = u - \Pi u, \qquad \eta_b = u - \pi_b u, \tag{5.1}$$

5.1. **Interior Patch $\widetilde{\mathcal{M}}_\sigma^{\ell,\mathrm{int}}$.** For the interior reference mesh patch $\widetilde{\mathcal{M}}_\sigma^{\ell,\mathrm{int}}$, we take

$$\Pi u := \pi_b u \quad \text{on } \widetilde{\mathcal{M}}_\sigma^{\ell,\mathrm{int}}, \tag{5.2}$$

Since $\widetilde{\mathcal{M}}_\sigma^{\ell,\mathrm{int}}$ contains finitely many regular refinements, Πu in (5.2) yields a conforming piecewise polynomial approximation over the patch $\widetilde{\mathcal{M}}_\sigma^{\ell,\mathrm{int}}$, cp. Lemma 4.4 and Assumptions 3.1, 3.2. No further liftings are required, and the bound (3.28) over $\widetilde{\mathcal{M}}_\sigma^{\ell,\mathrm{int}}$ holds trivially and without any loss in p.

Proposition 5.1. *We have $\Upsilon_{\widetilde{\mathcal{M}}_\sigma^{\ell,\mathrm{int}}}[\eta] \lesssim \Upsilon_{\widetilde{\mathcal{M}}_\sigma^{\ell,\mathrm{int}}}[\eta_b]$.*

5.2. **Edge Patch $\widetilde{\mathcal{M}}_\sigma^{\ell,\boldsymbol{e}}$.** Next, we analyze the reference edge patch $\widetilde{\mathcal{M}}_\sigma^{\ell,\boldsymbol{e}}$, where irregular faces across arise due to irregular geometric refinements perpendicular to edges, as illustrated in Figure 1 (middle). As the edge-patch analysis will be a building block also for the corner-edge case, we consider here a more general edge patch $\widetilde{\mathcal{M}}_\sigma^{\ell,\boldsymbol{e}}$ whose edge-parallel size is determined by the parameter $h^\parallel$ (not necessarily of order one). Our estimates will then be made explicit in $h^\parallel$. According to (4.8), we write $\widetilde{\mathcal{M}}_\sigma^{\ell,\boldsymbol{e}} = \widetilde{\mathfrak{O}}_\sigma^{\ell,\boldsymbol{e}} \dot\cup \widetilde{\mathfrak{T}}_\sigma^{\ell,\boldsymbol{e}}$ and consider the two submeshes separately.

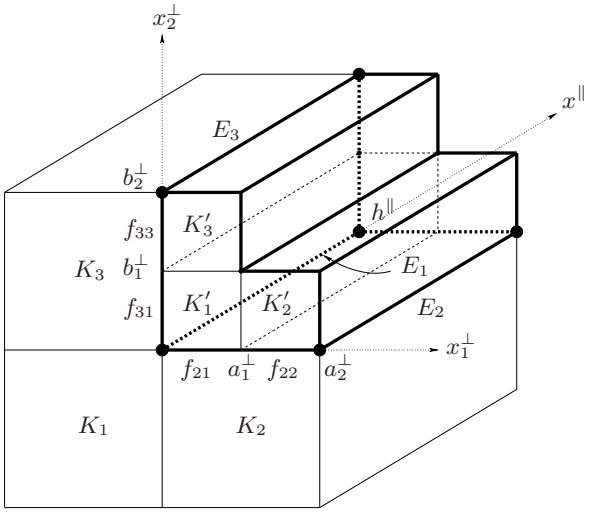

FIGURE 2. Interface between layers $\widetilde{\mathfrak{L}}_\sigma^{\ell'-1,\boldsymbol{e}} = \{K_1, K_2, K_3\}$ and $\widetilde{\mathfrak{L}}_\sigma^{\ell',\boldsymbol{e}} = \{K_1', K_2', K_3'\}$ for $\sigma = 0.5$ and length parameters $h^\parallel$, $a_1^\perp, a_2^\perp$, $b_1^\perp, b_2^\perp$. The irregular faces $f_{21}, f_{22}, f_{31}, f_{33}$ are illustrated.

5.2.1. *Interior Elements in* $\widetilde{\mathfrak{O}}_\sigma^{\ell,\boldsymbol{e}}$. By (3.5), the interior mesh $\widetilde{\mathfrak{O}}_\sigma^{\ell,\boldsymbol{e}}$ can be partitioned into ℓ layers as $\widetilde{\mathfrak{O}}_\sigma^{\ell,\boldsymbol{e}} = \dot\cup_{\ell'=0}^{\ell-1} \widetilde{\mathfrak{L}}_\sigma^{\ell',\boldsymbol{e}}$. By Lemma 4.4 and Remark 4.5, the base projector $\pi_b u$ is continuous over elements within each layer ℓ', and satisfies the homogeneous boundary conditions on appropriate patch boundary faces. For $1 \le \ell' \le \ell - 1$, we thus need to introduce trace liftings on the interface of the two adjacent mesh layers $\widetilde{\mathfrak{L}}_\sigma^{\ell'-1,\boldsymbol{e}} = \{K_1, K_2, K_3\}$ and $\widetilde{\mathfrak{L}}_\sigma^{\ell',\boldsymbol{e}} = \{K_1', K_2', K_3'\}$ as illustrated in Figure 2. In the coordinate system there, the singular edge $\boldsymbol{e}$ on the patch corresponds to $\boldsymbol{e} = \{\boldsymbol{x} = (\boldsymbol{x}^\perp, x^\parallel) : x_1^\perp = a_2^\perp, x_2^\perp = b_2^\perp, x^\parallel \in e^\parallel\}$, with $e^\parallel := (0, h^\parallel)$. As in (3.6), we write the elements in the product form

$$K_i = K_i^\perp \times e^\parallel, \qquad K_i' = (K_i')^\perp \times e^\parallel,$$

where $K_i^\perp$ and $(K_i')^\perp$ are shape-regular and axiparallel rectangles of diameters $\operatorname{diam}(K_i^\perp) \simeq h^\perp$, with $h^\perp \lesssim h^\parallel$. We use the notation $f_{ij} := f_{K_i,K_j'} = \operatorname{int}(\partial K_i \cap \partial K_j')$, and note that the faces $f_{21}, f_{22}, f_{31}, f_{33}$ are irregular, cp. Figure 2. We further set $f_{ij}' := f_{K_i',K_j'} = \operatorname{int}(\partial K_i' \cap \partial K_j')$, and observe that f_{12}' and f_{13}' match regularly. As indicated in Figure 2, the precise locations of the elements, faces and edges in each layer are determined by the length parameters $a_1^\perp, a_2^\perp$ and $b_1^\perp, b_2^\perp$, which do not change from layer to layer. Finally, we note that $h_{\min,K_i}^\perp \simeq h_{\min,K_i'}^\perp \simeq h^\perp$. We then consider the polynomial face jumps

$$[\![\pi_b u]\!]_{f_{ij}} = [\![\pi_b u]\!]_{f_{K_i,K_j'}} = \big(\pi_b|_{K_i} u|_{K_i} - \pi_b|_{K_j'} u|_{K_j'}\big)|_{f_{ij}}\,. \tag{5.3}$$

Similarly, we denote the jumps across f_{ij}' by $[\![\pi_b u]\!]_{f_{ij}'} := [\![\pi_b u]\!]_{f_{K_i',K_j'}}$.

Remark 5.2. The jumps (5.3) have a natural tensor-product structure. To describe it, we write $f_{ij} := e_{ij}^\perp \times e^\parallel$. The tensor-product definitions (4.1), (4.4) imply $\pi_b|_K = \pi_b^\parallel|_K \otimes \pi_b^\perp|_K$ with $\pi_b^\parallel|_K$ denoting the univariate projector $\pi_{p,2}^{(3)}|_K$ acting

in $x^{\|}$-direction, and $\pi_b^{\perp}|_K = \pi_{p,2}^{(1)}|_K \otimes \pi_{p,2}^{(2)}|_K$ the two-dimensional tensor-product projectors considered already in [16, Theorem 4.72]. It can be readily seen that

$$[\![\pi_b u]\!]_{f_{ij}} = [\![\pi_b^{\perp} u]\!]_{e_{ij}^{\perp}} \otimes \pi_b^{\|}, \qquad \text{on } f_{ij} = e_{ij}^{\perp} \times e^{\|}, \tag{5.4}$$

with $[\![\pi_b^{\perp} u]\!]_{e_{ij}^{\perp}}$ denoting two-dimensional jumps in direction perpendicular to the edge $\boldsymbol{e}$ on the slice $x^{\|} \in e^{\|}$. The jumps $[\![\pi_b u]\!]_{f'_{ij}}$ have an analogous tensor-product structure.

In addition, we point out that, for $x^{\|} = 0$ (and analogously for $x^{\|} = h^{\|}$), the nodal exactness property of the univariate projector $\pi_b^{\|}$ in Lemma 4.1 implies

$$(\pi_b u)(\boldsymbol{x}^{\perp}, 0) = (\pi_b^{\perp} u(\cdot, 0))(\boldsymbol{x}^{\perp}), \qquad \boldsymbol{x}^{\perp} = (x_1^{\perp}, x_2^{\perp}) \in \{K_i^{\perp} \cup (K_i')^{\perp}\}_{i=1}^{3} . \tag{5.5}$$

In conjunction with Assumptions 3.1, 3.2, property (5.5) implies the conformity of the base projections $\pi_b u$ in parallel direction over (the corresponding mesh layers of) different patches across $x^{\|} = 0$ (or $x^{\|} = h^{\|}$); see also the discussion in Remark 4.5.

The next lemma records several other results for the polynomial jumps (5.3). To state them, we introduce the elemental edges $E_1 = \{x_1^{\perp} = 0, x_2^{\perp} = 0, x^{\|} \in e^{\|}\}$, $E_2 = \{x_1^{\perp} = a_2^{\perp}, x_2^{\perp} = 0, x^{\|} \in e^{\|}\}$ and $E_3 = \{x_1^{\perp} = 0, x_2^{\perp} = b_2^{\perp}, x^{\|} \in e^{\|}\}$, as depicted in Figure 2.

Lemma 5.3. *There holds:*

(i) *The jumps $[\![\pi_b u]\!]_{f_{21}}$, $[\![\pi_b u]\!]_{f_{22}}$ are continuous across $x_1^{\perp} = a_1^{\perp}$; the jumps $[\![\pi_b u]\!]_{f_{31}}$, $[\![\pi_b u]\!]_{f_{31}}$ are continuous across $x_2^{\perp} = b_1^{\perp}$.*

(ii) *For the elemental edges E_1, E_2, E_3 in Figure 2, there holds*

$$[\![\pi_b u]\!]_{f_{21}} \equiv 0 \text{ on } \overline{E}_1, \qquad [\![\pi_b u]\!]_{f_{31}} \equiv 0 \text{ on } \overline{E}_1, \tag{5.6}$$

$$[\![\pi_b u]\!]_{f_{22}} \equiv 0 \text{ on } \overline{E}_2, \qquad [\![\pi_b u]\!]_{f_{33}} \equiv 0 \text{ on } \overline{E}_3 . \tag{5.7}$$

Proof. In item (i), we establish the continuity of the jumps over f_{21}, f_{22} at $x_1^{\perp} = a_1^{\perp}$ (the second statement is proved in an analogous manner). Let $\boldsymbol{x} = (a_1^{\perp}, 0, x^{\|})$. By (5.3) and since f_{21} and f_{22} lie on $x_2^{\perp} = 0$, we have

$$[\![\pi_b u]\!]_{f_{21}}(\boldsymbol{x}) = \big(\pi_b|_{K_2} u|_{K_2} - \pi_b|_{K_1'} u|_{K_1'}\big)(\boldsymbol{x}),$$
$$[\![\pi_b u]\!]_{f_{22}}(\boldsymbol{x}) = \big(\pi_b|_{K_2} u|_{K_2} - \pi_b|_{K_2'} u|_{K_2'}\big)(\boldsymbol{x}).$$

Since K_1' and K_2' match regularly over f_{12}', property (4.5) in Lemma 4.4 implies $\pi_b|_{K_1'} u|_{K_1'}(\boldsymbol{x}) = \pi_b|_{K_2'} u|_{K_2'}(\boldsymbol{x})$.

To prove (5.6), (5.7), we may consider exemplarily the edge $\overline{E}_1 \subset \overline{f}_{21}$ given by $x_1^{\perp} = x_2^{\perp} = 0$ (the proofs of the other cases being analogous). By using the tensor-structure (5.4) and the nodal exactness property (4.3) (for the perpendicular tensor projector $\pi_b^{\perp}$), we see that, for $\boldsymbol{x} = (0, 0, x^{\|})$,

$$[\![\pi_b u]\!]_{f_{21}}(\boldsymbol{x}) = \big([\![\pi_b^{\perp} u]\!]_{e_{21}^{\perp}} \otimes \pi_b^{\|}\big)(\boldsymbol{x}) = [\![\pi_b^{\|} u]\!]_{f_{21}}(\boldsymbol{x}) = 0 ,$$

which finishes the proof. □

The tensor-product structure (5.4) of the polynomial jumps (5.3) motivates tensor-product constructions of jump liftings from the irregular faces f_{ij} into the

smaller elements K_j'. To that end, we define the polynomial jump lifting operator $\mathcal{L}_{\boldsymbol{e}}[\pi_b u]$ by

$$\mathcal{L}_{\boldsymbol{e}}[\pi_b u] := \begin{cases} [\![\pi_b u]\!]_{f_{21}}(1 - x_2^\perp/b_1^\perp) + [\![\pi_b u]\!]_{f_{31}}(1 - x_1^\perp/a_1^\perp) & \text{on } K_1', \\ [\![\pi_b u]\!]_{f_{22}}(1 - x_2^\perp/b_1^\perp) & \text{on } K_2', \\ [\![\pi_b u]\!]_{f_{33}}(1 - x_1^\perp/a_1^\perp) & \text{on } K_3', \\ 0 & \text{on } \{K_i\}_{i=1}^3. \end{cases} \tag{5.8}$$

Lemma 5.4. *There holds:*

(i) $\mathcal{L}_{\boldsymbol{e}}[\pi_b u]|_{K_j'} \in \mathbb{Q}_p(K_j')$ *for* $j = 1, 2, 3$, *and* $\mathcal{L}_{\boldsymbol{e}}[\pi_b u] \in C^0(\overline{K_1'} \cup \overline{K_2'} \cup \overline{K_3'})$.

(ii) *The lifting* $\mathcal{L}_{\boldsymbol{e}}[\pi_b u]$ *vanishes on* $\partial K_2' \cap \{x_1^\perp = a_2^\perp\}$, $\partial K_2' \cap \{x_2^\perp = b_1^\perp\}$, *and on* $\partial K_3' \cap \{x_1^\perp = a_1^\perp\}$, $\partial K_3' \cap \{x_2^\perp = b_2^\perp\}$. *That is, its support does not extend into layer* $\ell' + 1$ *and beyond the patch borders within layer* ℓ'.

(iii) *We have:*

$$\big(\mathcal{L}_{\boldsymbol{e}}[\pi_b u]|_{K_1'}\big)\,|_{f_{21}} = [\![\pi_b u]\!]_{f_{21}}, \qquad \big(\mathcal{L}_{\boldsymbol{e}}[\pi_b u]|_{K_1'}\big)\,|_{f_{31}} = [\![\pi_b u]\!]_{f_{31}}, \tag{5.9}$$

$$\big(\mathcal{L}_{\boldsymbol{e}}[\pi_b u]|_{K_2'}\big)\,|_{f_{22}} = [\![\pi_b u]\!]_{f_{22}}, \qquad \big(\mathcal{L}_{\boldsymbol{e}}[\pi_b u]|_{K_3'}\big)\,|_{f_{33}} = [\![\pi_b u]\!]_{f_{33}}. \tag{5.10}$$

Proof. By definition, $\mathcal{L}_{\boldsymbol{e}}[\pi_b u]$ is piecewise polynomial in layer ℓ'. The continuity over $\overline{K_1'} \cup \overline{K_2'} \cup \overline{K_3'}$ follows readily from the construction of the lifting and Lemma 5.3. This implies item (i).

Next, let us establish the properties in item (ii) for element K_2'. From the definition (5.8), it follows immediately that the lifting vanishes on $\partial K_2' \cap \{x_2^\perp = b_1^\perp\}$. Next, we consider the boundary $\partial K_2' \cap \{x_1^\perp = a_2^\perp\}$. By property (5.7) and since f_{22} lies on $x_2^\perp = 0$, there holds $[\![\pi_b u]\!]_{f_{22}}(a_2^\perp, 0, x^\parallel) = 0$. Hence, the lifting also vanishes on $\partial K_2' \cap \{x_1^\perp = a_2^\perp\}$. The proof for K_3' is analogous.

To prove (5.9), (5.10) we only consider in detail the face f_{21} on $\partial K_1' \cap \{x_2^\perp = 0\}$ (the other faces are treated analogously). Then, since the face f_{31} lies on $x_1^\perp = 0$,

$$\mathcal{L}_{\boldsymbol{e}}[\pi_b u]|_{K_1'}(x_1^\perp, 0, x^\parallel) = [\![\pi_b u]\!]_{f_{21}}(x_1^\perp, 0, x^\parallel) + [\![\pi_b u]\!]_{f_{31}}(0, 0, x^\parallel)(1 - x_1^\perp/a_1^\perp)\,.$$

Due to (5.6), it follows that $[\![\pi_b u]\!]_{f_{31}}(0, 0, x^\parallel) = 0$, which yields the assertion. □

Remark 5.5. From (5.4), we have $\mathcal{L}_{\boldsymbol{e}}[\pi_b u] = \mathcal{L}^\perp_{\boldsymbol{e}^\perp}[\pi_b^\perp u] \otimes \pi_b^\parallel$, where $\mathcal{L}^\perp_{\boldsymbol{e}^\perp}$ is (a slight modification of) the two-dimensional polynomial trace lifting operator introduced in [16, Theorem 4.72] in the slice at $x^\parallel \in e^\parallel$ in edge-perpendicular direction; cp. Figure 2. Hence, for $x^\parallel = 0$ (and analogously for $x^\parallel = h^\parallel$), property (5.5) implies

$$\mathcal{L}_{\boldsymbol{e}}[\pi_b u](\boldsymbol{x}^\perp, 0) = (\mathcal{L}^\perp_{\boldsymbol{e}^\perp}[\pi_b^\perp u(\cdot, 0)])(\boldsymbol{x}^\perp)\,, \qquad \boldsymbol{x}^\perp \in (K_i')^\perp\,,\ \ i = 1, 2, 3\,. \tag{5.11}$$

It also follows that the lifting $\mathcal{L}_{\boldsymbol{e}}[\pi_b u]$ does not generally vanish at the edge-perpendicular patch borders situated on $x^\parallel = 0$ or $x^\parallel = h^\parallel$. However, under Assumptions 3.1, 3.2 and upon introducing corresponding liftings in the adjacent patches, the tensor-product structure of the base projectors and liftings in (5.5) and (5.11), respectively, guarantee the conformity of the patch projectors $\mathcal{L}_{\boldsymbol{e}}[\pi_b u]$ over the corresponding mesh layers of different patches on the edge-perpendicular patch interfaces $x^\parallel = 0$ or $x^\parallel = h^\parallel$.

Lemma 5.4 and the definition of the jumps in (5.3) imply that the lifted projector $\Pi u := \pi_b u + \mathcal{L}_{\boldsymbol{e}}[\pi_b u]$ gives a continuous and piecewise polynomial approximation over the mesh layers $\ell' - 1$ and ℓ', cp. (5.9), (5.10), which does not affect the base projection $\pi_b u$ at the interface to the next layer $\ell' + 1$. In view of Lemma 5.4

and property (4.6), Πu also satisfies homogeneous Dirichlet boundary conditions which might possibly arise within layer ℓ' on $\partial K_2' \cap \{x_1^\perp = a_2^\perp\}$ or $\partial K_3' \cap \{x_2^\perp = b_2^\perp\}$. Finally, the projection Πu gives rise to a continuous function over the corresponding mesh layers across $x^\parallel = 0$ or $x^\parallel = h^\parallel$; cp. Remarks 5.2 and 5.5.

As we show next, the jump lifting $\mathcal{L}_{\boldsymbol{e}}[\pi_b u]$ is stable and the (weighted) H^1-norm of $\eta = u - \Pi u$ can be controlled in terms of $\eta_b = u - \pi_b u$.

Lemma 5.6. *We have the bounds*

$$\begin{aligned} N_{K_1'}[\mathcal{L}_{\boldsymbol{e}}[\pi_b u]]^2 &\lesssim p^4 (h^\perp)^{-1} \big(\|[\![\pi_b u]\!]_{f_{21}}\|^2_{L^2(f_{21})} + \|[\![\pi_b u]\!]_{f_{31}}\|^2_{L^2(f_{31})} \big), \\ N_{K_2'}[\mathcal{L}_{\boldsymbol{e}}[\pi_b u]]^2 &\lesssim p^4 (h^\perp)^{-1} \|[\![\pi_b u]\!]_{f_{22}}\|^2_{L^2(f_{22})}, \\ N_{K_3'}[\mathcal{L}_{\boldsymbol{e}}[\pi_b u]]^2 &\lesssim p^4 (h^\perp)^{-1} \|[\![\pi_b u]\!]_{f_{33}}\|^2_{L^2(f_{33})}, \end{aligned} \tag{5.12}$$

and

$$\sum_{i=1}^3 \big(N_{K_i}[\eta]^2 + N_{K_i'}[\eta]^2 \big) \lesssim p^4 \sum_{i=1}^3 \big(N_{K_i}[\eta_b]^2 + N_{K_i'}[\eta_b]^2 \big) \ . \tag{5.13}$$

Proof. We only prove (5.12) for K_1' (the other bounds are analogous). To do so, we first assume that the configuration is of unit size, i.e., $h^\perp \simeq h^\parallel \simeq O(1)$. Then, by definition of $\mathcal{L}_{\boldsymbol{e}}[\pi_b u]$ in (5.8), it readily follows that

$$\|\mathcal{L}_{\boldsymbol{e}}[\pi_b u]\|^2_{L^2(K_1')} \lesssim \big(\|[\![\pi_b u]\!]_{f_{21}}\|^2_{L^2(f_{21})} + \|[\![\pi_b u]\!]_{f_{31}}\|^2_{L^2(f_{31})} \big).$$

With the standard inverse inequality (see e.g. [16]), we have

$$\|\nabla v\|^2_{L^2(\widehat{K})} \lesssim p^4 \|v\|^2_{L^2(\widehat{K})} \qquad \forall\, v \in \mathbb{Q}_p(\widehat{K}) \ , \tag{5.14}$$

and, hence,

$$\|\nabla \mathcal{L}_{\boldsymbol{e}}[\pi_b u]\|^2_{L^2(K_1')} \lesssim p^4 \big(\|[\![\pi_b u]\!]_{f_{21}}\|^2_{L^2(f_{21})} + \|[\![\pi_b u]\!]_{f_{31}}\|^2_{L^2(f_{31})} \big).$$

In the general case as shown in Figure 2, we use the bounds above in conjunction with the anisotropic scalings in Lemma 3.3, exploiting the assumption $h^\perp \lesssim h^\parallel \lesssim 1$. This results in

$$\|\mathcal{L}_{\boldsymbol{e}}[\pi_b u]\|^2_{L^2(K_1')} \lesssim h^\perp \big(\|[\![\pi_b u]\!]_{f_{21}}\|^2_{L^2(f_{21})} + \|[\![\pi_b u]\!]_{f_{31}}\|^2_{L^2(f_{31})} \big), \tag{5.15}$$

$$\|\nabla \mathcal{L}_{\boldsymbol{e}}[\pi_b u]\|^2_{L^2(K_1')} \lesssim p^4 (h^\perp)^{-1} \big(\|[\![\pi_b u]\!]_{f_{21}}\|^2_{L^2(f_{21})} + \|[\![\pi_b u]\!]_{f_{31}}\|^2_{L^2(f_{31})} \big). \tag{5.16}$$

From these bounds and since $h^\perp_{\min,K_1'} \simeq h^\perp$, we conclude that

$$N_{K_1'}[\mathcal{L}_{\boldsymbol{e}}[\pi_b u]]^2 \lesssim p^4 (h^\perp)^{-1} \big(\|[\![\pi_b u]\!]_{f_{21}}\|^2_{L^2(f_{21})} + \|[\![\pi_b u]\!]_{f_{31}}\|^2_{L^2(f_{31})} \big),$$

which proves the bound in (5.12).

To establish (5.13), we note that, with the triangle inequality,

$$\sum_{i=1}^3 \big(N_{K_i}[\eta]^2 + N_{K_i'}[\eta]^2 \big) \lesssim \sum_{i=1}^3 \big(N_{K_i}[\eta_b]^2 + N_{K_i'}[\eta_b]^2 + N_{K_i'}[\mathcal{L}_{\boldsymbol{e}}[\pi_b u]]^2 \big) .$$

We next bound the term $N_{K_2'}[\mathcal{L}_{\boldsymbol{e}}[\pi_b u]]^2$. From (5.12) and (3.9) (with the fact that $[\![\pi_b u]\!]_{f_{22}} = [\![\eta_b]\!]_{f_{22}}$), we see that

$$N_{K_2'}[\mathcal{L}_{\boldsymbol{e}}[\pi_b u]]^2 \le p^4 (h^\perp)^{-1} \|[\![\pi_b u]\!]_{f_{22}}\|^2_{L^2(f_{22})} \lesssim p^4 \left(N_{K_2}[\eta_b]^2 + N_{K_2'}[\eta_b]^2 \right).$$

Similar bounds for the other terms $N_{K_i'}[\mathcal{L}_{\boldsymbol{e}}[\pi_b u]]$ give the assertion. □

5.2.2. *Terminal Layer Elements in $\widetilde{\mathfrak{T}}_\sigma^{\ell,\boldsymbol{e}}$.* We next consider the interface from $\widetilde{\mathfrak{O}}_\sigma^{\ell,\boldsymbol{e}}$ to $\widetilde{\mathfrak{T}}_\sigma^{\ell,\boldsymbol{e}}$ illustrated in Figure 3. We use the same notations as in Section 5.2.1. The set $\widetilde{\mathfrak{L}}_\sigma^{\ell-1,\boldsymbol{e}} = \{K_1, K_2, K_3\}$ forms layer $\ell-1$ of $\widetilde{\mathfrak{O}}_\sigma^{\ell,\boldsymbol{e}}$, and $\widetilde{\mathfrak{T}}_\sigma^{\ell,\boldsymbol{e}} = \{K_1'\}$ is the terminal layer. The base projector $\pi_b u$ is set to zero in K_1' as per (4.9). Thus, even though the faces f_{21} and f_{31} are now regularly matching, the jumps $[\![\pi_b u]\!]_{f_{21}}$ and $[\![\pi_b u]\!]_{f_{31}}$ do not vanish in general. In addition, the key properties (5.6), (5.7) are not valid anymore.

Remark 5.7. Due to Assumptions 3.1, 3.2, the base projectors $\pi_b u$ are continuous in parallel direction over (the corresponding mesh layers of) different patches across $x^\parallel = 0$ or $x^\parallel = h^\parallel$; cp. Remark 5.2 and the definition of the base projectors in (4.9).

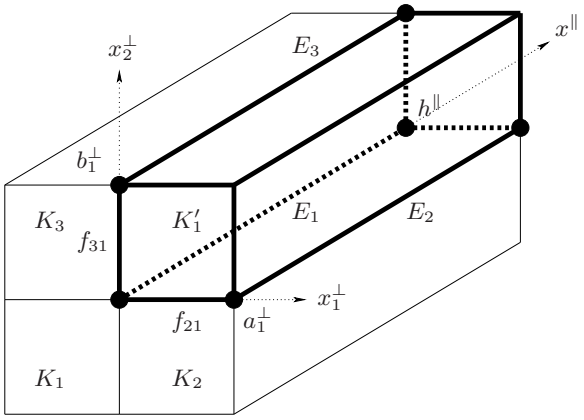

FIGURE 3. Interface between mesh layer $\widetilde{\mathfrak{L}}_\sigma^{\ell-1,\boldsymbol{e}} = \{K_1, K_2, K_3\}$ and the terminal layer $\widetilde{\mathfrak{T}}_\sigma^{\ell,\boldsymbol{e}} = \{K_1'\}$ for $\sigma = 0.5$ and length parameters $h^\parallel, a_1^\perp, a_2^\perp, b_1^\perp, b_2^\perp$. The faces f_{21}, f_{31} and the edges E_1, E_2, E_3 are illustrated.

To overcome the above difficulties, we modify the lifting procedure in (5.8), by introducing suitable edge liftings associated with the edges E_1, E_2, E_3 shown in Figure 3. We focus in detail on edge E_1.

Lemma 5.8. *We have $[\![\pi_b u]\!]_{f_{21}} = [\![\pi_b u]\!]_{f_{31}}$ on $\overline{E}_1$. Analogous identities hold on E_2 and E_3 (across patch borders).*

Proof. Let $\boldsymbol{x} \in \overline{E}_1$. Then, since $\pi_b u = 0$ on K_1', we have $[\![\pi_b u]\!]_{f_{21}}(\boldsymbol{x}) = \pi_b|_{K_2} u|_{K_2}(\boldsymbol{x})$ and $[\![\pi_b u]\!]_{f_{31}}(\boldsymbol{x}) = \pi_b|_{K_3} u|_{K_3}(\boldsymbol{x})$. Since the elements K_1, K_2, K_3 in layer $\ell-1$ match regularly, property (4.5) implies

$$\pi_b|_{K_2} u|_{K_2}(\boldsymbol{x}) = \pi_b|_{K_1} u|_{K_1}(\boldsymbol{x}) = \pi_b|_{K_3} u|_{K_3}(\boldsymbol{x}),$$

which proves the assertion. □

With Lemma 5.8, we set $[\![\pi_b u]\!]_{E_1} := [\![\pi_b u]\!]_{f_{21}}|_{E_1} = [\![\pi_b u]\!]_{f_{31}}|_{E_1}$, and introduce the edge jump lifting

$$\mathcal{L}_{\boldsymbol{e}}^{E_1}[\pi_b u] := \begin{cases} [\![\pi_b u]\!]_{E_1}(1 - x_1^\perp/a_2^\perp)(1 - x_2^\perp/b_1^\perp) & \text{on } K_1', \\ 0 & \text{on } \{K_i\}_{i=1}^3. \end{cases} \tag{5.17}$$

By construction, $\mathcal{L}_{\boldsymbol{e}}^{E_1}[\pi_b u] \in \mathbb{Q}_p(K_1')$. Furthermore, the lifting vanishes on the elemental faces $\partial K_1' \cap \{x_1^\perp = a_1^\perp\}$ and $\partial K_1' \cap \{x_2^\perp = b_1^\perp\}$; see Figure 3.

Remark 5.9. The lifting $\mathcal{L}_{\boldsymbol{e}}^{E_1}[\cdot]$ has the tensor-product structure

$$\mathcal{L}_{\boldsymbol{e}}^{E_1} = \mathcal{L}_N^\perp \otimes \pi_b^\parallel, \tag{5.18}$$

where the lifting $\mathcal{L}_N^\perp$ is a two-dimensional nodal lifting in perpendicular direction into $(K_1')^\perp$ on the slice $x^\parallel \in e^\parallel$, with $N = (0, 0, x^\parallel)$.

Lemma 5.10. *We have the bounds*

$$\begin{aligned} N_{K_1'}[\mathcal{L}_{\boldsymbol{e}}^{E_1}[\pi_b u]]^2 &\lesssim p^6 (h^\perp)^{-1} \|[\![\pi_b u]\!]_{f_{21}}\|^2_{L^2(f_{21})}, \\ N_{K_1'}[\mathcal{L}_{\boldsymbol{e}}^{E_1}[\pi_b u]]^2 &\lesssim p^6 (h^\perp)^{-1} \|[\![\pi_b u]\!]_{f_{31}}\|^2_{L^2(f_{31})}, \end{aligned} \tag{5.19}$$

and

$$\begin{aligned} N_{K_1'}[\mathcal{L}_{\boldsymbol{e}}^{E_1}[\pi_b u]]^2 &\lesssim p^6 \big(N_{K_2}[\eta_b]^2 + N_{K_1'}[\eta_b]^2\big), \\ N_{K_1'}[\mathcal{L}_{\boldsymbol{e}}^{E_1}[\pi_b u]]^2 &\lesssim p^6 \big(N_{K_3}[\eta_b]^2 + N_{K_1'}[\eta_b]^2\big). \end{aligned} \tag{5.20}$$

Proof. We establish the bounds associated with face f_{21}; the proof of the other ones is analogous. If the configuration in Figure 3 is of unit size, the two-dimensional polynomial trace inequality in [16, Theorem 4.76] yields

$$\|[\![\pi_b u]\!]_{E_1}\|^2_{L^2(E_1)} \lesssim p^2 \|[\![\pi_b u]\!]_{f_{21}}\|^2_{L^2(f_{21})}, \tag{5.21}$$

since $[\![\pi_b u]\!]_{E_1} = [\![\pi_b u]\!]_{f_{21}}|_{E_1}$. With this estimate, it readily follows that

$$\|\mathcal{L}_{\boldsymbol{e}}^{E_1}[\pi_b u]\|^2_{L^2(K_1')} \lesssim \|[\![\pi_b u]\!]_{E_1}\|^2_{L^2(E_1)} \lesssim p^2 \|[\![\pi_b u]\!]_{f_{21}}\|^2_{L^2(f_{21})}.$$

As before, the inverse inequality (5.14) implies

$$\|\nabla \mathcal{L}_{\boldsymbol{e}}^{E_1}[\pi_b u]\|^2_{L^2(K_1')} \lesssim p^6 \|[\![\pi_b u]\!]_{f_{21}}\|^2_{L^2(f_{21})}.$$

This implies (5.17) in the reference case. In the general case, we apply the scalings in Lemma 3.3, cp. (5.15) and (5.16), and obtain the first bound in (5.19).

This bound, the jump estimate (3.9) (with the fact that $[\![u]\!]_{f_{21}} = 0$) and the triangle inequality yield

$$N_{K_1'}[\mathcal{L}_{\boldsymbol{e}}^{E_1}[\pi_b u]]^2 \lesssim p^6 \big(N_{K_2}[\eta_b]^2 + N_{K_1'}[\eta_b]^2\big).$$

This shows the first estimate in (5.20). □

Next, we define the full edge lifting

$$\mathcal{L}_{\boldsymbol{e}}^{E}[\pi_b u] = \sum_{j=1}^{3} \mathcal{L}_{\boldsymbol{e}}^{E_j}[\pi_b u], \tag{5.22}$$

where $\mathcal{L}_{\boldsymbol{e}}^{E_2}[\pi_b u]$, $\mathcal{L}_{\boldsymbol{e}}^{E_3}[\pi_b u]$ are edge liftings associated with the edges E_2, E_3 in Figure 3. They are defined as in (5.17). If the elemental edge E_2 or E_3 corresponds to a boundary edge, the resulting edge lifting is identically zero, in accordance with property (4.7) for element K_2 or K_3. From stability bounds analogous to (5.19), we conclude that

$$N_{K_1'}[\mathcal{L}_{\boldsymbol{e}}^{E}[\pi_b u]]^2 \lesssim p^6 \big(N_{K_2}[\eta_b]^2 + N_{K_3}[\eta_b]^2 + N_{K_1'}[\eta_b]^2\big). \tag{5.23}$$

Remark 5.11. The introduction of corresponding edge liftings $\mathcal{L}_{\boldsymbol{e}}^E[\pi_b u]$ in terminal layer elements of adjacent patches readily yields continuity across patch borders in $x_1^\perp$-direction or $x_2^\perp$-direction. In addition, the tensor-product property (5.18) ensures the conformity of $\mathcal{L}_{\boldsymbol{e}}^E[\pi_b u]$ in terminal layer elements across $x^\parallel = 0$ or $x^\parallel = h^\parallel$; cp. Assumptions 3.1, 3.2.

We modify the base projector on K_1' and set

$$\pi_b^E u := \begin{cases} \pi_b u + \mathcal{L}_{\boldsymbol{e}}^E[\pi_b u] & \text{on } K_1', \\ \pi_b u & \text{on } \{K_i\}_{i=1}^3. \end{cases} \tag{5.24}$$

By construction, the projector $\pi_b^E u$ satisfies properties (5.6), (5.7) in the terminal layer setting of Figure 3.

Lemma 5.12. *There holds:*

$$[\![\pi_b^E u]\!]_{f_{21}} \equiv 0 \text{ on } \overline{E}_1, \qquad [\![\pi_b^E u]\!]_{f_{31}} \equiv 0 \text{ on } \overline{E}_1, \tag{5.25}$$

$$[\![\pi_b^E u]\!]_{f_{21}} \equiv 0 \text{ on } \overline{E}_2, \qquad [\![\pi_b^E u]\!]_{f_{31}} \equiv 0 \text{ on } \overline{E}_3\ . \tag{5.26}$$

Proof. We verify (5.25) for the face f_{21} (the proof for the other faces is analogous). By construction and the definition (5.3) of the jumps, we have, for $\boldsymbol{x} \in \overline{E}_1$,

$$\begin{aligned} [\![\pi_b^E u]\!]_{f_{21}}(\boldsymbol{x}) &= [\![\pi_b u]\!]_{f_{21}}(\boldsymbol{x}) + [\![\mathcal{L}_{\boldsymbol{e}}^E[\pi_b u]]\!]_{f_{21}}(\boldsymbol{x}) \\ &= [\![\pi_b u]\!]_{f_{21}}(\boldsymbol{x}) - \big(\mathcal{L}_{\boldsymbol{e}}^{E_1}[\pi_b u]|_{K_1'}\big)|_{f_{21}}(\boldsymbol{x}) \\ &= [\![\pi_b u]\!]_{f_{21}}(\boldsymbol{x}) - [\![\pi_b u]\!]_{f_{21}}(\boldsymbol{x}) = 0. \end{aligned}$$

This yields the assertion. □

Then, we adapt the face lifting $\mathcal{L}_{\boldsymbol{e}}[\cdot]$ in (5.8) to the configuration in Figure 3:

$$\mathcal{L}_{\boldsymbol{e}}^{K_1'}[\pi_b u] := \begin{cases} [\![\pi_b^E u]\!]_{f_{21}}(1 - x_2^\perp/b_1^\perp) + [\![\pi_b^E u]\!]_{f_{31}}(1 - x_1^\perp/a_1^\perp) & \text{on } K_1', \\ 0 & \text{on } \{K_i\}_{i=1}^3. \end{cases} \tag{5.27}$$

With (5.25), (5.26), the lifting $\mathcal{L}_{\boldsymbol{e}}^{K_1'}[\pi_b u]$ vanishes on $\partial K_1' \cap \{x_1^\perp = a_1^\perp\}$ and $\partial K_1' \cap \{x_2^\perp = b_1^\perp\}$; cp. Lemma 5.4. Furthermore, $\mathcal{L}_{\boldsymbol{e}}^{K_1'}[\pi_b u]$ has a tensor-product structure similar to (5.11).

Lemma 5.13. *There holds*

$$N_{K_1'}[\mathcal{L}_{\boldsymbol{e}}^{K_1'}[\pi_b u]]^2 \lesssim p^{10}\big(N_{K_2}[\eta_b]^2 + N_{K_3}[\eta_b]^2 + N_{K_1'}[\eta_b]^2\big). \tag{5.28}$$

Proof. By proceeding as in the proof of (5.12), we see that

$$N_{K_1'}[\mathcal{L}_{\boldsymbol{e}}^{K_1'}[\pi_b u]]^2 \lesssim p^4 (h^\perp)^{-1}\big(\|[\![\pi_b^E u]\!]_{f_{21}}\|_{L^2(f_{21})}^2 + \|[\![\pi_b^E u]\!]_{f_{31}}\|_{L^2(f_{31})}^2\big).$$

Then, the jump bound (3.9) (noting that $[\![u]\!]_{f_{21}} = [\![u]\!]_{f_{32}} = 0$), the definition of the edge lifting and the triangle inequality yield

$$\begin{aligned} N_{K_1'}[\mathcal{L}_{\boldsymbol{e}}^{K_1'}[\pi_b u]]^2 &\lesssim p^4 \left(N_{K_2}[\eta_b]^2 + N_{K_3}[\eta_b]^2 + N_{K_1'}[u - \pi_b^E u]^2\right) \\ &\lesssim p^4 \left(N_{K_2}[\eta_b]^2 + N_{K_3}[\eta_b]^2 + N_{K_1'}[\eta_b]^2 + N_{K_1'}[\mathcal{L}_{\boldsymbol{e}}^E[\pi_b u]]^2\right)\ . \end{aligned}$$

Invoking (5.23) yields the desired bound. □

In the configuration of Figure 3, we finally introduce the following lifting:

$$\mathcal{L}_{\boldsymbol{e}}^{\mathfrak{T}}[\pi_b u] := \begin{cases} \mathcal{L}_{\boldsymbol{e}}^{E}[\pi_b u] + \mathcal{L}_{\boldsymbol{e}}^{K_1'}[\pi_b u] & \text{on } K_1', \\ 0 & \text{on } \{K_i\}_{i=1}^3. \end{cases} \tag{5.29}$$

By Remark 5.11, the combination of the base interpolant and edge jump liftings $\mathcal{L}_{\boldsymbol{e}}^{E}[\pi_b u]$ in (5.29) give rise to a conforming function across neighboring patches. The lifting $\mathcal{L}_{\boldsymbol{e}}^{K_1'}[\pi_b u]$ is piecewise polynomial and vanishes at the patch borders $\partial K_1' \cap \{x_1^\perp = a_1^\perp\}$ and $\partial K_1' \cap \{x_2^\perp = b_1^\perp\}$. Hence, it preserves essential boundary data which possibly arise on these patch faces.

Remark 5.14. The lifting $\mathcal{L}_{\boldsymbol{e}}^{\mathfrak{T}}[\pi_b u]$ does not generally vanish on $x^\parallel = 0$ or $x^\parallel = h^\parallel$. However, as in Section 5.2.1, the tensor-product structure of the liftings $\mathcal{L}_{\boldsymbol{e}}^{E}[\pi_b u]$ and $\mathcal{L}_{\boldsymbol{e}}^{K_1'}[\pi_b u]$ ensures the continuity of $\mathcal{L}_{\boldsymbol{e}}^{\mathfrak{T}}[\pi_b u]$ in terminal layer elements across $x^\parallel = 0$ or $x^\parallel = h^\parallel$; cp. Assumptions 3.1, 3.2 and the nodal exactness of the univariate projector $\pi_b^\parallel$ in edge-parallel direction in Lemma 4.1.

Lemma 5.15. *There holds:*

$$\big(\mathcal{L}_{\boldsymbol{e}}^{\mathfrak{T}}[\pi_b u]|_{K_1'}\big)\,|_{f_{21}} = [\![\pi_b u]\!]_{f_{21}}, \qquad \big(\mathcal{L}_{\boldsymbol{e}}^{\mathfrak{T}}[\pi_b u]|_{K_1'}\big)\,|_{f_{31}} = [\![\pi_b u]\!]_{f_{31}}. \tag{5.30}$$

Proof. We show (5.30) for f_{21} (the proof for f_{31} is analogous). By (5.25) and as in the proof of (5.9), we have

$$\big(\mathcal{L}_{\boldsymbol{e}}^{K_1'}[\pi_b u]|_{K_1'}\big)|_{f_{21}} = [\![\pi_b^E u]\!]_{f_{21}}.$$

Hence, with the definition of $\pi_b^E u$ and the jumps in (5.24) and (5.3), respectively, we conclude that

$$\begin{aligned}\big(\mathcal{L}_{\boldsymbol{e}}^{\mathfrak{T}}[\pi_b u]|_{K_1'}\big)|_{f_{21}} &= \big(\mathcal{L}_{\boldsymbol{e}}^{E}[\pi_b u]|_{K_1'}\big)|_{f_{21}} + [\![\pi_b^E u]\!]_{f_{21}} \\ &= \big(\mathcal{L}_{\boldsymbol{e}}^{E}[\pi_b u]|_{K_1'}\big)|_{f_{21}} + [\![\pi_b u]\!]_{f_{21}} - \big(\mathcal{L}_{\boldsymbol{e}}^{E}[\pi_b u]|_{K_1'}\big)|_{f_{21}} = [\![\pi_b u]\!]_{f_{21}},\end{aligned}$$

which gives the assertion. □

In view of Remark 5.14 and Lemma 5.15, the lifted projector $\Pi u := \pi_b u + \mathcal{L}_{\boldsymbol{e}}^{\mathfrak{T}}[\pi_b u]$ yields a piecewise polynomial and conforming approximation in the setting of Figure 3. The analog of the bound (5.13) in Lemma 5.6 reads as follows.

Lemma 5.16. *We have the bound*

$$\sum_{i=1}^{3} N_{K_i}[\eta]^2 + N_{K_1'}[\eta]^2 \lesssim p^{10}\big(\sum_{i=1}^{3} N_{K_i}[\eta_b]^2 + N_{K_1'}[\eta_b]^2\big). \tag{5.31}$$

Proof. The triangle inequality yields

$$\begin{aligned}&\sum_{i=1}^{3} N_{K_i}[\eta]^2 + N_{K_1'}[\eta]^2 \\ &\qquad\lesssim \sum_{i=1}^{3} N_{K_i}[\eta_b]^2 + N_{K_1'}[\eta_b]^2 + N_{K_1'}[\mathcal{L}_{\boldsymbol{e}}^{E}[\pi_b u]]^2 + N_{K_1'}[\mathcal{L}_{\boldsymbol{e}}^{K_1'}[\pi_b^E u]]^2.\end{aligned}$$

Referring to (5.23) and Lemma 5.13 finishes the proof. □

Lemma 5.6 (for submesh $\widetilde{\mathfrak{D}}_\sigma^{\ell,\boldsymbol{e}}$) and Lemma 5.16 (for submesh $\widetilde{\mathfrak{T}}_\sigma^{\ell,\boldsymbol{e}}$) show the bound (3.28) over the reference edge patch $\widetilde{\mathcal{M}}_\sigma^{\ell,\boldsymbol{e}}$. More precisely, the subsequent estimate holds.

Proposition 5.17. *We have* $\Upsilon_{\widetilde{\mathcal{M}}_\sigma^{\ell,\boldsymbol{e}}}[\eta] \lesssim p^{10}\Upsilon_{\widetilde{\mathcal{M}}_\sigma^{\ell,\boldsymbol{e}}}[\eta_b]$.

5.3. **Corner Patch $\widetilde{\mathcal{M}}_\sigma^{\ell,\boldsymbol{c}}$.** We consider the reference corner patch $\widetilde{\mathcal{M}}_\sigma^{\ell,\boldsymbol{c}}$, where irregular faces appear due to hanging nodes located in the interior of faces, cp. Figure 1 (left); these faces involve only shape-regular elements. We proceed as in Section 5.2, by writing $\widetilde{\mathcal{M}}_\sigma^{\ell,\boldsymbol{c}} = \widetilde{\mathfrak{O}}_\sigma^{\ell,\boldsymbol{c}} \,\dot\cup\, \widetilde{\mathfrak{T}}_\sigma^{\ell,\boldsymbol{c}}$, cp. (4.8), and by analyzing the two submeshes separately.

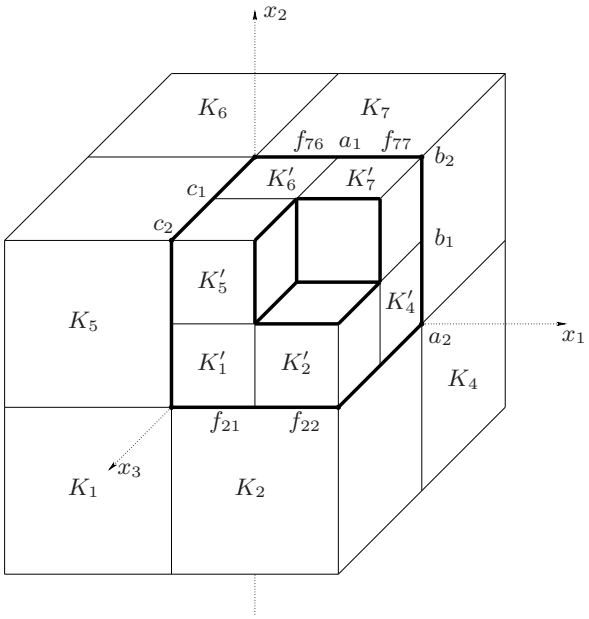

FIGURE 4. Interface between layers $\widetilde{\mathfrak{L}}_\sigma^{\ell'-1,\boldsymbol{c}} = \{K_i\}_{i=1}^7$ and $\widetilde{\mathfrak{L}}_\sigma^{\ell',\boldsymbol{c}} = \{K_i'\}_{i=1}^7$ for $\sigma = 0.5$ and length parameters a_i, b_i, c_i, $i = 1, 2$. The irregular faces $f_{21}, f_{22}, f_{76}, f_{77}$ are illustrated.

5.3.1. *Interior Elements in $\widetilde{\mathfrak{O}}_\sigma^{\ell,\boldsymbol{c}}$.* As in the edge patch case, we partition $\widetilde{\mathfrak{O}}_\sigma^{\ell,\boldsymbol{e}}$ into ℓ layers: $\widetilde{\mathfrak{O}}_\sigma^{\ell,\boldsymbol{e}} = \dot\cup_{\ell'=0}^{\ell-1} \widetilde{\mathfrak{L}}_\sigma^{\ell',\boldsymbol{c}}$; cp. (3.5). For $1 \le \ell' \le \ell - 1$, we consider the interface of the two adjacent mesh layers $\widetilde{\mathfrak{L}}_\sigma^{\ell'-1,\boldsymbol{c}} = \{K_i\}_{i=1}^7$ and $\widetilde{\mathfrak{L}}_\sigma^{\ell',\boldsymbol{c}} = \{K_i'\}_{i=1}^7$ shown in Figure 4. The elements are shape-regular (uniformly in ℓ) with $h_{K_i} \simeq h_{K_i'} \simeq h^\perp_{\min,K_i} \simeq h^\perp_{\min,K_i'} \simeq h$. As in Section 5.2, we introduce the faces $f_{ij} = f_{K_i,K_j'}$ and $f_{ij}' = f_{K_i',K_j'}$. The faces $f_{21}, f_{22}, f_{76}, f_{77}$ are illustrated in Figure 4. The locations of the elements, faces and edges in this configuration are determined by the length parameters a_1, a_2 in x_1-direction, by b_1, b_2 in x_2-direction, and by c_1, c_2 in x_3-direction, respectively. Again, these values do not change from layer to layer. By Remark 4.5, the base projector $\pi_b u$ defined in (4.9) is continuous across elements K_i, K_j within layer $\ell' - 1$, respectively across the faces f_{ij}' within layer ℓ', and satisfies possible homogeneous Dirichlet boundary conditions on patch boundary faces. The polynomial face jumps $[\![\pi_b u]\!]_{f_{ij}}$ are defined as in (5.3).

As further illustrated in Figure 5, there are three faces which constitute the interface between layer $\ell' - 1$ and ℓ': $F_1 := \partial K_2 \cap \{\, x_2 = 0 \,\}$, $F_2 := \partial K_7 \cap \{\, x_3 = 0 \,\}$,

and $F_3 := \partial K_5 \cap \{ x_1 = 0 \}$. The elemental edges of these faces are denoted by $E_1, \ldots, E_9$ and are also depicted in Figure 5.

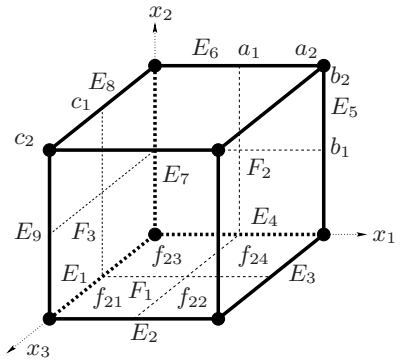

FIGURE 5. Illustration of the faces F_1, F_2, F_3 constituting the interface from layer $\ell' - 1$ to layer ℓ' for $\sigma = 0.5$. The edges of these faces are denoted by $E_1, \ldots, E_9$. The face F_1 consists of the four irregular faces $f_{21}, f_{22}, f_{23}, f_{24}$.

We define the polynomial jump across face F_1 by

$$[\![\pi_b u]\!]_{F_1} := [\![\pi_b u]\!]_{f_{2j}} \quad \text{on } f_{2j},\ 1 \le j \le 4. \tag{5.32}$$

The jumps $[\![\pi_b u]\!]_{F_2}$ and $[\![\pi_b u]\!]_{F_3}$ are defined analogously.

Lemma 5.18. *There holds:*

(i) *We have* $[\![\pi_b u]\!]_{F_1} \in C^0(\overline{F}_1)$ *and*

$$[\![\pi_b u]\!]_{F_1}(0,0,0) = 0, \qquad [\![\pi_b u]\!]_{F_1}(0,0,c_2) = 0, \tag{5.33}$$
$$[\![\pi_b u]\!]_{F_1}(a_2,0,0) = 0, \qquad [\![\pi_b u]\!]_{F_1}(a_2,0,c_2) = 0. \tag{5.34}$$

(ii) *We have* $[\![\pi_b u]\!]_{F_1} = [\![\pi_b u]\!]_{F_3}$ *on* $\overline{E}_1$.

Analogous properties hold for the jumps $[\![\pi_b u]\!]_{F_2}$ *and* $[\![\pi_b u]\!]_{F_3}$ *(possibly across patch borders).*

Proof. The continuity of $[\![\pi_b u]\!]_{F_1}$ follows from the fact that elements $K_1', \ldots, K_4'$ match regularly in across the faces $f_{12}', f_{14}', f_{45}', f_{25}$. Properties (5.33), (5.34) are direct consequences of the nodal exactness (4.3). This verifies item (i).

For item (ii), we proceed as in the proof of Lemma 5.8 and consider $\boldsymbol{x} \in \overline{E}_1 \cap \partial K_j'$ for $j \in \{1,3\}$. Then,

$$[\![\pi_b u]\!]_{F_1}(\boldsymbol{x}) = [\![\pi_b u]\!]_{f_{2j}}(\boldsymbol{x}) = \pi_b|_{K_2} u|_{K_2}(\boldsymbol{x}) - \pi_b|_{K_j'} u|_{K_j'}(\boldsymbol{x}),$$
$$[\![\pi_b u]\!]_{F_3}(\boldsymbol{x}) = [\![\pi_b u]\!]_{f_{5j}}(\boldsymbol{x}) = \pi_b|_{K_5} u|_{K_5}(\boldsymbol{x}) - \pi_b|_{K_j'} u|_{K_j'}(\boldsymbol{x}).$$

Since the elements $\{K_i\}_{i=1}^7$ in layer $\ell' - 1$ match regularly, by property (4.5), we obtain $\pi_b|_{K_2} u|_{K_2}(\boldsymbol{x}) = \pi_b|_{K_1} u|_{K_1}(\boldsymbol{x}) = \pi_b|_{K_5} u|_{K_5}(\boldsymbol{x})$. This finishes the proof. □

We begin our construction by introducing edge jump liftings associated with the edges $E_1, \ldots, E_9$ in Figure 5; cp. Section 5.2.2. We consider in detail edge E_1.

Then, with Lemma 5.18, we may set $[\![\pi_b u]\!]_{E_1} := ([\![\pi_b u]\!]_{F_1})|_{E_1} = ([\![\pi_b u]\!]_{F_3})|_{E_1}$, and define the edge lifting

$$\mathcal{L}_{\boldsymbol{c}}^{E_1}[\pi_b u] := \begin{cases} [\![\pi_b u]\!]_{E_1}(1-x_1/a_1)(1-x_2/b_1) & \text{in } K_1',\, K_3', \\ 0 & \text{otherwise.} \end{cases} \tag{5.35}$$

The lifting $\mathcal{L}_{\boldsymbol{c}}^{E_1}[\pi_b u]$ defines a piecewise polynomial and continuous function in $\overline{K_1'} \cup \overline{K_3'}$; cp. Lemma 5.18, which reproduces the edge jump $[\![\pi_b u]\!]_{E_1}$ on E_1. By construction and due to (5.34) it vanishes on edges E_2, E_4, as well as on $\{x_1 = a_1\}$, $\{x_2 = b_1\}$. By proceeding as in the proof of (5.20) (with isotropic element scaling), the following bound can be readily verified.

Lemma 5.19. *We have the bound*

$$N_{K_1'}[\mathcal{L}_{\boldsymbol{c}}^{E_1}[\pi_b u]]^2 + N_{K_3'}[\mathcal{L}_{\boldsymbol{c}}^{E_1}[\pi_b u]]^2 \lesssim p^6 \left(N_{K_2}[\eta_b]^2 + N_{K_1'}[\eta_b]^2 + N_{K_3'}[\eta_b]^2\right) . \tag{5.36}$$

In the setting of Figure 5, we then define the full edge lifting $\mathcal{L}_{\boldsymbol{c}}^{E}[\pi_b u]$ as

$$\mathcal{L}_{\boldsymbol{c}}^{E}[\pi_b u] := \sum_{j=1}^{9} \mathcal{L}_{\boldsymbol{c}}^{E_j}[\pi_b u], \tag{5.37}$$

where $\mathcal{L}_{\boldsymbol{c}}^{E_j}[\pi_b u]$ is an edge lifting associated with E_j as in (5.35). The function $\mathcal{L}_{\boldsymbol{c}}^{E}[\pi_b u]$ is piecewise polynomial and continuous in $\overline{K_1'} \cup \ldots \cup \overline{K_7'}$.

Remark 5.20. If E_j corresponds to a boundary edge, the resulting edge lifting is identically zero, cp. (4.7). As in Remark 5.11, the introduction of corresponding edge jump liftings in adjacent patches yields conformity over patch border; cp. Assumptions 3.1, 3.2.

From estimates as in (5.36), we conclude that, over face F_1, we have

$$\sum_{i=1}^{4} N_{K_i'}[\mathcal{L}_{\boldsymbol{c}}^{E}[\pi_b u]]^2 \lesssim p^6 \big(N_{K_2}[\eta_b]^2 + \sum_{i=1}^{4} N_{K_i'}[\eta_b]^2\big). \tag{5.38}$$

Similar bounds hold over F_2 and F_3. Proceeding as in Section 5.2.2, we introduce the modified projector

$$\pi_b^E u := \pi_b u + \mathcal{L}_{\boldsymbol{c}}^{E}[\pi_b u] \, . \tag{5.39}$$

Lemma 5.21. *There holds:*

(i) *We have* $[\![\pi_b^E u]\!]_{F_1} \in C^0(\overline{F}_1)$.
(ii) *We have* $[\![\pi_b^E u]\!]_{F_1} \equiv 0$ *on* $\overline{E}_j$ *for* $1 \le j \le 4$.

Analogous properties hold on F_2 *and* F_3.

Proof. To prove item (i), we note that

$$[\![\pi_b^E u]\!]_{F_1} = [\![\pi_b u]\!]_{f_{2j}} - \big(\mathcal{L}_{\boldsymbol{c}}^{E}[\pi_b u]|_{K_j'}\big)|_{f_{2j}} \quad \text{on } f_{2j},\ 1 \le j \le 4. \tag{5.40}$$

Hence, the continuity of $[\![\pi_b^E u]\!]_{F_1}$ follows from the continuity of $[\![\pi_b u]\!]_{F_1}$ shown in Lemma 5.18 and the continuity of the edge liftings. To verify item (ii), let $\boldsymbol{x} \in \overline{E}_1 \cap \partial K_j'$ for $j \in \{1,3\}$. By (5.40),

$$\begin{aligned} [\![\pi_b^E u]\!]_{F_1}(\boldsymbol{x}) &= [\![\pi_b u]\!]_{f_{2j}}(\boldsymbol{x}) - \big(\mathcal{L}_{\boldsymbol{c}}^{E_1}[\pi_b u]|_{K_1'}\big)|_{f_{2j}}(\boldsymbol{x}) \\ &= [\![\pi_b u]\!]_{f_{2j}}(\boldsymbol{x}) - [\![\pi_b u]\!]_{f_{2j}}(\boldsymbol{x}) = 0 \, . \end{aligned}$$

Analogous arguments for the other edges complete the proof. □

Next, we define the face lifting of $[\![\pi_b^E u]\!]_{F_1}$ over F_1 from K_2 into layer ℓ' by

$$\mathcal{L}_{\boldsymbol{c}}^{F_1,K_2}[\pi_b u] := \begin{cases} [\![\pi_b^E u]\!]_{F_1}(1-x_2/b_1) & \text{on } \{K_i'\}_{i=1}^4, \\ 0 & \text{otherwise.} \end{cases} \tag{5.41}$$

Notice that, due to Lemma 5.21, this lifting vanishes on the sets $\{\boldsymbol{x} : (x_1,0,x_3) \in \partial F_1, x_2 \in (0,b_1)\}$ and $\{x_2 = b_1\}$, respectively, and in particular on the other faces F_2 and F_3. In addition, it reproduces the jump of $\pi_b^E u$ on F_1:

$$\big(\mathcal{L}_{\boldsymbol{c}}^{F_1,K_2}[\pi_b u]|_{K_j'}\big)|_{f_{2j}} = [\![\pi_b^E u]\!]_{f_{2j}}, \qquad 1 \le j \le 4\,. \tag{5.42}$$

Lemma 5.22. *We have the bound*

$$\sum_{i=1}^4 N_{K_i'}[\mathcal{L}_{\boldsymbol{c}}^{F_1,K_2}[\pi_b u]]^2 \lesssim p^{10}\big(N_{K_2}[\eta_b]^2 + \sum_{i=1}^4 N_{K_i'}[\eta_b]^2\big). \tag{5.43}$$

Proof. Proceeding as in the proof of (5.12) yields

$$\sum_{i=1}^4 N_{K_i'}[\mathcal{L}_{\boldsymbol{c}}^{F_1,K_2}[\pi_b u]]^2 \lesssim p^4 h^{-1} \sum_{i=1}^4 \|[\![\pi_b^E u]\!]_{f_{2i}}\|_{L^2(f_{2i})}^2.$$

Applying the jump estimate (3.9) (with the fact that $[\![u]\!]_{f_{2i}} = 0$) in conjunction with the bound (5.38) implies the asserted bound. □

Next, we introduce the full trace lifting $\mathcal{L}_{\boldsymbol{c}}^{F_1}[\pi_b u]$ associated with the face F_1 as

$$\mathcal{L}_{\boldsymbol{c}}^{F_1}[\pi_b u] := \begin{cases} \mathcal{L}_{\boldsymbol{c}}^{E}[\pi_b u] + \mathcal{L}_{\boldsymbol{c}}^{F_1,K_2}[\pi_b u] & \text{on } \{K_i'\}_{i=1}^4, \\ 0 & \text{otherwise,} \end{cases} \tag{5.44}$$

with $\mathcal{L}_{\boldsymbol{c}}^{E}[\pi_b u]$ and $\mathcal{L}_{\boldsymbol{c}}^{F_1,K_2}[\pi_b u]$ defined in (5.37) and (5.41), respectively. The lifting $\mathcal{L}_{\boldsymbol{c}}^{F_1}[\pi_b u]$ is piecewise polynomial and continuous in $\cup_{i=1}^4 \overline{K_i'}$. By construction and definition of the edge liftings, it vanishes on the elemental boundaries on the plane $\{x_2 = b_1\}$. That is, it does not extend into layer $\ell'+1$ in x_2-direction; cp. Figure 4. Moreover, since $\mathcal{L}_{\boldsymbol{c}}^{F_1,K_2}[\pi_b u]$ vanishes on the faces F_2, F_3, the lifting $\mathcal{L}_{\boldsymbol{c}}^{F_1}[\pi_b u]$ affects the values of $\pi_b u$ on the other faces F_1, F_2 only through the edge lifting $\mathcal{L}_{\boldsymbol{c}}^{E}[\pi_b u]$, which gives rise to a continuous function in layer ℓ' and over patch borders; cp. Remark 5.20.

Lemma 5.23. *There holds*

$$\big(\mathcal{L}_{\boldsymbol{c}}^{F_1}[\pi_b u]|_{K_i'}\big)|_{f_{2j}} = [\![\pi_b u]\!]_{f_{2j}}, \qquad 1 \le j \le 4, \tag{5.45}$$

and

$$\sum_{i=1}^4 N_{K_i'}[\mathcal{L}_{\boldsymbol{c}}^{F_1}[\pi_b u]]^2 \lesssim p^{10}\big(N_{K_2}[\eta_b]^2 + \sum_{i=1}^4 N_{K_i'}[\eta_b]^2\big)\,. \tag{5.46}$$

Proof. We establish (5.45) for K_1' (the proof for the other elements is analogous). By property (5.42) and the definition of $\pi_b^E u$ in (5.39), we have

$$\begin{aligned} \big(\mathcal{L}_{\boldsymbol{c}}^{F_1}[\pi_b u]|_{K_1'}\big)|_{f_{21}} &= \big(\mathcal{L}_{\boldsymbol{c}}^{E}[\pi_b u]|_{K_1'}\big)|_{f_{21}} + \big(\mathcal{L}_{\boldsymbol{c}}^{F_1,K_2}[\pi_b u]|_{K_1'}\big)|_{f_{21}} \\ &= \big(\mathcal{L}_{\boldsymbol{c}}^{E}[\pi_b u]|_{K_1'}\big)|_{f_{21}} + [\![\pi_b u]\!]_{f_{21}} + [\![\mathcal{L}_{\boldsymbol{c}}^{E}[\pi_b u]]\!]_{f_{21}} \\ &= \big(\mathcal{L}_{\boldsymbol{c}}^{E}[\pi_b u]|_{K_1'}\big)|_{f_{21}} + [\![\pi_b u]\!]_{f_{21}} - \big(\mathcal{L}_{\boldsymbol{c}}^{E}[\pi_b u]|_{K_1'}\big)|_{f_{21}} = [\![\pi_b u]\!]_{f_{21}}. \end{aligned}$$

The estimate (5.46) follows with the triangle inequality, by combining the bounds in (5.38) and (5.43). □

Upon constructing corresponding face liftings $\mathcal{L}_{\boldsymbol{c}}^{F_2}[\pi_b u]$ and $\mathcal{L}_{\boldsymbol{c}}^{F_3}[\pi_b u]$ over the faces F_2 and F_3, respectively, we finally define the corner lifting $\mathcal{L}_{\boldsymbol{c}}[\pi_b u]$ by

$$\mathcal{L}_{\boldsymbol{c}}[\pi_b u] := \sum_{i=1}^{3} \mathcal{L}_{\boldsymbol{c}}^{F_i}[\pi_b u]. \tag{5.47}$$

The lifted interpolant $\Pi u := \pi_b u + \mathcal{L}_{\boldsymbol{c}}[\pi_b u]$ now gives rise to a piecewise polynomial and conforming interpolant across layer $\ell' - 1$ and ℓ', cp. (5.45). The support of the trace lifting does not extend into layer $\ell' + 1$ and preserves homogeneous Dirichlet boundary conditions.

Lemma 5.24. *We have the bound*

$$\sum_{i=1}^{7} \left(N_{K_i}[\eta]^2 + N_{K_i'}[\eta]^2 \right) \lesssim p^{10} \sum_{i=1}^{7} \left(N_{K_i}[\eta_b]^2 + N_{K_i'}[\eta_b]^2 \right). \tag{5.48}$$

Proof. This follows readily from the triangle inequality and bounds as in (5.46). □

5.3.2. *Terminal Layer Elements in $\widetilde{\mathfrak{T}}_\sigma^{\ell,\boldsymbol{c}}$.* We consider the interface from the mesh layer $\widetilde{\mathfrak{L}}_\sigma^{\ell-1,\boldsymbol{c}} = \{K_i\}_{i=1}^7$ to the terminal layer $\widetilde{\mathfrak{T}}_\sigma^{\ell,\boldsymbol{c}} = \{K_1'\}$ shown in Figure 6. We employ notation as in Section 5.3.1: we denote by h the diameter of the shape-regular elements involved. Analogously to Figure 5, we introduce the elemental faces F_1, F_2, F_3 of K_1', as well as the elemental edges $E_1, \dots, E_9$. In contrast to Section 5.3.2, these faces are now regularly matching elemental faces of K_1'. Nevertheless, the jumps $[\![\pi_b u]\!]_{F_i}$ (defined in analogy to the definitions in (5.3), (5.32)) do not vanish in general, since the base projector vanishes on K_1', cp. (4.9). Another consequence of this choice is that properties (5.33), (5.34) are not valid anymore.

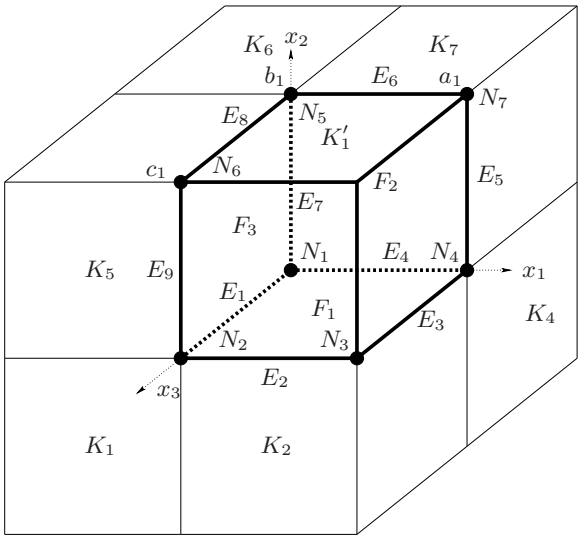

FIGURE 6. Interface between mesh layer $\widetilde{\mathfrak{L}}_\sigma^{\ell-1,\boldsymbol{c}} = \{K_i\}_{i=1}^7$ and the terminal layer $\widetilde{\mathfrak{T}}_\sigma^{\ell,\boldsymbol{c}} = \{K_1'\}$ for $\sigma = 0.5$ and length parameters a_1, b_1, c_1. The faces F_1, F_2, F_3, the edges $E_1, \dots, E_9$ and the nodes $N_1, \dots, N_9$ are illustrated.

To overcome these difficulties, we introduce polynomial nodal liftings associated with the nodes $N_1, \dots N_7$ shown in Figure 6. Here, we emphasize that, under our regularity assumption $u \in M^3_{-1-\boldsymbol{b}_\iota}(\widetilde{Q})$, the point values $u(N_j)$ are well-defined (since the nodes are separated from the singular edge $\boldsymbol{e}$). We now focus on node $N_1 = (0,0,0)$. By the nodal exactness (4.3) of $\pi_b u$ in layer $\ell - 1$, we have

$$[\![\pi_b u]\!]_{F_1}(N_1) = [\![\pi_b u]\!]_{F_2}(N_1) = [\![\pi_b u]\!]_{F_3}(N_1) = u(N_1). \tag{5.49}$$

This prompts us to define the polynomial vertex jump lifting $\mathcal{L}^{N_1}_{\boldsymbol{c}}[\pi_b u]$ by

$$\mathcal{L}^{N_1}_{\boldsymbol{c}}[\pi_b u] := \begin{cases} [\![\pi_b u]\!]_{F_1}(N_1) L_{N_1}(\boldsymbol{x}) & \text{on } K_1', \\ 0 & \text{on } \{K_i\}_{i=1}^7, \end{cases} \tag{5.50}$$

with the nodal basis function $L_{N_1}(\boldsymbol{x}) := (1-x_1/a_1)(1-x_2/b_1)(1-x_3/c_3) \in \mathbb{Q}_1(K_1')$.

Lemma 5.25. *We have the bounds*

$$N_{K_1'}[\mathcal{L}^{N_1}_{\boldsymbol{c}}[\pi_b u]]^2 \lesssim p^8 h^{-1} \|[\![\pi_b u]\!]_{F_1}\|^2_{L^2(F_1)}, \tag{5.51}$$

and

$$N_{K_1'}[\mathcal{L}^{N_1}_{\boldsymbol{c}}[\pi_b u]]^2 \lesssim p^8 \big(N_{K_1'}[\eta_b]^2 + N_{K_2}[\eta_b]^2\big). \tag{5.52}$$

Proof. As in the proof of Lemma 5.6, we first let the configuration in Figure 3 be of unit size. With the inverse inequality in [16, Theorem 4.76], we conclude that

$$\|\mathcal{L}^{N_1}_{\boldsymbol{c}}[\pi_b u]\|^2_{L^2(K_1')} \lesssim |[\![\pi_b u]\!]_{F_1}(N_1)|^2 \lesssim \|[\![\pi_b u]\!]_{F_1}\|^2_{L^\infty(F_1)} \lesssim p^4 \|[\![\pi_b u]\!]_{F_1}\|^2_{L^2(F_1)}\,.$$

Moreover, applying the inverse inequality (5.14) yields

$$\|\nabla \mathcal{L}^{N_1}_{\boldsymbol{c}}[\pi_b u]\|^2_{L^2(K_1')} \lesssim p^8 \|[\![\pi_b u]\!]_{F_1}\|^2_{L^2(F_1)},$$

which shows the assertion in the reference case. In the general case, (isotropic versions of) the scalings in Lemma 3.3 imply the bound (5.51); cp. (5.15) and (5.16). The bound (5.52) follows from (5.51) and the jump bound (3.9) (since $[\![u]\!]_{F_1} = 0$ and $F_1 = \operatorname{int}(\partial K_2 \cap \partial K_1')$. □

Similar constructions for the other nodes in Figure 6 give rise to nodal liftings $\mathcal{L}^{N_j}_{\boldsymbol{c}}[\pi_b u]$, for $1 \le j \le 7$, with analogous properties. We then define the full vertex lifting

$$\mathcal{L}^{N}_{\boldsymbol{c}}[\pi_b u] := \sum_{j=1}^{7} \mathcal{L}^{N_j}_{\boldsymbol{c}}[\pi_b u]. \tag{5.53}$$

From bounds analogous to (5.52), we have

$$N_{K_1'}[\mathcal{L}^{N}_{\boldsymbol{c}}[\pi_b u]]^2 \lesssim p^8 \big(N_{K_2}[\eta_b]^2 + N_{K_5}[\eta_b]^2 + N_{K_7}[\eta_b]^2 + N_{K_1'}[\eta_b]^2\big). \tag{5.54}$$

Remark 5.26. We note that, if N_j corresponds to a boundary node, then the resulting vertex lifting $\mathcal{L}^{N_j}_{\boldsymbol{c}}[\pi_b u]$ is identically zero; cp. property (5.49). Moreover, the definitions of corresponding vertex liftings in the terminal layers of adjacent patches (matching regularly over patch interfaces due to Assumptions 3.1, 3.2) yield conformity of the nodal liftings $\mathcal{L}^{N}_{\boldsymbol{c}}[\pi_b u]$ across patch borders.

The modified base projector

$$\pi_b^N u := \begin{cases} \pi_b u + \mathcal{L}^{N}_{\boldsymbol{c}}[\pi_b u] & \text{on } K_1', \\ \pi_b u & \text{otherwise.} \end{cases} \tag{5.55}$$

satisfies the properties analogous to those in Lemma 5.18.

Lemma 5.27. *There holds:*

(i) *We have* $[\![\pi_b^N u]\!]_{F_1} = [\![\pi_b^N u]\!]_{F_3}$ *on* $\overline{E}_1$.
(ii) *We have* $[\![\pi_b^N u]\!]_{F_1}(N_j) = 0$ *for* $1 \le j \le 4$.

Analogous identities hold on the other faces and edges (possibly across patch borders).

Proof. For $\boldsymbol{x} \in \overline{E}_1$, we have

$$[\![\pi_b^N u]\!]_{F_1}(\boldsymbol{x}) = \pi_b|_{K_2} u|_{K_2}(\boldsymbol{x}) - \mathcal{L}_{\boldsymbol{c}}^N[\pi_b u]|_{K_1'}(\boldsymbol{x}),$$

and

$$[\![\pi_b^N u]\!]_{F_3}(\boldsymbol{x}) = \pi_b|_{K_5} u|_{K_5}(\boldsymbol{x}) - \mathcal{L}_{\boldsymbol{c}}^N[\pi_b u]|_{K_1'}(\boldsymbol{x}).$$

As in the proof of Lemma 5.18, since $\{K_i\}_{i=1}^7$ match regularly in layer $\ell - 1$, we conclude with (4.5) that $\pi_b|_{K_2} u|_{K_2}(\boldsymbol{x}) = \pi_b|_{K_5} u|_{K_5}(\boldsymbol{x})$, which implies item (i). Then, for node N_j, we have, by construction and the definition of the jumps,

$$\begin{aligned}[\![\pi_b^N u]\!]_{F_1}(N_j) &= [\![\pi_b u]\!]_{F_1}(N_j) - \mathcal{L}_{\boldsymbol{c}}^N[\pi_b u]|_{K_1'}(N_j) \\ &= [\![\pi_b u]\!]_{F_1}(N_j) - \mathcal{L}_{\boldsymbol{c}}^{N_j}[\pi_b u]|_{K_1'}(N_j) = [\![\pi_b u]\!]_{F_1}(N_j) - [\![\pi_b u]\!]_{F_1}(N_j) = 0.\end{aligned}$$

This yields the assertion on the face F_1. □

With Lemma 5.27, we now continue our analysis along the lines of Section 5.3.1, by employing the projector $\pi_b^N u$ instead of $\pi_b u$. To do so, we first introduce edge liftings associated with the edge jumps $[\![\pi_b^N u]\!]_{E_i}$ and defined similarly to those in (5.17), (5.35), (5.37). Second, we adapt the polynomial face lifting $\mathcal{L}_{\boldsymbol{c}}^{F_1}[\cdot]$ in (5.44) (and analogously $\mathcal{L}_{\boldsymbol{c}}^{F_2}[\cdot]$, $\mathcal{L}_{\boldsymbol{c}}^{F_3}[\cdot]$) to the slightly different setting in Figure 6, giving rise to a polynomial corner lifting $\mathcal{L}_{\boldsymbol{c}}^{K_1'}[\pi_b^N u]$ as in (5.47), (5.48), but defined only over K_1'. By construction, this lifting satisfies

$$\big(\mathcal{L}_{\boldsymbol{c}}^{K_1'}[\pi_b^N u]|_{K_1'}\big)|_{F_j} = [\![\pi_b^N u]\!]_{F_j}, \qquad 1 \le j \le 3, \tag{5.56}$$

cp. (5.45). In the configuration of Figure 6, we introduce the terminal layer lifting

$$\mathcal{L}_{\boldsymbol{c}}^{\mathfrak{T}}[\pi_b u] := \mathcal{L}_{\boldsymbol{c}}^N[\pi_b u] + \mathcal{L}_{\boldsymbol{c}}^{K_1'}[\pi_b^N u]\,. \tag{5.57}$$

Lemma 5.28. *We have*

$$\big(\mathcal{L}_{\boldsymbol{c}}^{\mathfrak{T}}[\pi_b u]|_{K_1'}\big)|_{F_j} = [\![\pi_b u]\!]_{F_j}, \qquad 1 \le j \le 3, \tag{5.58}$$

and

$$N_{K_1'}[\mathcal{L}_{\boldsymbol{c}}^{\mathfrak{T}}[\pi_b u]]^2 \lesssim p^{18}\left(N_{K_1'}[\eta_b]^2 + N_{K_2}[\eta_b]^2 + N_{K_5}[\eta_b]^2 + N_{K_7}[\eta_b]^2\right). \tag{5.59}$$

Proof. For (5.58), we employ identity (5.56) and the definition of the jumps to obtain

$$\begin{aligned}\big(\mathcal{L}_{\boldsymbol{c}}^{\mathfrak{T}}[\pi_b u]|_{K_1'}\big)|_{F_j} &= \big(\mathcal{L}_{\boldsymbol{c}}^N[\pi_b u]|_{K_1'}\big)|_{F_j} + [\![\pi_b^N u]\!]_{F_j} \\ &= \big(\mathcal{L}_{\boldsymbol{c}}^N[\pi_b u]|_{K_1'}\big)|_{F_j} + [\![\pi_b u]\!]_{F_j} + [\![\mathcal{L}_{\boldsymbol{c}}^N[\pi_b u]]\!]_{F_j} \\ &= \big(\mathcal{L}_{\boldsymbol{c}}^N[\pi_b u]|_{K_1'}\big)|_{F_j} + [\![\pi_b u]\!]_{F_j} - \big(\mathcal{L}_{\boldsymbol{c}}^N[\pi_b u]|_{K_1'}\big)|_{F_j} = [\![\pi_b u]\!]_{F_j}.\end{aligned}$$

To establish (5.59), we first note that

$$N_{K_1'}[\mathcal{L}_{\boldsymbol{c}}^{\mathfrak{T}}[\pi_b u]]^2 \lesssim N_{K_1'}[\mathcal{L}_{\boldsymbol{c}}^N[\pi_b u]]^2 + N_{K_1'}[\mathcal{L}_{\boldsymbol{c}}^{K_1'}[\pi_b^N u]]^2.$$

According to (5.54), we have

$$N_{K_1'}[\mathcal{L}_{\boldsymbol{c}}^N[\pi_b u]]^2 \lesssim p^8\left(N_{K_1'}[\eta_b]^2 + N_{K_2}[\eta_b]^2 + N_{K_5}[\eta_b]^2 + N_{K_7}[\eta_b]^2\right).$$

Moreover, by proceeding as in the proof of (5.46) we find

$$N_{K_1'}[\mathcal{L}_{\boldsymbol{c}}^{K_1'}[\pi_b^N u]]^2 \lesssim p^{10}\left(N_{K_2}[\eta_b]^2 + N_{K_5}[\eta_b]^2 + N_{K_7}[\eta_b]^2 + N_{K_1'}[u-\pi_b^N u]^2\right).$$

Finally, with the triangle inequality and as above with (5.54),

$$\begin{aligned} p^{10} N_{K_1'}[u-\pi_b^N u]^2 &\lesssim p^{10}\left(N_{K_1'}[\eta_b]^2 + N_{K_1'}[\mathcal{L}_{\boldsymbol{c}}^N[\pi_b u]]^2\right) \\ &\lesssim p^{18}\left(N_{K_1'}[\eta_b]^2 + N_{K_2}[\eta_b]^2 + N_{K_5}[\eta_b]^2 + N_{K_7}[\eta_b]^2\right) . \end{aligned}$$

This completes the proof. □

With Lemma 5.28 the lifted interpolant $\Pi u := \pi_b u + \mathcal{L}_{\boldsymbol{c}}^{\mathfrak{T}}[\pi_b u]$ is conforming across layers $\ell-1$ and ℓ, and preserves the essential boundary conditions. Analogously to Section 5.2.2 and with the estimate (5.59), the terminal layer version of Lemma 5.24 follows.

Lemma 5.29. *We have the bound*

$$N_{K_1'}[\eta]^2 + \sum_{i=1}^{7} N_{K_i}[\eta]^2 \lesssim p^{18}\big(N_{K_1'}[\eta_b]^2 + \sum_{i=1}^{7} N_{K_i}[\eta_b]^2\big) . \tag{5.60}$$

This completes the construction of the jump liftings for the corner patch $\widetilde{\mathcal{M}}_\sigma^{\ell,\boldsymbol{c}}$. Lemma 5.24 (for submesh $\widetilde{\mathfrak{O}}_\sigma^{\ell,\boldsymbol{c}}$) and Lemma 5.29 (for submesh $\widetilde{\mathfrak{T}}_\sigma^{\ell,\boldsymbol{c}}$) give the bound (3.28) over the reference corner patch $\widetilde{\mathcal{M}}_\sigma^{\ell,\boldsymbol{c}}$.

Proposition 5.30. *We have* $\Upsilon_{\widetilde{\mathcal{M}}_\sigma^{\ell,\boldsymbol{c}}}[\eta] \lesssim p^{18}\Upsilon_{\widetilde{\mathcal{M}}_\sigma^{\ell,\boldsymbol{c}}}[\eta_b]$.

5.4. **Corner-edge Patch $\widetilde{\mathcal{M}}_\sigma^{\ell,\boldsymbol{ce}}$.** We finally address the polynomial liftings in the reference corner-edge patch $\widetilde{\mathcal{M}}_\sigma^{\ell,\boldsymbol{ce}}$ depicted in Figure 1 (right). We consider in detail the case of a corner-edge patch with geometric refinements along a single edge $\boldsymbol{e}$, and comment on the case with refinements along two or three edges in Section 5.4.8 ahead.

5.4.1. *Patch Decomposition.* We partition the corner-edge patch mesh on $\widetilde{Q}$ into

$$\widetilde{\mathcal{M}}_\sigma^{\ell,\boldsymbol{ce}} := \widetilde{\mathfrak{T}}_\sigma^{\ell,\boldsymbol{c}} \,\dot\cup\, \widetilde{\mathfrak{O}}_\sigma^{\ell,\boldsymbol{c},\perp} \,\dot\cup\, \widetilde{\mathcal{M}}_\sigma^{\ell,\boldsymbol{ce},\parallel} , \qquad \ell \geq 1 , \tag{5.61}$$

where $\widetilde{\mathfrak{T}}_\sigma^{\ell,\boldsymbol{c}}$ consists of a single and isotropic terminal layer element at the corner $\boldsymbol{c}$, and the mesh $\widetilde{\mathfrak{O}}_\sigma^{\ell,\boldsymbol{c},\perp}$ is a corner-patch type mesh consisting of shape-regular elements and refined into the corner $\boldsymbol{c}$. The mesh $\widetilde{\mathcal{M}}_\sigma^{\ell,\boldsymbol{ce},\parallel}$ consists of a sequence of ℓ geometrically scaled edge-patch meshes, properly translated along the edge $\boldsymbol{e}$. More precisely,

$$\widetilde{\mathcal{M}}_\sigma^{\ell,\boldsymbol{ce},\parallel} = \bigcup_{\ell'=1}^{\ell} \widetilde{\Psi}^{\ell',\boldsymbol{ce}}(\widetilde{\mathcal{M}}_\sigma^{\ell',\boldsymbol{e}}) , \tag{5.62}$$

where we denote by $\widetilde{\Psi}^{\ell',\boldsymbol{ce}}$ the operation of translation with respect to the edge-parallel variable $x^\parallel$ combined with a dilation by a factor only depending on σ, ℓ, ℓ', and where the mesh $\widetilde{\mathcal{M}}_\sigma^{\ell',\boldsymbol{e}}$ is a reference edge patch on $\widetilde{Q}$ with $\ell'+1$ mesh layers; cp. (3.5). In Figure 7, a schematic illustration of the patch decomposition (5.61), (5.62) is provided.

The two outermost edge-patch meshes $\widetilde{\Psi}^{\ell-1,\boldsymbol{ce}}(\widetilde{\mathcal{M}}_\sigma^{\ell-1,\boldsymbol{e}})$ and $\widetilde{\Psi}^{\ell,\boldsymbol{ce}}(\widetilde{\mathcal{M}}_\sigma^{\ell,\boldsymbol{e}})$ are illustrated in Figure 8 (left). There, the hexahedra K_3', K_4', K_6' in $\widetilde{\Psi}^{\ell-1,\boldsymbol{ce}}(\widetilde{\mathcal{M}}_\sigma^{\ell-1,\boldsymbol{e}})$,

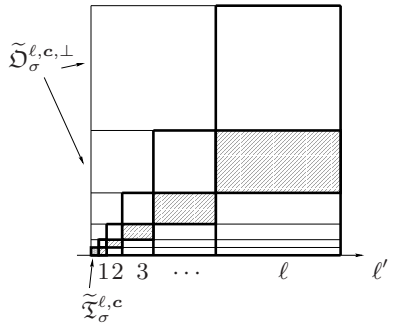

FIGURE 7. Decomposition (5.61), (5.62) for $\sigma = 0.5$ and $\ell = 5$. The scaled edge-patch meshes for $\ell' = 1, \dots, \ell$ are illustrated in boldface. The subdiagonal elements in $\mathcal{D}_{\ell'}$ are shaded. The single terminal layer element in $\widetilde{\mathfrak{T}}_\sigma^{\ell,\boldsymbol{c}}$ is indicated. The remaining elements belong to the corner-type mesh $\widetilde{\mathfrak{O}}_\sigma^{\ell,\boldsymbol{c},\perp}$.

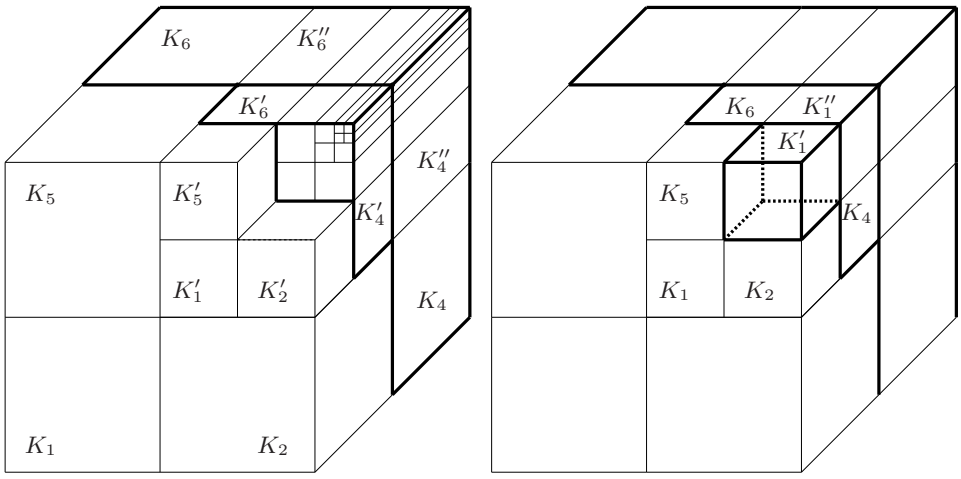

FIGURE 8. Left: The edge-patch meshes $\widetilde{\Psi}^{\ell-1,\boldsymbol{ce}}(\widetilde{\mathcal{M}}_\sigma^{\ell-1,\boldsymbol{e}})$ and $\widetilde{\Psi}^{\ell,\boldsymbol{ce}}(\widetilde{\mathcal{M}}_\sigma^{\ell,\boldsymbol{e}})$ for $\sigma = 0.5$ and $\ell = 5$. Right: Interface between $\widetilde{\mathfrak{T}}_\sigma^{\ell,\boldsymbol{c}} = \{K_1'\}$ and the first edge-patch block $\widetilde{\Psi}^{1,\boldsymbol{ce}}(\widetilde{\mathcal{M}}_\sigma^{1,\boldsymbol{e}})$ for $\sigma = 0.5$ and $\ell = 2$.

and K_3, K_4, K_6 in $\widetilde{\Psi}^{\ell,\boldsymbol{ce}}(\widetilde{\mathcal{M}}_\sigma^{\ell,\boldsymbol{e}})$ will be referred to as *diagonal elements*. Moreover, the immediate neighbors of K_3', K_4', K_6' across the patch interface are denoted by

$$\mathcal{D}_\ell := \{K_3'', K_4'', K_6''\}, \tag{5.63}$$

and are called the *subdiagonal elements*. (Note that K_3, K_3', K_3'' are not explicitly labelled in Figure 8). The diagonal and subdiagonal elements are shape-regular (uniformly in ℓ). We may thus assume that

$$h_{K_i} \simeq h_{K_i'} \simeq h_{K_i''} \simeq h, \qquad i \in \{3, 4, 6\}. \tag{5.64}$$

Corresponding conventions will be employed in the other scaled edge-patch meshes for $2 \le \ell' \le \ell$. In particular, we denote by $\mathcal{D}_{\ell'}$ the corresponding set of subdiagonal elements. In Figure 8 (right), we further illustrate the interface between $\widetilde{\mathfrak{T}}_\sigma^{\ell,\boldsymbol{c}} = \{K_1'\}$ and $\widetilde{\Psi}^{1,\boldsymbol{ce}}(\widetilde{\mathcal{M}}_\sigma^{1,\boldsymbol{e}})$. The diagonal elements are K_3, K_4, K_6, while the set

$$\mathcal{D}_1 := \{K_1''\} \tag{5.65}$$

consists of single subdiagonal element in $\widetilde{\Psi}^{1,\boldsymbol{ce}}(\widetilde{\mathcal{M}}_\sigma^{1,\boldsymbol{e}})$.

In the sequel, we construct polynomial jump liftings over irregular faces of $\widetilde{\mathcal{M}}_\sigma^{\ell,\boldsymbol{ce}}$ in (5.61), (5.62) starting from the base projector $\pi_b u$ defined in (4.9). We proceed in several steps.

5.4.2. *Edge-patch Liftings.* On all irregular faces which are situated parallel to $\boldsymbol{e}$ and which belong to an edge-patch mesh $\widetilde{\Psi}^{\ell',\boldsymbol{ce}}(\widetilde{\mathcal{M}}_\sigma^{\ell',\boldsymbol{e}})$, $1 \le \ell' \le \ell$, we apply the (scaled) jump liftings $\mathcal{L}_{\boldsymbol{e}}[\pi_b u]$ and $\mathcal{L}_{\boldsymbol{e}}^{\mathfrak{T}}[\pi_b u]$ constructed in (5.8) and (5.17), respectively. For $\ell' = 1$, only a scaled version of $\mathcal{L}_{\boldsymbol{e}}^{\mathfrak{T}}[\pi_b u]$ is employed. As shown in Lemma 5.4 (for $\mathcal{L}_{\boldsymbol{e}}[\pi_b u]$) and Lemma 5.15 (for $\mathcal{L}_{\boldsymbol{e}}^{\mathfrak{T}}[\pi_b u]$), these liftings remove the polynomial face jumps across irregular faces situated as in Figures 2 and 3. We denote by $\pi_b^\star u$ the intermediate base projector thus constructed from $\pi_b u$ over $\widetilde{\mathcal{M}}_\sigma^{\ell,\boldsymbol{ce},\|}$. This yields a continuous projector within each edge-patch block.

Lemma 5.31. *We have* $\Upsilon_{\widetilde{\mathcal{M}}_\sigma^{\ell,\boldsymbol{ce},\|}}[u - \pi_b^\star u] \lesssim p^{10} \Upsilon_{\widetilde{\mathcal{M}}_\sigma^{\ell,\boldsymbol{ce},\|}}[u - \pi_b u]$.

Proof. This follows from the bound in Proposition 5.17, which holds true for edge-parallel hexahedra of general aspect ratio with $0 < h^\perp \lesssim h^\| \lesssim 1$. □

We analyze the continuity properties of $\pi_b^\star u$ over $\widetilde{\mathcal{M}}_\sigma^{\ell,\boldsymbol{ce},\|}$ in edge-parallel direction (i.e., across interfaces perpendicular to $\boldsymbol{e}$). First, as in Remarks 5.5 and 5.14, the tensor-product structure of the projector $\pi_b u$ and the liftings $\mathcal{L}_{\boldsymbol{e}}[\pi_b u]$, $\mathcal{L}_{\boldsymbol{e}}^{\mathfrak{T}}[\pi_b u]$ ensures the continuity of the intermediate projection $\pi_b^\star u$ across the scaled edge-patch mesh $\widetilde{\Psi}^{\ell,\boldsymbol{ce}}(\widetilde{\mathcal{M}}_\sigma^{\ell,\boldsymbol{e}})$ into an adjacent edge or corner-edge patch where the same jump liftings are applied. Second, to discuss the conformity between adjacent edge-patch blocks across interfaces perpendicular to $\boldsymbol{e}$, we may again focus on the two adjacent edge-patch blocks $\widetilde{\Psi}^{\ell-1,\boldsymbol{ce}}(\widetilde{\mathcal{M}}_\sigma^{\ell-1,\boldsymbol{e}})$, $\widetilde{\Psi}^{\ell,\boldsymbol{ce}}(\widetilde{\mathcal{M}}_\sigma^{\ell,\boldsymbol{e}})$ shown in Figure 8 (left). Then, with the same arguments as above, $\pi_b^\star u$ is continuous across such interfaces, *with the exception of the perpendicular faces associated with the subdiagonal elements* K_3'', K_4'', K_6'' *of* $\widetilde{\Psi}^{\ell,\boldsymbol{ce}}(\widetilde{\mathcal{M}}_\sigma^{\ell,\boldsymbol{e}})$. Indeed, by definition of the liftings $\mathcal{L}_{\boldsymbol{e}}[\pi_b u]$ in (5.8), we have

$$\pi_b^\star u = \pi_b u \qquad \text{on } \{K_3, K_3', K_4, K_4', K_6, K_6'\}, \tag{5.66}$$

since the diagonal elements constitute the outermost layers in the scaled edge-patch blocks $\widetilde{\Psi}^{\ell-1,\boldsymbol{ce}}(\widetilde{\mathcal{M}}_\sigma^{\ell-1,\boldsymbol{e}})$ and $\widetilde{\Psi}^{\ell,\boldsymbol{ce}}(\widetilde{\mathcal{M}}_\sigma^{\ell,\boldsymbol{e}})$. However, on the subdiagonal elements K_3'', K_4'', K_6'' in $\widetilde{\Psi}^{\ell,\boldsymbol{ce}}(\widetilde{\mathcal{M}}_\sigma^{\ell,\boldsymbol{e}})$ depicted in Figure 8 (left), the base projector $\pi_b u$ is altered by the addition of the (scaled) lifting $\mathcal{L}_{\boldsymbol{e}}[\pi_b u]$ which does not generally vanish on the interface $x_3 = 0$; cp. Remark 5.5. As a consequence, the projector $\pi_b^\star u$ is generally *not continuous* over the faces $f_{K_3',K_3''}$, $f_{K_4',K_4''}$ and $f_{K_6',K_6''}$. By the self-similar structure of the mesh $\widetilde{\mathcal{M}}_\sigma^{\ell,\boldsymbol{ce},\|}$, the same difficulty arises in the subdiagonal elements of each scaled edge patch $\widetilde{\Psi}^{\ell',\boldsymbol{ce}}(\widetilde{\mathcal{M}}_\sigma^{\ell',\boldsymbol{e}})$, for $2 \le \ell' \le \ell$, cp. Figure 7. In addition, in the case $\ell' = 1$, see Figure 8 (right), it follows similarly that

$$\pi_b^\star u = \pi_b u \qquad \text{on } \{K_3, K_4, K_6, K_1'\}, \tag{5.67}$$

and that $\pi_b u$ is in general non-conforming over the face $f_{K_1',K_1''}$.

5.4.3. *Conformity over Subdiagonal Elements.* To correct for the non-conformity across the critical faces above, we proceed in several steps.

Subdiagonal Elements for $2 \le \ell' \le \ell$. In Figure 9 and for $2 \le \ell' \le \ell$, we illustrate the three subdiagonal elements K_3'', K_4'', K_6'' on the patch interface between $\widetilde{\Psi}^{\ell'-1,\boldsymbol{ce}}(\widetilde{\mathcal{M}}_\sigma^{\ell'-1,\boldsymbol{e}})$ and $\widetilde{\Psi}^{\ell',\boldsymbol{ce}}(\widetilde{\mathcal{M}}_\sigma^{\ell',\boldsymbol{e}})$, employing the notation in Figure 8 (left). Without loss of generality, we may assume that the interface lies on $x_3 = 0$.

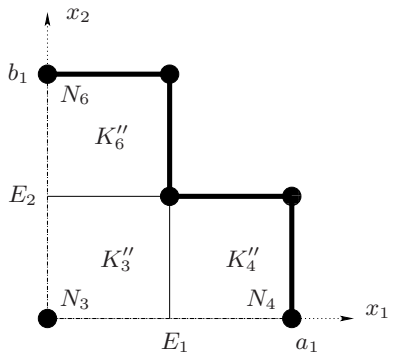

FIGURE 9. Subdiagonal elements K_3'', K_4'', K_6'' on the interface $x_3 = 0$ between two adjacent edge-patch blocks for $\sigma = 0.5$ and $2 \le \ell' \le \ell$. The nodes N_3, N_4, N_6 and the edges E_1, E_2 are indicated.

Lemma 5.32. *Let* $2 \le \ell' \le \ell$. *In the setting of Figure 9, there holds:*

(i) *For* $i \in \{3,4,6\}$, *we have*

$$\pi_b^\star|_{K_i'} u|_{K_i'}(N_i) = \pi_b^\star|_{K_i''} u|_{K_i''}(N_i), \tag{5.68}$$

for the nodes $N_3 = (0,0,0)$, $N_4 = (a_1,0,0)$ *and* $N_6 = (0,b_1,0)$.

(ii) *We have* $\pi_b^\star|_{K_i'} u|_{K_i'} = \pi_b^\star|_{K_i''} u|_{K_i''}$ *on each (closed) line segment shown in boldface and for the corresponding index* $i \in \{3,4,6\}$.

(iii) *For* $i \in \{3,4\}$ *and edge* $E_i = E_1 \cap \partial K_i'$, *we have*

$$\big(\pi_b^\star|_{K_i'} u|_{K_i'}\big)|_{E_i} = \big(\pi_b|_{K_2} u|_{K_2}\big)|_{E_i} = \big(\pi_b|_{K_4} u|_{K_4}\big)|_{E_i}. \tag{5.69}$$

Similarly, for $i \in \{3,6\}$ *and edge* $E_i = E_2 \cap \partial K_i'$, *we have*

$$\big(\pi_b^\star|_{K_i'} u|_{K_i'}\big)|_{E_i} = \big(\pi_b|_{K_5} u|_{K_5}\big)|_{E_i} = \big(\pi_b|_{K_6} u|_{K_6}\big)|_{E_i}. \tag{5.70}$$

Proof. We verify (5.68) for $i = 3$. With the properties (5.66), (4.5), the definition of $\pi_b^\star u$ and the identities (5.6), (5.6), we conclude that

$$\pi_b^\star|_{K_3'} u|_{K_3'}(N_3) = \pi_b|_{K_3'} u|_{K_3'}(N_3) = \pi_b|_{K_3''} u|_{K_3''}(N_3) = \pi_b^\star|_{K_3''} u|_{K_3''}(N_3).$$

Moreover, consider a line segment and the corresponding index $i \in \{3,4,6\}$. Hence, by Lemma 5.4, item (ii), $\pi_b^\star|_{K_i''} u|_{K_i''}$ is identical equal to $\pi_b|_{K_i''} u|_{K_i''}$, which in turn is equal to $\pi_b|_{K_i'} u|_{K_i'} = \pi_b^\star|_{K_i'} u|_{K_i'}$; cp. property (4.5). This yields item (ii). Properties (5.69) and (5.70) follow from (5.66) and the fact that $\pi_b u$ is continuous over f_{K_2,K_4} and f_{K_5,K_6}. □

Next, we adjust the projector $\pi_b^\star u$ on the faces of the subdiagonal elements of $\mathcal{D}_{\ell'}$ in (5.63). To that end, for an axiparallel hexahedral element K, we will express $\pi_b^\star|_K u|_K$ as a linear combination of the Lagrangian basis functions associated with the (mapped) $(p+1)$-point tensor-product Gauss-Lobatto interpolation nodes on K; cp. [3, 18].

Fix the subdiagonal element $K_i'' \in \mathcal{D}_{\ell'}$ for $i \in \{3,4,6\}$. We denote by f_i the face $f_{K_i',K_i''}$. On K_i'', we modify $\pi_b^\star u$ to $\pi_b^{\mathcal{D},\star} u$, by explicitly altering the $(p+1)^2$ Gauss-Lobatto face degrees of freedom of $(\pi_b^\star u)|_{K_i''}$ on $\overline{f}_i \subset \partial K_i''$ so that we have

$$\big(\pi_b^{\mathcal{D},\star}|_{K_i''} u|_{K_i''}\big)|_{\overline{f}_i} = \big(\pi_b^\star|_{K_i'} u|_{K_i'}\big)|_{\overline{f}_i}, \qquad i \in \{3,4,6\}. \tag{5.71}$$

By construction and in view of Lemma 5.32, the projector $\pi_b^{\mathcal{D},\star} u$ yields a conforming approximation, which is now continuous across the critical faces $\overline{f}_i = f_{K_i',K_i''}$ for $i \in \{3,4,6\}$ and has the same continuity properties as $\pi_b^\star u$ elsewhere. It also preserves homogeneous Dirichlet boundary conditions.

Lemma 5.33. *Let $2 \le \ell' \le \ell$. Then:*

$$\pi_b^{\mathcal{D},\star} u = \pi_b^\star u = \pi_b u \qquad \text{on } \{K_3, K_3', K_4, K_4', K_6, K_6'\}. \tag{5.72}$$

In addition, we have the bounds

$$N_{K_i''}[\pi_b^{\mathcal{D},\star} u - \pi_b^\star u]^2 \lesssim p^2 h^{-1} \|\pi_b^{\mathcal{D},\star} u - \pi_b^\star u\|^2_{L^2(f_i)}, \qquad i \in \{3,4,6\}, \tag{5.73}$$

with the mesh size h in (5.64)*, and*

$$\sum_{i\in\{3,4,6\}} N_{K_i''}[\pi_b^{\mathcal{D},\star} u - \pi_b^\star u]^2 \lesssim p^2 \sum_{i\in\{3,4,6\}} (N_{K_i'}[u - \pi_b^\star u]^2 + N_{K_i''}[u - \pi_b^\star u]^2). \tag{5.74}$$

Proof. Property (5.72) follows from (5.66) and the definition in (5.71). To verify (5.73), we note that, upon an isotropic scaling argument as in Lemma 3.3 and (5.15), (5.16), it is sufficient to consider the case where K_i'' and K_i' are of unit size. By (5.71), the difference $(\pi_b^{\mathcal{D},\star} u - \pi_b^\star u)|_{K_i''}$ then vanishes in the interior Gauss-Lobatto tensor-product points on K_i''. The inequality in [3, Lemma 3.1, Equation (16)] thus yields

$$\|\pi_b^{\mathcal{D},\star} u - \pi_b^\star u\|^2_{L^2(K_i'')} \lesssim p^{-2} \|\pi_b^{\mathcal{D},\star} u - \pi_b^\star u\|^2_{L^2(f_i)}.$$

Again, the inverse inequality (5.14) shows that

$$\|\nabla(\pi_b^{\mathcal{D},\star} u - \pi_b^\star u)\|^2_{L_2(K_i'')} \lesssim p^2 \|\pi_b^{\mathcal{D},\star} u - \pi_b^\star u\|^2_{L^2(f_i')},$$

which implies (5.73).

To establish (5.74), we start from the bound (5.73) and employ the triangle inequality (along with the fact that u is continuous over f_i), property (5.71), and the trace inequality [14, Lemma 4.2] (with $t = 2$); cp. the bound (3.9). This readily results in

$$\begin{aligned} N_{K_i''}[\pi_b^{\mathcal{D},\star} u - \pi_b^\star u]^2 &\lesssim p^2 h^{-1} \big(\|u|_{K_i'} - (\pi_b^{\mathcal{D},\star} u)|_{K_i''}\|^2_{L^2(f_i)} + \|(u - \pi_b^\star u)|_{K_i''}\|^2_{L^2(f_i)}\big) \\ &\lesssim p^2 h^{-1} \big(\|(u - \pi_b^\star u)|_{K_i'}\|^2_{L^2(f_i)} + \|(u - \pi_b^\star u)|_{K_i''}\|^2_{L^2(f_i)}\big) \\ &\lesssim p^2 \big(N_{K_i'}[u - \pi_b^\star u]^2 + N_{K_i''}[u - \pi_b^\star u]^2\big). \end{aligned}$$

The assertion follows. □

Subdiagonal Elements for $\ell' = 1$. Second, we treat the single subdiagonal element $K_1'' \in \mathcal{D}_1$ as illustrated in Figure 8 (right). In accordance to (5.71), we define $\pi_b^{\mathcal{D},\star}u$ on $K_1'' \in \mathcal{D}_1$ so that

$$\big(\pi_b^{\mathcal{D},\star}|_{K_1''}u|_{K_1''}\big)|_{\overline{f}_1} = \big(\pi_b^{\star}|_{K_1'}u|_{K_1'}\big)|_{\overline{f}_1}, \tag{5.75}$$

over the face $f_1 = f_{K_1',K_1''}$. The projector $\pi_b^{\mathcal{D},\star}u$ is conforming over the face $f_{K_1',K_1''}$ in Figure 8 (right) and preserves potential homogeneous Dirichlet boundary conditions on patch faces. The analog of (5.74) reads as follows.

Lemma 5.34. *Let $\ell' = 1$. Then:*

$$\pi_b^{\mathcal{D},\star}u = \pi_b^{\star}u = \pi_b u \qquad \text{on } \{K_3, K_4, K_6, K_1'\}. \tag{5.76}$$

In addition, we have the bound

$$N_{K_1''}[\pi_b^{\mathcal{D},\star}u - \pi_b^{\star}u]^2 \lesssim p^2(N_{K_1'}[u - \pi_b^{\star}u]^2 + N_{K_1''}[u - \pi_b^{\star}u]^2). \tag{5.77}$$

The Projector $\pi_b^{\mathcal{D},\star}u$. In conclusion, the projector $\pi_b^{\mathcal{D},\star}u$ defined in (5.71), (5.75) gives piecewise polynomial and conforming over the entire mesh $\widetilde{\mathcal{M}}_\sigma^{\ell,\boldsymbol{ce},\parallel}$ in (5.62). In addition, it is conforming over the interface between $\widetilde{\mathcal{M}}_\sigma^{\ell,\boldsymbol{ce},\parallel}$ and $\widetilde{\mathfrak{T}}_\sigma^{\ell,\boldsymbol{c}}$ in edge-parallel direction (i.e., over the face $f_{K_1',K_1''}$ in Figure 8 (right)). The projector $\pi_b^{\mathcal{D},\star}u$ satisfies homogeneous Dirichlet boundary conditions on corresponding patch boundaries.

Lemma 5.35. *We have $\Upsilon_{\widetilde{\mathcal{M}}_\sigma^{\ell,\boldsymbol{ce},\parallel}}[u - \pi_b^{\mathcal{D},\star}u] \lesssim p^{12}\Upsilon_{\widetilde{\mathcal{M}}_\sigma^{\ell,\boldsymbol{ce},\parallel}}[u - \pi_b u]$.* .

Proof. By employing the triangle inequality, this follows from Lemmas 5.33, 5.34 in combination with the bound in Lemma 5.31. □

5.4.4. *Interfaces between $\widetilde{\mathcal{M}}_\sigma^{\ell,\boldsymbol{ce},\parallel}$ and $\widetilde{\mathfrak{O}}_\sigma^{\ell,\boldsymbol{c},\perp}$.* To address the continuity across faces between $\widetilde{\Psi}^{\ell',\boldsymbol{ce}}(\widetilde{\mathcal{M}}_\sigma^{\ell',\boldsymbol{e}})$ and $\widetilde{\mathfrak{O}}_\sigma^{\ell,\boldsymbol{c},\perp}$, $1 \le \ell' \le \ell$, we consider again the two configurations in Figure 8. For $2 \le \ell' \le \ell$, the projector $\pi_b^{\mathcal{D},\star}u$ is already continuous over the regular faces f_{K_1,K_3}, f_{K_2,K_4}, and f_{K_5,K_6}, due to properties (5.72) and (4.5). Similarly, $\pi_b^{\mathcal{D},\star}u$ is conforming over the faces $f_{K_1',K_3'}$, $f_{K_2',K_4'}$, $f_{K_5',K_6'}$. For $\ell' = 1$, continuity of $\pi_b^{\mathcal{D},\star}u$ is ensured across f_{K_1,K_3}, f_{K_2,K_4} and f_{K_5,K_6}; cp. (5.76).

5.4.5. *Continuity across Irregular Faces in $\widetilde{\mathfrak{O}}_\sigma^{\ell,\boldsymbol{c},\perp}$.* In Figure 8 (left), there are in general nonzero polynomial face jumps across the irregular faces $f_{2i} = f_{K_2,K_i'}$, $i \in \{1,2,3,4\}$, and $f_{5i} = f_{K_5,K_i'}$ for $i \in \{1,4,5,6\}$, as well as over analogous faces in the omitted mesh structure (recall from (5.72) that $\pi_b^{\mathcal{D},\star}u = \pi_b u$ on K_3', K_4', K_6'). The geometric situation is similar to that in the corner patch $\widetilde{\mathcal{M}}_\sigma^{\ell,\boldsymbol{c}}$ shown in Figure 4. Over these irregular faces, we thus construct polynomial face jump liftings similarly to $\mathcal{L}_{\boldsymbol{c}}[\pi_b u]$ in (5.44), (5.47) (with the aid of associated edge liftings as in (5.35), (5.37)). The face liftings are supported in $\overline{K_1'} \cup \overline{K_2'} \cup \overline{K_3'} \cup \overline{K_4'}$ and $\overline{K_1'} \cup \overline{K_4'} \cup \overline{K_5'} \cup \overline{K_6'}$ and are stable polynomially in p, as was shown in Section 5.3. We also note that conformity across the corner-edge patch into a neighboring patch is guaranteed by Assumptions 3.1, 3.2.

We denote by $\pi_b^{\star\star}u$ the lifted projector thus obtained from the base projector $\pi_b u$ on $\widetilde{\mathfrak{O}}_\sigma^{\ell,\boldsymbol{c},\perp}$. Lemma 5.24 implies the ensuing bound.

Lemma 5.36. *We have $\Upsilon_{\widetilde{\mathfrak{O}}_\sigma^{\ell,\boldsymbol{ce},\perp}}[u - \pi_b^{\star\star}u] \lesssim p^{10}\Upsilon_{\widetilde{\mathfrak{O}}_\sigma^{\ell,\boldsymbol{ce},\perp}}[u - \pi_b u]$.*

5.4.6. *Continuity into* $\widetilde{\mathfrak{T}}_{\boldsymbol{c}}^{\ell}$. The projector $\pi_b^{\mathcal{D},\star}u$ over $\widetilde{\mathcal{M}}_\sigma^{\ell,\boldsymbol{ce},\|}$ is continuous across $f_{K_1',K_1''}$ in Figure 8 (right). Hence, it remains to enforce the conformity of $\pi_b^{\star\star}u$ over $\widetilde{\mathfrak{O}}_\sigma^{\ell,\boldsymbol{c},\perp}$ from K_2, K_5 into the corner element K_1'. Since $\pi_b^{\star\star}u = \pi_b u$ on the faces $f_{K_2,K_1'}$, $f_{K_5,K_1'}$, this can be achieved with the introduction of face jump liftings for $\pi_b^{\star\star}u$ over $f_{K_2,K_1'}$ and $f_{K_5,K_1'}$, similarly to $\mathcal{L}_{\boldsymbol{c}}^{\mathfrak{T}}[\pi_b u]$ in (5.57) and in conjunction with vertex and edge jump liftings as in Section 5.3.2. A bound analogous to (5.60) holds for the lifted projector still denoted by $\pi_b^{\star\star}u$, with an algebraic loss of p^{18}.

Lemma 5.37. *We have* $\Upsilon_{\widetilde{\mathfrak{T}}_\sigma^{\ell,\boldsymbol{c}}}[u - \pi_b^{\star\star}u] \lesssim p^{18}\Upsilon_{\widetilde{\mathfrak{T}}_\sigma^{\ell,\boldsymbol{c}}}[u - \pi_b u]$.

5.4.7. *Conclusion.* We now define the lifted patch projector Πu over the corner-edge patch $\widetilde{\mathcal{M}}_\sigma^{\ell,\boldsymbol{ce}}$ as $\Pi u := \pi_b^{\mathcal{D},\star}u$ on $\widetilde{\mathcal{M}}_\sigma^{\ell,\boldsymbol{ce},\|}$ and $\Pi u := \pi_b^{\star\star}u$ on $\widetilde{\mathfrak{O}}_\sigma^{\ell,\boldsymbol{c},\perp} \dot\cup \widetilde{\mathfrak{T}}_\sigma^{\ell,\boldsymbol{c}}$. It is conforming over the entire corner-edge patch and preserves essential boundary conditions. With the bounds in Lemmas 5.35, 5.36 and 5.37, we conclude that bound (3.28) holds over the corner-edge patch $\widetilde{\mathcal{M}}_\sigma^{\ell,\boldsymbol{ce}}$.

Proposition 5.38. *We have* $\Upsilon_{\widetilde{\mathcal{M}}_\sigma^{\ell,\boldsymbol{ce}}}[u - \Pi u] \lesssim p^{18}\Upsilon_{\widetilde{\mathcal{M}}_\sigma^{\ell,\boldsymbol{ce}}}[u - \pi_b u]$.

This completes the construction of the reference corner-edge patch projector in the case of refinement along one edge $\boldsymbol{e}$.

5.4.8. *Simultaneous Refinements.* Finally, we comment on extensions to the case where $\widetilde{\mathcal{M}}_\sigma^{\ell,\boldsymbol{ce}}$ is simultaneously refined towards two or three edges.

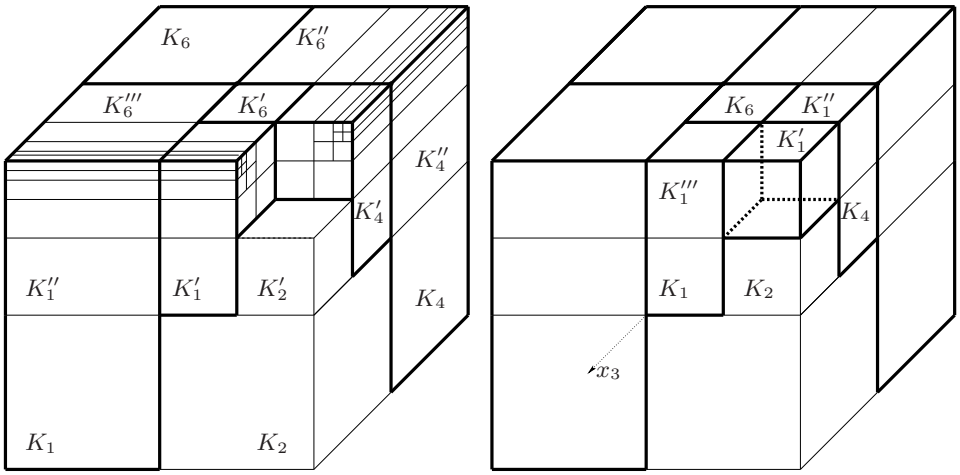

FIGURE 10. Refinement towards two edges. Left: Outermost edge-patch blocks for $\sigma = 0.5$ and $\ell = 5$. Right: Interface between $\widetilde{\mathfrak{T}}_\sigma^{\ell,\boldsymbol{c}} = \{K_1'\}$ and the first edge-patch blocks for $\sigma = 0.5$ and $\ell = 2$.

Refinement Along Two Edges. Let us first consider refinements towards two edges $\boldsymbol{e}_1, \boldsymbol{e}_2$ as shown in Figure 10. In this situation and analogously to (5.61), we write

$$\widetilde{\mathcal{M}}_\sigma^{\ell,\boldsymbol{ce}} := \widetilde{\mathfrak{T}}_\sigma^{\ell,\boldsymbol{c}} \dot\cup \widetilde{\mathfrak{O}}_\sigma^{\ell,\boldsymbol{c},x_3} \dot\cup \big(\widetilde{\mathcal{M}}_\sigma^{\ell,\boldsymbol{ce}_1,\|} \cup \widetilde{\mathcal{M}}_\sigma^{\ell,\boldsymbol{ce}_2,\|}\big), \tag{5.78}$$

where $\widetilde{\mathfrak{T}}_\sigma^{\ell,\boldsymbol{c}}$ consists again of the single terminal layer element abutting at the corner $\boldsymbol{c}$, and $\widetilde{\mathfrak{O}}_\sigma^{\ell,\boldsymbol{c},x_3}$ is a corner-type mesh in x_3-direction. The submeshes $\widetilde{\mathcal{M}}_\sigma^{\ell,\boldsymbol{ce}_1,\|}$

and $\widetilde{\mathcal{M}}_\sigma^{\ell,\boldsymbol{ce}_2,\|}$ are two *non-disjoint sequences* of ℓ scaled edge-patch meshes as in (5.62); they overlap over the mutual diagonal elements K_3, K_6 and K_3', K_6' as illustrated in Figure 10 (left) (the overlap in the omitted mesh structure is analogous).

In the submeshes $\widetilde{\mathcal{M}}_\sigma^{\ell,\boldsymbol{ce}_1,\|}$ and $\widetilde{\mathcal{M}}_\sigma^{\ell,\boldsymbol{ce}_2,\|}$, we proceed as in Section 5.4.2, and apply the liftings $\mathcal{L}_{\boldsymbol{e}}[\pi_b u]$, $\mathcal{L}_{\boldsymbol{e}}^{\mathfrak{T}}[\pi_b u]$ in (5.8), (5.29). As in (5.66), these liftings leave the base projector $\pi_b u$ unchanged on the diagonal elements, which are given by K_1, K_3, K_4, K_6 and K_1', K_3', K_4', K_6' for blocks away from $\boldsymbol{c}$ (case $2 \le \ell' \le \ell$) and by K_1, K_3, K_4, K_6 and K_1' for the last configuration abutting at $\boldsymbol{c}$ (case $\ell' = 1$). Similarly to the discussion in Section 5.4.2, the resulting lifted projector $\pi_b^\star u$ is generally non-conforming over the regular faces $f_{K_1',K_1''}$, $f_{K_3',K_3''}$, $f_{K_3',K_3'''}$, $f_{K_4',K_4''}$ $f_{K_6',K_6''}$, and $f_{K_6',K_6'''}$ in the case of edge-patch block ℓ' with $2 \le \ell' \le \ell$, as well as over $f_{K_1',K_1''}$ and $f_{K_1',K_1'''}$ in the case $\ell' = 1$. (Note that the elements K_3, K_3', K_3'', K_3''' are not explicitly labelled in Figure 10). The definitions (5.71), (5.75) of the projector $\pi_b^{\mathcal{D},\star} u$ can be readily extended to the configuration in Figure 10, by replacing the set $\mathcal{D}_{\ell'}$ in (5.66), (5.67) by

$$\mathcal{D}_{\ell'} = \begin{cases} \{K_1'', K_3'', K_3''', K_4'', K_6'', K_6'''\}, & 2 \le \ell' \le \ell, \\ \{K_1'', K_1'''\}, & \ell' = 1, \end{cases} \tag{5.79}$$

where we employ notation as in Figure 10. The projector $\pi_b^{\mathcal{D},\star} u$ coincides with $\pi_b u$ on the diagonal elements indicated in Figure 10; cp. properties (5.72), (5.76). Moreover, corresponding variants of Lemma 5.33, Lemma 5.34 and Lemma 5.35 hold true.

Continuity across faces between $\widetilde{\mathfrak{O}}_\sigma^{\ell,\boldsymbol{c},x_3}$ and $\widetilde{\mathcal{M}}_\sigma^{\ell,\boldsymbol{ce}_1,\|}$, $\widetilde{\mathcal{M}}_\sigma^{\ell,\boldsymbol{ce}_2,\|}$ follows as in Section 5.4.4, by invoking property (4.5) across regular faces. Polynomial jumps over irregular faces within $\widetilde{\mathfrak{O}}_\sigma^{\ell,\boldsymbol{c},x_3}$ are lifted as in Section 5.4.5, and the corner element K_1' in $\widetilde{\mathfrak{T}}_{\boldsymbol{c}}^\ell$ is treated similarly to Section 5.4.6, thereby providing estimates as in Lemmas 5.36 and 5.37.

Consequently, Proposition 5.38 holds true also for corner-edge patches which are refined along two edges.

Refinement Along Three Edges. The case of refinement towards the three edges $\boldsymbol{e}_1, \boldsymbol{e}_2, \boldsymbol{e}_3$ is illustrated in Figure 11. In this case, we decompose the corner-edge patch into

$$\widetilde{\mathcal{M}}_\sigma^{\ell,\boldsymbol{ce}} := \widetilde{\mathfrak{T}}_\sigma^{\ell,\boldsymbol{c}} \,\dot\cup\, \big(\widetilde{\mathcal{M}}_\sigma^{\ell,\boldsymbol{ce}_1,\|} \cup \widetilde{\mathcal{M}}_\sigma^{\ell,\boldsymbol{ce}_2,\|} \cup \widetilde{\mathcal{M}}_\sigma^{\ell,\boldsymbol{ce}_3,\|}\big). \tag{5.80}$$

The set $\widetilde{\mathfrak{T}}_\sigma^{\ell,\boldsymbol{c}}$ contains the single corner element, and $\widetilde{\mathcal{M}}_\sigma^{\ell,\boldsymbol{ce}_i,\|}$ is sequence of ℓ scaled edge-patch blocks as in (5.62) along edge $\boldsymbol{e}_i$. These sequences overlap on the mutual diagonal elements as illustrated in Figure 10. The overlap is similar in the omitted mesh structure. The intermediate projector $\pi_b^\star u$ is obtained from $\pi_b u$ after application of the liftings $\mathcal{L}_{\boldsymbol{e}}[\pi_b u]$ and $\mathcal{L}_{\boldsymbol{e}}^{\mathfrak{T}}[\pi_b u]$ on each of the submeshes $\widetilde{\mathcal{M}}_\sigma^{\ell,\boldsymbol{ce}_i,\|}$; cp. Section 5.4.2. While we have $\pi_b^\star u = \pi_b u$ on diagonal elements, the approximation $\pi_b^\star u$ is non-conforming across edge-perpendicular faces of the subdiagonal elements given by

$$\mathcal{D}_{\ell'} = \begin{cases} \{K_1'', K_1''', K_3'', K_3''', K_3'''', K_4'', K_4''', K_6'', K_6'''\}, & 2 \le \ell' \le \ell, \\ \{K_1'', K_1''', K_1''''\}, & \ell' = 1, \end{cases} \tag{5.81}$$

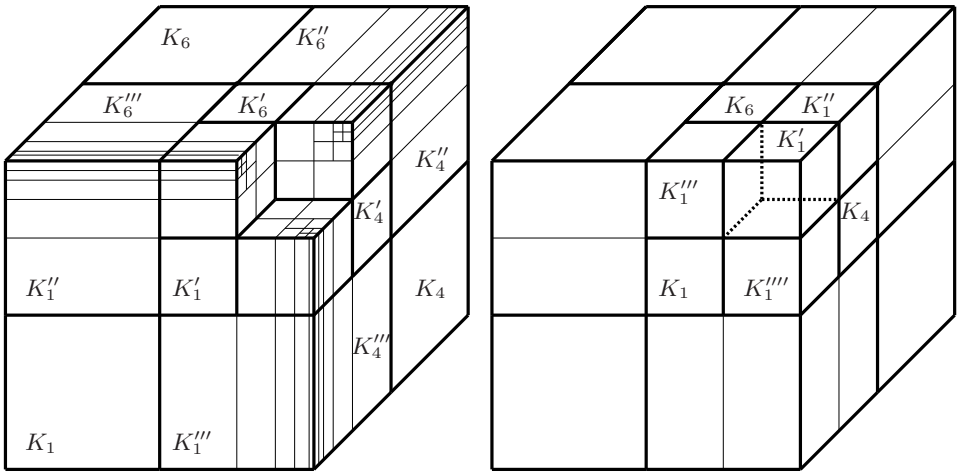

FIGURE 11. Refinement toward three edges. Left: Outermost edge-patch blocks for $\sigma = 0.5$ and $\ell = 5$. Right: Interface between $\widetilde{\mathfrak{T}}_\sigma^{\ell,\boldsymbol{c}} = \{K_1'\}$ and the first edge-patch block for $\sigma = 0.5$ and $\ell = 2$.

employing notation as in Figure 11. As before, the definitions (5.71), (5.75) of the projector $\pi_b^{\mathcal{D},\star}u$ can be generalized to the configuration in Figure 11, by using the subdiagonal elements in (5.81). This gives rise to a conforming approximation $\pi_b^{\mathcal{D},\star}u$ over $\cup_{i=1}^3 \widetilde{\mathcal{M}}_\sigma^{\ell,\boldsymbol{c}\boldsymbol{e}_i,\|}$. It is also continuous across the faces $f_{K_1',K_1''}$,$f_{K_1',K_1'''}$ and $f_{K_1',K_1''''}$ in Figure 11 (right). Since $\pi_b u$ is identically zero on $K_1' \in \widetilde{\mathfrak{T}}_\sigma^{\ell,\sigma}$, cp. (4.9), there is no need for further liftings into $\widetilde{\mathfrak{T}}_\sigma^{\ell,\boldsymbol{c}}$.

Therefore, Proposition 5.38 remains valid for corner-edge patches which are geometrically refined along three edges.

REFERENCES

[1] I. Babuška and B. Q. Guo. Regularity of the solution of elliptic problems with piecewise analytic data. I. Boundary value problems for linear elliptic equation of second order. *SIAM J. Math. Anal.*, 19(1):172–203, 1988.

[2] I. Babuška and B. Q. Guo. Approximation properties of the *h-p* version of the finite element method. *Comput. Methods Appl. Mech. Engrg.*, 133(3-4):319–346, 1996.

[3] E. Burman and A. Ern. Continuous interior penalty *hp*-finite element methods for advection and advection-diffusion equations. *Math. Comp.*, 76(259):1110–1140, 2007.

[4] M. Costabel, M. Dauge, and S. Nicaise. Analytic regularity for linear elliptic systems in polygons and polyhedra. *Math. Models Methods Appl. Sci.*, 22(8), 2012.

[5] M. Costabel, M. Dauge, and Ch. Schwab. Exponential convergence of *hp*-FEM for Maxwell's equations with weighted regularization in polygonal domains. *Math. Models Methods Appl. Sci.*, 15(4):575–622, 2005.

[6] W. Dahmen and K. Scherer. Best approximation by piecewise polynomials with variable knots and degrees. *J. Approx. Theory*, 26(1):1–13, 1979.

[7] L. Demkowicz, Jason J. Kurtz, D. Pardo, M. Paszyński, W. Rachowicz, and A. Zdunek. *Computing with hp-Adaptive Finite Elements. Vol. 2: Frontiers: Three Dimensional Elliptic and Maxwell Problems with Applications*. Chapman & Hall/CRC Applied Mathematics and Nonlinear Science Series. Chapman & Hall/CRC, Boca Raton, FL, 2007.

[8] P. Frauenfelder. *hp-Finite Element Methods on Anisotropically, Locally Refined Meshes in Three Dimensions with Stochastic Data*. PhD thesis, Swiss Federal Institute of Technology. Diss. ETH No. 15750, 2004. URL: http://e-collection.library.ethz.ch/.

[9] W. Gui and I. Babuška. The h, p and h-p versions of the finite element method in 1 dimension. II. The error analysis of the h- and h-p versions. *Numer. Math.*, 49(6):613–657, 1986.

[10] B. Q. Guo and I. Babuška. The hp-version of the finite element method. Part I: The basic approximation results. *Comp. Mech.*, 1:21–41, 1986.

[11] B. Q. Guo and I. Babuška. Regularity of the solutions for elliptic problems on nonsmooth domains in $\mathbb{R}^3$. I. Countably normed spaces on polyhedral domains. *Proc. Roy. Soc. Edinburgh Sect. A*, 127(1):77–126, 1997.

[12] B. Q. Guo and I. Babuška. Regularity of the solutions for elliptic problems on nonsmooth domains in $\mathbb{R}^3$. II. Regularity in neighbourhoods of edges. *Proc. Roy. Soc. Edinburgh Sect. A*, 127(3):517–545, 1997.

[13] K. Scherer. On optimal global error bounds obtained by scaled local error estimates. *Numer. Math.*, 36:257–277, 1981.

[14] D. Schötzau, Ch. Schwab, and T. P. Wihler. hp-DGFEM for second-order elliptic problems in polyhedra I: Stability on geometric meshes. *SIAM J. Numer. Anal.*, 51(3):1610–1633, 2013.

[15] D. Schötzau, Ch. Schwab, and T. P. Wihler. hp-DGFEM for second-order elliptic problems in polyhedra II: Exponential convergence. *SIAM J. Numer. Anal.*, 51(4):2005–2035, 2013.

[16] Ch. Schwab. *p- and hp-FEM – Theory and Application to Solid and Fluid Mechanics*. Oxford University Press, Oxford, 1998.

[17] Ch. Schwab and M. Suri. The optimal p-version approximation of singularities on polyhedra in the boundary element method. *SIAM J. Numer. Anal.*, 33(2):729–759, 1996.

[18] L. Zhu, S. Giani, P. Houston, and D. Schötzau. Energy norm a posteriori error estimation for hp-adaptive discontinuous Galerkin methods for elliptic problem in three dimensions. *Math. Models Methods Appl. Sci.*, 21(2):267–306, 2011.

Mathematics Department, University of British Columbia, Vancouver, BC V6T 1Z2, Canada

E-mail address: schoetzau@math.ubc.ca

Seminar of Applied Mathematics, ETH Zürich, 8092 Zürich, Switzerland

E-mail address: schwab@math.ethz.ch

Recent Research Reports

Nr.	Authors/Title

2014-28 D. Ray and P. Chandrashekar and U. Fjordholm and S. Mishra
Entropy stable schemes on two-dimensional unstructured grids

2014-29 H. Rauhut and Ch. Schwab
Compressive sensing Petrov-Galerkin approximation of high-dimensional parametric operator equations

2014-30 M. Hansen
A new embedding result for Kondratiev spaces and application to adaptive approximation of elliptic PDEs

2014-31 F. Mueller and Ch. Schwab
Finite elements with mesh refinement for elastic wave propagation in polygons

2014-32 R. Casagrande and C. Winkelmann and R. Hiptmair and J. Ostrowski
DG Treatment of Non-Conforming Interfaces in 3D Curl-Curl Problems

2014-33 U. Fjordholm and R. Kappeli and S. Mishra and E. Tadmor
Construction of approximate entropy measure valued solutions for systems of conservation laws.

2014-34 S. Lanthaler and S. Mishra
Computation of measure valued solutions for the incompressible Euler equations.

2014-35 P. Grohs and A. Obermeier
Ridgelet Methods for Linear Transport Equations

2014-36 P. Chen and Ch. Schwab
Sparse-Grid, Reduced-Basis Bayesian Inversion

2014-37 R. Kaeppeli and S. Mishra
Well-balanced schemes for gravitationally stratified media